EUROPEAN ORGANISATION FOR NUCLEAR RESEARCH (CERN)

JHEP 11 (2022) 040
DOI: DOI:10.1007/JHEP11(2022)040

CERN-EP-2021-263
1st December 2022

Measurement of the polarisation of single top quarks and antiquarks produced in the t-channel at $\sqrt{s} = 13$ TeV and bounds on the tWb dipole operator from the ATLAS experiment

The ATLAS Collaboration

A simultaneous measurement of the three components of the top-quark and top-antiquark polarisation vectors in t-channel single-top-quark production is presented. This analysis is based on data from proton–proton collisions at a centre-of-mass energy of 13 TeV corresponding to an integrated luminosity of 139 fb^{-1}, collected with the ATLAS detector at the LHC. Selected events contain exactly one isolated electron or muon, large missing transverse momentum and exactly two jets, one being b-tagged. Stringent selection requirements are applied to discriminate t-channel single-top-quark events from the background contributions. The top-quark and top-antiquark polarisation vectors are measured from the distributions of the direction cosines of the charged-lepton momentum in the top-quark rest frame. The three components of the polarisation vector for the selected top-quark event sample are $P_{x'} = 0.01 \pm 0.18$, $P_{y'} = -0.029 \pm 0.027$, $P_{z'} = 0.91 \pm 0.10$ and for the top-antiquark event sample they are $P_{x'} = -0.02 \pm 0.20$, $P_{y'} = -0.007 \pm 0.051$, $P_{z'} = -0.79 \pm 0.16$. Normalised differential cross-sections corrected to a fiducial region at the stable-particle level are presented as a function of the charged-lepton angles for top-quark and top-antiquark events inclusively and separately. These measurements are in agreement with Standard Model predictions. The angular differential cross-sections are used to derive bounds on the complex Wilson coefficient of the dimension-six O_{tW} operator in the framework of an effective field theory. The obtained bounds are $C_{tW} \in [-0.9, 1.4]$ and $C_{itW} \in [-0.8, 0.2]$, both at 95% confidence level.

1 Introduction

Single-top-quark production through the electroweak (EW) charged current at hadron colliders proceeds mostly, according to the Standard Model (SM) prediction, via three modes that can be defined at leading order (LO) in quantum chromodynamics (QCD): the exchange of a virtual W boson in either the t- or s-channel, and the associated production of a top quark and a W boson (named tW). At the LHC, in proton–proton (pp) collision data, the t-channel is the dominant process and the subject of the measurements presented in this paper. In the t-channel process, a light-flavour quark q from one of the colliding protons interacts with a b-quark, which can be considered as being emitted directly from the other colliding proton (five-flavour scheme or 5FS) or as originating from gluon splitting (four-flavour scheme or 4FS). The incoming light-flavour quark exchanges a space-like virtual W boson, producing a top quark t and a recoiling light-flavour quark q', called the *spectator quark*. Two subprocesses contribute to the t-channel process in the production of either single top quarks (t) or single top antiquarks ($\bar{t}$) at LO. The dominant subprocess is the scattering of the incoming up-type (down-type) quark from a bottom quark (antiquark), to produce a down-type (up-type) spectator quark and a top quark (antiquark), as illustrated in Figures 1(a) and 1(d). The subdominant subprocess is the scattering of a down-type (up-type) antiquark from a bottom quark (antiquark), to produce an up-type (down-type) spectator antiquark and a top quark (antiquark), as illustrated in Figures 1(b) and 1(c). The production cross-section of single top quarks is about twice as large as that of single top antiquarks.

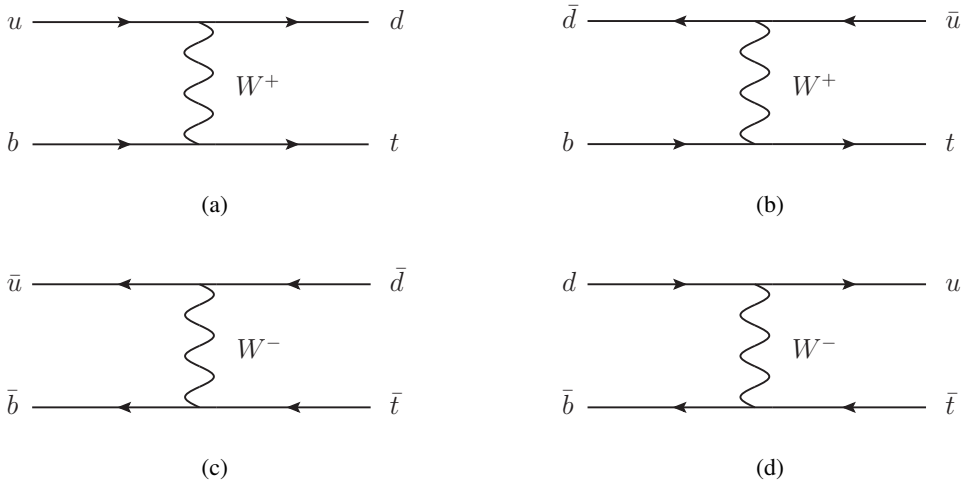

Figure 1: Feynman diagrams for the processes contributing to t-channel single-top-quark production at LO, in the five-flavour scheme. In the dominant subprocess, an up- or down-type quark from one of the colliding protons interacts with a bottom quark or antiquark from the other proton by exchanging a virtual W boson to produce a (a) top quark or (d) top antiquark. In the subdominant subprocess, a down- or up-type antiquark from one of the colliding protons interacts with a bottom quark or antiquark from another proton by exchanging a virtual W boson to produce a (b) top quark or (c) top antiquark.

The QCD $pp \to t\bar{t}$ process produces unpolarised top quarks because of parity conservation in QCD [1–4], while single-top-quark production yields a large sample of highly polarised top quarks and top antiquarks. In the t-channel at LO, as a consequence of the vector minus axial-vector ($V - A$) form of the tWb vertex, single top quarks are produced with their spin completely aligned along the direction of the

down-type quarks [5, 6]. For single top quarks produced by the dominant subprocess, this direction is the spectator-quark direction, while for the subdominant subprocess it is the direction of the incoming down-type antiquark. For single top-antiquark production, the spin aligns in the direction opposite to that of the incoming down-type quark in the dominant subprocess, and opposite to that of the spectator antiquark in the subdominant process. Thus, the degree of polarisation for a sample of single-top-quark or single-top-antiquark events depends on the mix of dominant and subdominant production processes and the relative alignment between the beam line and spectator-quark directions, averaged over the sample selected. The orientation of the polarisation vector is in the production plane. In all cases the direction is relative to the rest frame of the top quark or antiquark.

In the t-channel production process, the spectator-quark direction lies close to the beam direction. The predominant $ub \to dt$ process (or $ug \to dt\bar{b}$ in the 4FS), as well as the similarity of the two aforementioned directions, produces very high (though not 100%) top-quark polarisation along the direction of the spectator quark when both the dominant and subdominant processes are considered. For top antiquarks, the two subprocesses contribute to different degrees, but also lead to nearly 100% polarisation, this time in the direction opposite to that of the spectator quark. At LO in the SM, the expected values of the polarisations of top quarks and top antiquarks along the direction of the spectator quark are 0.90 and −0.86, respectively, computed in the 4FS as detailed in Ref. [7]. However, effects beyond LO as well as acceptance requirements, which have a large effect on the polarisation, are not accounted for in that calculation. A calculation at next-to-next-to-leading order (NNLO), based on Ref. [8], predicts top-quark polarisation along the direction of the spectator quark of $0.965 \pm 0.003\ (\text{scale})^{+0.003}_{-0.004}\ (\text{PDF} + \alpha_\text{s})$ for top quarks and $-0.957^{-0.003}_{+0.012}\ (\text{scale})^{+0.004}_{-0.002}\ (\text{PDF} + \alpha_\text{s})$ for top antiquarks. These values are obtained from a parton-level calculation at fixed order using the CT18NNLO [9] set of parton distribution functions (PDFs) with the renormalisation (μ_r) and factorisation (μ_f) scales set to half of the top-quark mass (m_t). This calculation considers stable single top quarks produced in the t-channel from pp collisions at $\sqrt{s} = 13$ TeV, in a region with exactly one light-flavour jet, where jets are clustered with the anti-k_t algorithm [10] with a radius parameter of 0.4, and they are required to have $p_\text{T} > 30$ GeV and $|\eta| < 4.5$. Additional acceptance criteria for the light-flavour jet, implementing the acceptance requirement defined in Eq. (2) and described in Section 4, were also applied in calculating the prediction. The effect of the scale uncertainty is calculated by varying the renormalisation and factorisation scales by factors of 2.0 and 0.5 from their central value. The effect of the α_s uncertainty is calculated by varying $\alpha_\text{s}(m_Z)$ by 0.001 from its central value. The PDF uncertainty is calculated from the 68% confidence level (CL) eigenvectors in the CT18NNLO PDF sets at the most similar α_s value. The effects of the α_s and PDF uncertainties are summed in quadrature. Similar calculations were previously carried out for pp collisions at LO at $\sqrt{s} = 14$ TeV [6], at next-to-leading order (NLO) at $\sqrt{s} = 7$ TeV [11], and in proton–antiproton collisions at LO at Tevatron energies [5]. A general trend is that typical acceptance requirements increase the top-quark polarisation, while effects beyond LO reduce it. NLO EW corrections to the tWb vertex are calculated in Refs. [12–16], and Ref. [15] explicitly calculates the effect on top-quark polarisation. While that calculation is done for the full phase space of single-top-quark production, rather than the restricted space of the calculation described in this paper, the EW corrections are smaller than those from QCD.

This paper reports a direct measurement of the top-quark and top-antiquark polarisation vectors from a template fit to the joint distributions of the direction cosines of the charged-lepton momentum in the top-quark rest frame. Each component of the polarisation vector is thereby measured without any assumption about the other two components. In addition, normalised differential cross-sections corrected to a fiducial region at particle level are presented as a function of the charged-lepton angles for top-quark and top-antiquark events separately and inclusively, so that they can be combined with other experimental inputs, to derive bounds on complex Wilson coefficients in the framework of an effective field theory (EFT).

In this paper, the inclusive measurements are used to derive bounds on the complex Wilson coefficient of the dimension-six O_{tW} operator.

1.1 Decay angles from polarised top quarks and top antiquarks

This analysis exploits the $t \to Wb \to b\ell^+\nu$ decay mode of the top quark, as well as the charge-conjugate decay mode of the top antiquark. The lepton $\ell^\pm$ can be either an electron or a muon. In the decay, three orthogonal directions may be defined [7]. These serve to express the spin vector of the top quark. As illustrated in Figure 2, the $\hat{z}'$ direction is the direction of the momentum of the spectator quark, $\vec{p}_{q'}$, in the top-quark reference frame. The $\hat{y}'$ direction is taken along $\hat{z}' \times \hat{p}_q$, where $\hat{p}_q$ is the direction of the incoming light-flavour quark, in the top-quark reference frame. Then, the $\hat{x}'$ direction lies in the production plane, orthogonal to $\hat{y}'$ and $\hat{z}'$, such that $\{x', y', z'\}$ form a right-handed coordinate system: $\hat{z}' = \vec{p}_{q'}/|\vec{p}_{q'}|$, $\hat{y}' = (\hat{z}' \times \vec{p}_q)/|\hat{z}' \times \vec{p}_q|$ and $\hat{x}' = \hat{y}' \times \hat{z}'$.

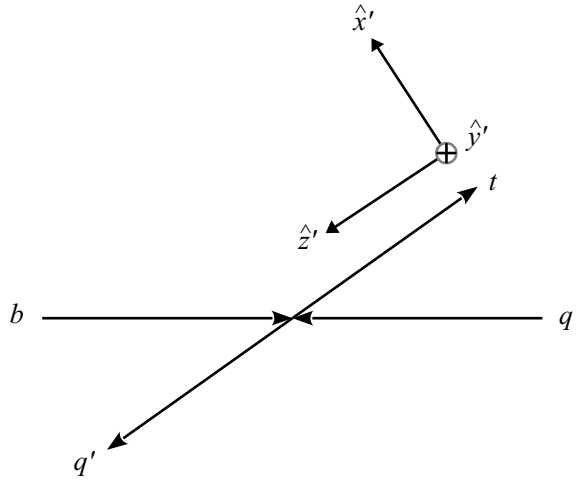

Figure 2: Diagram illustrating the three orthogonal directions $\hat{x}'$, $\hat{y}'$ and $\hat{z}'$ used in this analysis, as seen in the zero-momentum frame of the initial-state quarks. The $\hat{z}'$ direction is that of the spectator quark in the top-quark rest frame. The $\hat{x}'$ direction lies in the production plane, while the $\hat{y}'$ direction is perpendicular to the production plane.

The polarisation vector $\vec{P}$ is defined in this coordinate system; it satisfies $|\vec{P}| \leq 1$, equality holding if and only if the top quarks are produced in a pure quantum mechanical ensemble with respect to spin. Information about the spin of the top quark is transferred to the decay products, and therefore can be extracted from their angular distributions. This was already exploited in previous analyses [17–21] which measure spin observables in single-top-quark and/or $t\bar{t}$ events using LHC data. Previous measurement of t-channel single-top-quark polarisation at $\sqrt{s} = 8$ TeV from ATLAS [20] set a limit $\left|P_{z'}\right| > 0.72$ (at 95% CL) at parton level, where an average is taken over top quarks and top antiquarks. The spin asymmetry $A_\ell = (P_{z'}\alpha_\ell)/2$, where α_ℓ is the analysing power of the charged lepton (ℓ) in the top-quark decay, was determined to be 0.49 ± 0.06 by ATLAS [19] and 0.26 ± 0.11 by CMS [22] at $\sqrt{s} = 8$ TeV and measured to be 0.440 ± 0.070 by CMS at $\sqrt{s} = 13$ TeV [21]. In all these cases, this was done at parton level, and an average over top quarks and antiquarks was also taken.

As shown in Refs. [1–4], the charged lepton is the most sensitive probe of the top-quark spin, with analysing

power close to 1; for that reason the analysis is based upon angular distributions of the charged lepton from the top-quark decay. Angular distributions of single top quarks are discussed in Ref. [23], where the four-dimensional fully differential decay distribution for the top-(anti)quark decays with polarisation $\vec{P}$ is presented. Equation (11) in that reference is used as the basis for a custom decay model, valid at LO, which is interfaced with the LO Protos [24] event generator, in order to generate simulated event samples containing pure ensembles of events fully polarised along the x', y', or z' direction. Calculations of top-quark angular decay distributions at NLO and NNLO [25, 26] indicate that higher-order effects are small compared to the precision of this analysis. A fitting function describing angular distributions of event samples with arbitrary polarisation is constructed by taking linear combinations of templates derived from simulated pure ensembles with x', y', or z' polarisation at reconstruction level. The fitting function is then used in a template fit to data, in which the three components of polarisation, $\{P_{x'}, P_{y'}, P_{z'}\}$ are allowed to float without imposing the $|\vec{P}| \leq 1$ constraint. This is the strategy followed in this analysis to measure all components of the polarisation vector $\vec{P}$ for top-quark and top-antiquark events separately. Details of the fit model are given in Section 9.

In the coordinate system previously defined, and considering $\theta_{\ell i}$ as the polar angle of the charged-lepton momentum with respect to the i^{th} axis ($i = x', y', z'$), one can obtain the differential angular distributions associated with the three different polarisation components $\{P_{x'}, P_{y'}, P_{z'}\}$. These differential angular distributions are distorted by the inefficiencies and acceptance of the detector, smeared by the reconstruction procedures, and sculpted by the event selection criteria. In this paper, the detector effects are unfolded and the measured normalised differential angular distributions are compared directly with theoretical predictions within a fiducial region as detailed in Section 10.

1.2 Sensitivity of polarised top-quark decay angles to effective field theory operators

Measurements of polarisation observables in t-channel single-top-quark production are sensitive to new physics phenomena affecting the tWb vertex. In the framework of SM EFT [27], the SM Lagrangian ($\mathcal{L}_{\text{SM}}$) is augmented with higher-dimensional operators invariant under the SM gauge symmetry. Since dimension-five operators do not contribute to top-quark production or decay [28], the leading contributions from higher-dimensional operators are from dimension-six operators ($O_k^{[6]}$). This analysis is therefore limited to those terms, with corresponding Wilson coefficients (C_k) scaled by $1/\Lambda^2$:

$$\mathcal{L}_{\text{EFT}} = \mathcal{L}_{\text{SM}} + \sum_k \frac{C_k}{\Lambda^2} O_k^{[6]} + \dots ,$$

where $\mathcal{L}_{\text{EFT}}$ is the effective Lagrangian, Λ is the scale of new physics chosen such that higher-dimensional operators are sufficiently suppressed by higher powers of Λ, and where k runs over all dimension-six operators. There are only three dimension-six effective operators that contribute at order $1/\Lambda^2$ at tree level in the t-channel production of the single top quark as presented in Ref. [29]. In the so-called 'Warsaw' basis, the three operators are $O_{\varphi q}$, O_{qq} and O_{tW} as described in Ref. [30], where φ stands for the Higgs field. Other effective operators such as O_{bW} and $O_{\varphi tb}$ contribute but are suppressed by a factor $1/\Lambda^4$ or by the small value of the bottom-quark mass relative to that of the top quark. Within the present limits set on these other operators [20, 31–36], their effect on the polarisation of the top quark is expected to be insignificant compared to the current precision of the measurement.

The operator $O_{\varphi q}$ affects the signal production cross-section and has no effect on normalised distributions. The four-fermion operator, O_{qq}, has a negligible effect on angular distributions [29] and can be ignored. Only the O_{tW} operator with its complex coefficient has an effect on the polarisation of the top quark. The real and imaginary parts of its coefficient are indicated in this work by C_{tW} and C_{itW}, respectively. The coefficient C_{tW} mostly affects $P_{x'}$, whereas C_{itW} affects $P_{y'}$. Since the SM prediction for $P_{z'}$ is already near the maximum allowed value, it is less sensitive to changes in C_{tW} or C_{itW}. A non-zero value for C_{itW} could be a hint of non-SM CP violation in the tWb vertex, making it especially interesting with regard to the matter–antimatter asymmetry present in nature.

This formalism is used to perform an interpretation of the unfolded normalised differential angular distributions presented in Section 1.1 in an EFT context, providing limits on the real and imaginary parts of the O_{tW} dipole operator.

This paper is organised as follows. Section 2 describes the data samples as well as the simulated event samples used to predict properties of the t-channel signal and the background processes. Section 3 describes the object and event reconstruction for the identification of signal events, while Section 4 presents the criteria used to define the signal region and the control regions. The procedures for modelling background processes are described in Section 6. The event yields comparing the predictions and the observed data are also shown in this section. Section 8 quantifies the systematic uncertainties in this measurement. Section 9 describes the measurement of the polarisation vector of an ensemble of top quarks or antiquarks. The particle-level differential measurement of the normalised angular distributions is described in Section 10, while the way these angular differential cross-section distributions are used to set limits on some EFT coefficients is presented in Section 11. The conclusions are given in Section 12.

2 Data and simulated event samples

The ATLAS detector[1] [37] at the LHC covers nearly the entire solid angle around the collision point. It consists of an inner tracking detector surrounded by a thin superconducting solenoid producing a 2 T axial magnetic field, electromagnetic and hadronic calorimeters, and an external muon spectrometer incorporating three large toroidal magnet assemblies. The analysis is performed using pp collision data collected at a centre-of-mass energy of 13 TeV from 2015 to 2018. Stringent detector and data quality requirements were applied [38], resulting in a data sample corresponding to a total integrated luminosity of 139 fb^{-1} [39, 40]. The events were selected by single-lepton[2] triggers [41, 42], imposing low thresholds on the transverse energy (E_{T}) of electrons and the transverse momentum (p_{T}) of muons, in addition to isolation requirements, or imposing a looser identification criterion and higher thresholds with no isolation requirement. The lowest thresholds varied from 20 to 26 GeV depending on the lepton flavour and the data-taking period.

Samples of simulated events were produced using different Monte Carlo (MC) event generators including parton shower (PS) and hadronisation models. The effect of multiple interactions in the same and neighbouring bunch crossings (pile-up) was modelled by overlaying the hard-scattering event with simulated minimum-bias events generated with Pythia 8.186 [43, 44] using the NNPDF2.3lo [45] PDF set

[1] ATLAS uses a right-handed coordinate system with its origin at the nominal interaction point (IP) in the centre of the detector and the z-axis along the beam pipe. The x-axis points from the IP to the centre of the LHC ring, and the y-axis points upward. Cylindrical coordinates (r, ϕ) are used in the transverse plane, ϕ being the azimuthal angle around the z-axis. The pseudorapidity is defined in terms of the polar angle θ as $\eta = -\ln\tan(\theta/2)$.

[2] Henceforth, 'lepton' indicates an electron or muon.

and the A3 set of tuned parameters [46]. Events were reweighted such that the distribution of the average number of interactions per bunch crossing matches that observed in data.

Single-top-quark t-channel events were generated with the NLO Powheg Box [47–50] v2 generator, which provides matrix elements (MEs) at NLO in the strong coupling constant α_s using the 4FS with the NNPDF3.0nlo nf4 [51] PDF set. The scales were set to $\mu_r^2 = \mu_f^2 = 16(m_b^2 + p_{T,b}^2)$, where m_b and $p_{T,b}$ are the mass and p_T of the b-quark from the initial gluon splitting.

Additional samples of simulated t-channel signal events were produced within the 4FS with the LO Protos 2.3 generator [24] using the CTEQ6L1 PDF set [52]. The scales were set to $\mu_f^2 = -p_W^2$ for the light-flavour quark distribution function and $\mu_f^2 = p_{T,\bar{b}}^2 + m_b^2$ for the gluon distribution function, where p_W and $p_{T,\bar{b}}$ are the momentum of the exchanged W boson and the p_T of the b-antiquark originating from the gluon splitting, respectively [24, 53]. In addition to a SM signal sample, six samples with tWb anomalous couplings [54, 55], $V_{L,R}$ and $g_{L,R}$, enabled in both the production and decay vertices were produced with the Protos event generator. The ranges chosen for the anomalous coupling event samples were based on previous established limits [20]: $\mathrm{Re}[g_R]/V_L = \pm 0.18$; $\mathrm{Im}[g_R]/V_L = \pm 0.07$; and $V_R/V_L = \pm 0.4$ and $g_L/V_L = \mp 0.32$. For $V_L = 1$ and $\Lambda = 1$ TeV, following Ref. [56], these correspond to $C_{tW} = \pm 2.0$, $C_{itW} = \pm 0.8$, and $C_{\varphi tb} = \pm 13$ and $C_{bW} = \mp 3.7$, respectively. The Protos generator was also modified with a special decay model allowing it to generate event samples with top quarks fully polarised along, or opposite to, the x', y', or z' axes as defined in Section 1.1, resulting in six simulated samples in total. These samples are used to produce templates for the determination of top-quark and top-antiquark polarisations.

Furthermore, five samples of simulated signal events with non-zero Wilson coefficients related to dimension-six effective operators were also produced. These simulation samples were generated at NLO, using the same set-up as in Ref. [29], with the MadGraph5_aMC@NLO 2.6.2 [57] generator using the NNPDF3.0nlo PDF set. The values of the non-zero Wilson coefficients in the different simulated event samples were set to: $C_{tW} = 2.0$; $C_{itW} = 1.75$; $C_{qq} = -0.4$; $C_{tW} = -2.0$ and $C_{qq} = -0.4$; and $C_{tW} = 2.0$ and $C_{itW} = -1.75$. The EFT operators were allowed to enter in the production vertex as well as the decay vertex, consistently including possible effects on the width of the top quark. The implementation of the NLO effective operators [58] makes use of the 5FS, indicating that the b-quark is treated as being massless and thus part of the proton. The two scales were set to $\mu_r = \mu_f = m_t$ in the MC generation.

The t-channel signal production cross-section was calculated at NLO [59] in perturbative QCD using Hathor 2.1 [60, 61]. For pp collisions at $\sqrt{s} = 13$ TeV, this cross-section corresponds to 136 ± 5 pb and 81 ± 4 pb for top-quark and top-antiquark production, respectively. The cross-section uncertainties connected with the PDFs and α_s were calculated using the PDF4LHC prescription [62] with the MSTW2008nlo 68% CL [63, 64], CT10nlo [65] and NNPDF2.3nlo PDF sets, and were added in quadrature to the effect of the scale uncertainty.

The production of $t\bar{t}$ events, as well as single-top-quark events in the tW process and in the s-channel, were modelled using the Powheg Box v2 generator, which provides MEs at NLO, with the NNPDF3.0nlo PDF set. In $t\bar{t}$ events, the Powheg Box h_{damp} parameter[3] was set to $1.5\,m_t$ [66]. For the $t\bar{t}$ process, the scales were set to $\mu_r^2 = \mu_f^2 = m_t^2 + p_{T,t}^2$, where $p_{T,t}$ is the p_T of the top quark, while for the tW and s-channel processes these scales were set to m_t. In the case of tW associated production, the diagram-removal scheme [67] was employed to handle the interference with $t\bar{t}$ production [66]. The $t\bar{t}$ cross-section

[3] The Powheg h_{damp} parameter controls the p_T of the first additional emission beyond the LO Feynman diagram in the PS and therefore regulates the high-p_T emission against which the $t\bar{t}$ system recoils.

was calculated at NNLO in QCD including resummation of next-to-next-to-leading logarithmic (NNLL) soft-gluon terms with Top++ 2.0 [68–73]. This cross-section is 832 ± 35 (PDF + α_s) $^{+20}_{-29}$ (scale) pb. The cross-section uncertainties due to the PDF and α_s were calculated using the PDF4LHC prescription with the MSTW2008nnlo 68% CL, CT10nnlo [74] and NNPDF2.3nnlo PDF sets, and were added in quadrature to the effect of the scale uncertainty. The tW events are normalised to the predicted production cross-section of 72 ± 4 pb calculated at NLO in QCD including NNLL soft-gluon corrections [75]. The uncertainty in the cross-section corresponds to the sum in quadrature of the uncertainty derived from the MSTW2008nnlo 90% CL PDF set and the effect of the scale uncertainties. For the s-channel process, the inclusive cross-section is corrected to the theory prediction calculated at NLO in QCD with Hathor. This cross-section is 10.3 ± 0.4 pb. The uncertainties in the cross-section due to the PDF and α_s were calculated using the PDF4LHC prescription, similarly to the t-channel.

Vector-boson production in association with jets (generally named V+jets, or W/Z+jets) was simulated with the multi-leg Sherpa 2.2.1 [76] generator. The NNPDF3.0nnlo set [51] of PDFs as well as the dedicated set of tuned PS parameters developed by the Sherpa authors for this version were used. The events were filtered according to their b-hadron and c-hadron content at the particle level. The ME+PS matching [77] was employed for different jet multiplicities, which were then merged into an inclusive sample using an improved CKKW matching procedure [78, 79] which is extended to NLO accuracy using the MEPS@NLO prescription [80]. These particular simulations are accurate to NLO for up to two additional partons and accurate to LO for up to four additional partons. The virtual QCD corrections for MEs at NLO accuracy are provided by the OpenLoops library [81, 82]. Fully leptonically and semileptonically decaying diboson (VV) samples were simulated with the Sherpa 2.2.1 ME+PS generator. The ME+PS matching is the same as for the single-boson processes. These particular simulations are accurate to NLO for up to one additional parton and accurate to LO for up to three additional parton emissions using factorised on-shell decays. The inclusive cross-sections for V+jets production were calculated to NNLO accuracy [83] with FEWZ program [84]. For W+jets production, the overall theoretical uncertainty is 34%. This is the result of adding in quadrature the overall cross-section normalisation uncertainty and 24% per additional jet, according to the Berends–Giele scaling [85].

The production of $t\bar{t}Z$, $t\bar{t}W$, tZq, tHq, and tWZ events was modelled by the MadGraph5_aMC@NLO 2.3.3 generator, which provides MEs at NLO in α_s, with the NNPDF3.0nlo PDF set. The production of $t\bar{t}H$ events was modelled using the Powheg Box generator at NLO with the NNPDF3.0nlo PDF set.

All the signal and background processes involving one or more top quarks were simulated assuming a top-quark mass of 172.5 GeV, and the top quark was assumed to decay only into a W boson and a b-quark. In these samples, top quarks and W and Z bosons were decayed at LO using MadSpin [86, 87] to preserve all spin correlations. Moreover, the PS, hadronisation and underlying-event (UE) modelling was simulated with Pythia 8.230 or 8.212, using the A14 set of tuned parameters (A14 tune) [88] and the NNPDF2.3lo PDF set. The decays of bottom and charm hadrons were simulated using the EvtGen 1.6.0 or 1.2.0 program [89].

Alternative samples of simulated single-top-quark and $t\bar{t}$ events were also produced, using either different generators or different values of parameters in Powheg+Pythia8 (further details are given in Section 8) to estimate the generator modelling uncertainties. For studies of the NLO matching method, MadGraph5_aMC@NLO 2.6.2 or 2.6.0 using either the NNPDF3.0nlo nf4 PDF set for the t-channel process or the NNPDF3.0nlo PDF set for the $t\bar{t}$, tW and s-channel processes, was used. In these cases, the ME generator was interfaced to Pythia 8.230 or 8.212. To study the PS, the hadronisation and the UE modelling, the Powheg Box v2 generator interfaced to Herwig 7.04 [90, 91] using the H7UE set of tuned parameters [91] and the MMHT2014lo PDF set [92] was used. In the case of tW associated production, a

simulated event sample using the diagram-subtraction scheme [67] is employed to estimate the uncertainty associated with the scheme used to handle the interference with $t\bar{t}$ production.

Dijet events were simulated using Pythia 8.186 with the A14 tune and the NNPDF2.3nlo PDF set, and the decays of bottom and charm hadrons were simulated using the EvtGen 1.2.0 program. Here, $2 \to 2$ QCD processes were generated, including multijet, $qg \to q\gamma$, $q\bar{q} \to g\gamma$, EW (W/Z) and $t\bar{t}$ production processes. This simulated sample was filtered at generator level to enrich the event sample with jets that are likely to resemble electrons with detector signatures. Events were kept if particles in the event (excluding neutrinos and muons) deposit >17 GeV of energy into a square area $\eta \times \phi = 0.1 \times 0.1$ of the electromagnetic calorimeter, mimicking the highly localised energy deposits characteristic of electrons.

All baseline simulated event samples were passed through the full simulation of the ATLAS detector [93] based on the Geant4 [94] framework. Simulated samples of fully polarised single top quarks and top antiquarks, used to estimate the impact of anomalous couplings or EFT on the differential measurements, and samples used to evaluate most of the systematic effects were processed with a fast simulation [93] which relies on a parameterisation of the calorimeter response [95].

An extensive software suite [96] is used in the reconstruction and analysis of real and simulated data, in detector operations, and in the trigger and data acquisition systems of the experiment.

3 Object definitions

Electron candidates are reconstructed from clusters of energy deposits in the electromagnetic calorimeter that are matched to a track in the inner-detector tracking system. They are required to satisfy $p_{\mathrm{T}} > 7$ GeV, $|\eta_{\mathrm{cluster}}| < 2.47$ and a 'tight' likelihood-based identification requirement [97]. Electron candidates are excluded if their calorimeter clusters lie within the transition region between the barrel and endcap sections of the electromagnetic calorimeter, $1.37 < |\eta_{\mathrm{cluster}}| < 1.52$. The track associated with the electron must pass the requirements $|z_0 \sin\theta| < 0.5$ mm and $|d_0/\sigma(d_0)| < 5$, where z_0 is the longitudinal impact parameter with respect to the reconstructed primary vertex, d_0 denotes the transverse impact parameter relative to the beam-line axis and $\sigma(d_0)$ is the uncertainty in d_0.

Muon candidates are reconstructed from tracks measured in the muon spectrometer matched to tracks measured in the inner-detector tracker in the pseudorapidity range of $|\eta| < 2.5$. They must satisfy $p_{\mathrm{T}} > 7$ GeV along with the 'medium' identification requirements defined in Ref. [98]. These include requirements on the number of hits in the different inner-detector and muon spectrometer subsystems and on the significance of the charge-to-momentum ratio q/p. In addition, the track associated with the muon candidate must have $|z_0 \sin\theta| < 0.5$ mm and $|d_0/\sigma(d_0)| < 3$.

Isolation criteria are applied to the selected electrons and muons. For electrons, the scalar sum of the p_{T} of tracks within a variable-size cone around the electron, excluding tracks originating from the electron itself, must be less than 6% of the electron p_{T}. The track isolation cone size $\Delta R = \sqrt{(\Delta\eta)^2 + (\Delta\phi)^2}$ is given by the smaller of $\Delta R = 10\,\mathrm{GeV}/p_{\mathrm{T}}$ and $\Delta R = 0.2$. In addition, the sum of the transverse energy of the calorimeter topo-clusters in a cone of $\Delta R = 0.2$ around the electron is required to be less than 6% of the electron p_{T}, excluding clusters originating from the electron itself. For muons, the scalar sum of the p_{T} of tracks within a variable-size cone around the muon (excluding its own track) must be less than 6% of the muon p_{T}, with the track isolation cone size being given by the smaller of $\Delta R = 10\,\mathrm{GeV}/p_{\mathrm{T}}$ and $\Delta R = 0.3$.

Jets are reconstructed from topological clusters of energy deposited in the calorimeter [99] using the anti-k_t algorithm with a radius parameter of 0.4. They are calibrated through the application of a jet energy scale derived from data and simulation [100]. These jets are required to have $p_{\mathrm{T}} > 30\,\mathrm{GeV}$ and $|\eta| < 4.5$. To suppress jets from additional pp interactions within a bunch crossing, the so-called jet-vertex tagger (JVT) [101] is applied to jets with $p_{\mathrm{T}} < 120\,\mathrm{GeV}$ and $|\eta| < 2.5$. Jets containing b-hadrons (named b-tagged jets) are identified (tagged) by the MV2c10 b-tagging algorithm [102, 103]. The algorithm calculates a multivariate discriminant from information about the impact parameters of associated charged-particle tracks, the properties of reconstructed secondary vertices, and the topology of b- and c-hadron decays inside the jets. The b-tagging efficiency is measured for jets in the pseudorapidity range $|\eta| < 2.5$ and with $p_{\mathrm{T}} > 20\,\mathrm{GeV}$ in simulated $t\bar{t}$ events. The chosen working point for this analysis corresponds to a b-tagging efficiency of 60% [104]. The corresponding mistagging rates for c-quark and light-flavour jets are approximately 2.9% and 0.065%, respectively, as predicted in simulated $t\bar{t}$ events and calibrated in data [105, 106].

The missing transverse momentum in the event, whose magnitude is denoted in the following by $E_{\mathrm{T}}^{\mathrm{miss}}$, is defined as the negative vector sum of the p_{T} of the reconstructed and calibrated objects in the event [107, 108]. This sum also includes a 'soft term' consisting of the transverse momenta of inner-detector tracks that are associated with the primary vertex but not with any other objects.

Objects can satisfy both the jet and lepton selection criteria and therefore a procedure called 'overlap removal' is applied to ensure that objects are matched to a unique hypothesis. If any electron shares a track with a muon, the electron is removed since it is very likely to correspond to the reconstructed muon. Similarly, if any jet is close to an electron (within $\Delta R < 0.2$), the closest jet is removed. Electrons close to jets (within $\Delta R < 0.4$) are also removed to reduce the impact of non-prompt leptons. To reduce contributions from muons which stem from heavy-flavour decays inside a jet, muons are removed if they are separated from the nearest jet by $\Delta R < 0.4$. Additionally, jets with fewer than three tracks and separated from a muon by $\Delta R < 0.4$ are removed to reduce the number of fake jets from muons depositing a large fraction of their energy in the calorimeters.

4 Event selection in the signal and control regions

Events are required to have at least one vertex reconstructed from at least two inner-detector tracks with transverse momenta of $p_{\mathrm{T}} > 0.5\,\mathrm{GeV}$. The primary vertex for each event is defined as the vertex with the highest sum of p_{T}^2 over all associated inner-detector tracks [109]. The analysis considers only W-boson decay modes to an electron or a muon. Events in which the W boson decays to a τ-lepton are thus included if the τ-lepton subsequently decays to an electron or a muon. The signal event candidates are selected by requiring a single isolated lepton, significant $E_{\mathrm{T}}^{\mathrm{miss}}$ and exactly two jets. Each muon (electron) is required to have $p_{\mathrm{T}} > 30\,\mathrm{GeV}$ and $|\eta| < 2.5$ ($|\eta| < 2.47$, excluding the region $1.37 < |\eta| < 1.52$), and to satisfy the identification and isolation criteria discussed in Section 3. To remove background events from $t\bar{t}$, Z + jets and diboson production, the event is vetoed if an additional 'loose' lepton candidate with $p_{\mathrm{T}} > 10\,\mathrm{GeV}$ is found when applying less stringent lepton identification criteria and no isolation requirements [97, 110, 111]. The value of $E_{\mathrm{T}}^{\mathrm{miss}}$ is required to be larger than 35 GeV. Jets in the endcap–forward transition region of the calorimeters, $2.75 < |\eta| < 3.5$, are required to satisfy the more stringent requirement $p_{\mathrm{T}} > 35\,\mathrm{GeV}$. Exactly one of the jets is required to be b-tagged and have $|\eta| < 2.5$. The other, non-b-tagged, jet is referred to as the 'spectator jet'.

Two additional multijet background rejection criteria are applied. The transverse mass of the lepton–$E_{\mathrm{T}}^{\mathrm{miss}}$ system,

$$m_{\mathrm{T}}(\ell, E_{\mathrm{T}}^{\mathrm{miss}}) = \sqrt{2 p_{\mathrm{T}}(\ell) E_{\mathrm{T}}^{\mathrm{miss}} \left(1 - \cos \Delta\phi(p_{\mathrm{T}}(\ell), E_{\mathrm{T}}^{\mathrm{miss}})\right)},$$

is required to be larger than 60 GeV, and $\Delta\phi(p_{\mathrm{T}}(\ell), E_{\mathrm{T}}^{\mathrm{miss}})$ is the azimuthal angle between the lepton momentum and the $E_{\mathrm{T}}^{\mathrm{miss}}$ direction. Further reduction of this background is achieved by imposing an additional requirement on events where the lepton and the leading jet in p_{T} have opposite directions in the transverse plane,

$$p_{\mathrm{T}}(\ell) > 50 \left(1 - \frac{\pi - |\Delta\phi(p_{\mathrm{T}}(j_1), p_{\mathrm{T}}(\ell))|}{\pi - 1}\right) \text{GeV}, \tag{1}$$

where $\Delta\phi(p_{\mathrm{T}}(j_1), p_{\mathrm{T}}(\ell))$ is the azimuthal angle between the lepton p_{T} and the leading jet in p_{T}. This requirement provides significant rejection of background originating from multijet events where two jets are produced back-to-back in the azimuthal plane and one of those is misreconstructed as a lepton. This set of requirements defines the preselection region.

The on-shell W boson originating from the decay of the top quark is reconstructed from the momenta of the lepton and the neutrino by imposing four-momentum conservation. Since the neutrino escapes undetected, the x and y components of the reconstructed $E_{\mathrm{T}}^{\mathrm{miss}}$ are assumed to correspond to the p_{T} of the neutrino. The unmeasured longitudinal component of the neutrino momentum, p_z^{ν}, is computed by imposing a W-boson mass constraint on the lepton–neutrino system. A quadratic expression is found for p_z^{ν}, and the solution closer to zero is taken. If the solutions are complex, the reconstructed $E_{\mathrm{T}}^{\mathrm{miss}}$ is rescaled, preserving its direction, in order to have a unique real solution for p_z^{ν}. The top-quark candidate is then reconstructed by combining the four-momenta of the reconstructed W boson and the selected b-tagged jet. Finally, the lepton momentum is boosted into the top-quark rest frame and the angles $\theta_{\ell i}$ ($i = x', y', z'$) are derived by its projection along the axes defined in Section 1.1. In doing so, the ambiguity in the direction of the incoming light quark in the laboratory frame is resolved by accepting the direction which is closer to that of the spectator quark, also in the laboratory frame.

Further discrimination between t-channel signal events and background events is achieved by applying additional criteria that optimise the signal-to-background ratio (S/B), and thereby determine the signal region. Thus, the following criteria are applied:

- The invariant mass of the lepton–b-tagged jet system, $m_{\ell b}$, is required to be lower than 153 GeV.
- The mass of the reconstructed top quark, $m_{\ell\nu b}$, is required to be within 120.6–234.6 GeV.
- The mass of the spectator-jet–top-quark system, $m_{j\ell\nu b}$, is required to be larger than 320 GeV.
- A trapezoidal requirement is imposed in order to reject background events from the two-dimensional correlation among the pseudorapidities of the spectator jet, η_j, and the reconstructed top quark, $\eta_{\ell\nu b}$. This requirement is:

$$\begin{aligned} \eta_j &< (4\,\eta_{\ell\nu b} + a) && \& \\ \eta_j &> (4\,\eta_{\ell\nu b} - a) && \& \\ (\eta_j &> (0.44\,\eta_{\ell\nu b} + b) && \text{OR} \\ \eta_j &< (0.44\,\eta_{\ell\nu b} - b))\,, \end{aligned} \tag{2}$$

where the intercept parameters a and b of the lines defining the trapezoid were optimised to be 10 and 2, respectively.

- The scalar sum of the p_{T} of all final-state objects, H_{T}, must be larger than 190 GeV, since the H_{T} distributions of the backgrounds peak at lower values than the t-channel signature.

Additionally, two specific background-enriched control regions, orthogonal to the signal region, are defined in order to estimate the contributions of the most important background processes in the t-channel signal region, coming from $t\bar{t}$ and W+jets events, by computing scale factors for the overall normalisations. These two specific background-enriched regions are:

- A control region enriched in $t\bar{t}$ events is defined by applying all the preselection requirements, except for the requirement of exactly one b-tagged jet; instead, exactly two b-tagged jets are required.
- A control region enriched in W+jets events is defined by selecting events satisfying the preselection requirements and at least one of the reversed requisites for $m_{\ell b}$, $m_{\ell\nu b}$, $m_{j\ell\nu b}$ or trapezoidal requirement, all from the selection criteria. This control region has a W+jets flavour composition similar to that in the signal region (in terms of W+light-jets and W+heavy-jets contributions).

Table 1 summarises the selection criteria defining the preselection, the signal region and the two control regions used in this analysis. For the separate measurements of top-quark and top-antiquark events, the selected events in each region are further divided into two different regions according to the lepton charge.

Common event selection criteria			
Exactly one electron or muon Veto secondary low-p_{T} charged loose leptons Exactly two jets $E_{\mathrm{T}}^{\mathrm{miss}} > 35$ GeV $m_{\mathrm{T}}(\ell, E_{\mathrm{T}}^{\mathrm{miss}}) > 60$ GeV $p_{\mathrm{T}}(\ell) > 50\left(1 - \frac{\pi - \lvert\Delta\phi(p_{\mathrm{T}}(j_1), p_{\mathrm{T}}(\ell))\rvert}{\pi - 1}\right)$ GeV			
Preselection region	Signal region	$t\bar{t}$ control region	W+jets control region
Exactly one b-tagged jet	Exactly one b-tagged jet $m_{\ell b} < 153$ GeV $m_{j\ell\nu b} > 320$ GeV Trapezoidal requirement $H_{\mathrm{T}} > 190$ GeV	Exactly two b-tagged jet	Exactly one b-tagged jet $m_{\ell b} > 153$ GeV $m_{j\ell\nu b} < 320$ GeV Veto trapezoidal requirement $H_{\mathrm{T}} < 190$ GeV

Table 1: Summary of the selection criteria defining the preselection, the signal region and the two control regions.

5 Particle-level object definition and fiducial region selection

In order to reduce the dependency on phenomenological models which describe colour reconnection, initial- and final-state radiation, and fragmentation, the measured differential angular distributions are unfolded to particle level.

5.1 Particle-level objects

The definitions of the particle-level objects are the same as the ones detailed in Ref. [112]. They are constructed from stable particles in the MC event record with a lifetime larger than 30 ps, within the observable pseudorapidity range.

Particle-level leptons are defined as electrons, muons or neutrinos that do not originate from hadron decays, either directly or via a τ-lepton decay. Thus, leptons from either a W- or Z-boson decay are considered, including those emerging from a subsequent τ-lepton decay. In t-channel single-top-quark events, exactly one such electron or muon is present. No isolation requirement is imposed on the selected charged lepton and the calculation of its four-momentum includes photons within a surrounding cone of size $\Delta R = 0.1$. The $E_{\mathrm{T}}^{\mathrm{miss}}$ is calculated from the vector sum of all the selected neutrinos.

Particle-level jets are reconstructed using the anti-k_t algorithm with a radius parameter of 0.4. All stable particles are used to reconstruct the jets, excluding electrons, muons, neutrinos, and photons used in the definition of the selected charged leptons. A particle-level jet is identified as a b-tagged jet if the jet is within $|\eta| < 2.5$ and an associated b-hadron is found with a ghost-matching technique [113]; the hadron must have $p_{\mathrm{T}} > 5\,\mathrm{GeV}$. All particle-level charged leptons identified within a cone of size $\Delta R = 0.4$ around a selected particle-level jet are removed.

5.2 Fiducial region definition

The differential angular distributions are unfolded to particle level in a fiducial region. This fiducial region is defined so as to be close to the measured phase space, using the particle-level objects defined in Section 3. Exactly one particle-level electron or muon with $p_{\mathrm{T}} > 30\,\mathrm{GeV}$ and $|\eta| < 2.5$ (excluding the region $1.37 < |\eta| < 1.52$ for the case of electrons) is required. There must be two particle-level jets with $p_{\mathrm{T}} > 30\,\mathrm{GeV}$; exactly one of these jets must be identified as a b-tagged jet with $|\eta| < 2.5$ while the other jet must satisfy $|\eta| < 4.5$. The particle-level $E_{\mathrm{T}}^{\mathrm{miss}}$ is required to be larger than 35 GeV. The two additional multijet background rejection criteria, i.e. $m_{\mathrm{T}}(\ell, E_{\mathrm{T}}^{\mathrm{miss}})$ larger than 60 GeV and the requirement in Eq. (1), and the remaining signal region requirements are also applied to the particle-level objects. The signal region criteria require the reconstruction of the top quark. In this case, a top-quark proxy, called a pseudo top quark [112], is defined by using the particle-level objects and following exactly the same method described in Section 4.

Table 2 summarises the signal selection criteria, applied to particle-level objects, for defining the fiducial region used in this analysis.

6 Background estimation

The largest background contributions to the fiducial region arise from $t\bar{t}$ and W+jets production. The former is difficult to distinguish from the t-channel single-top-quark signal since $t\bar{t}$ events contain real top quarks in the final state. The W+jets production process contributes to the background if there is a b-quark in the final state or if a c-jet or light-flavour jet is mistagged. Other minor backgrounds originate from tW, s-channel single-top-quark, Z+jets, diboson, $t\bar{t}Z$, $t\bar{t}W$, tZq, tHq, and tWZ production. Multijet events produced via the strong interaction can also contribute if, in addition to having two reconstructed jets, an extra jet is misidentified as an isolated lepton, or if a non-prompt lepton appears to be isolated.

Fiducial region
Exactly one electron or muon
Exactly two jets
Exactly one b-tagged jet
$E_{\mathrm{T}}^{\mathrm{miss}} > 35\,\mathrm{GeV}$
$m_{\mathrm{T}}(\ell, E_{\mathrm{T}}^{\mathrm{miss}}) > 60\,\mathrm{GeV}$
$p_{\mathrm{T}}(\ell) > 50\left(1 - \frac{\pi - \lvert\Delta\phi(p_{\mathrm{T}}(j_1), p_{\mathrm{T}}(\ell))\rvert}{\pi - 1}\right)\,\mathrm{GeV}$
$m_{\ell b} < 153\,\mathrm{GeV}$
$m_{\ell\nu b} \in [120.6, 234.6]\,\mathrm{GeV}$
$m_{j\ell\nu b} > 320\,\mathrm{GeV}$
Trapezoidal requirement
$H_{\mathrm{T}} > 190\,\mathrm{GeV}$

Table 2: Summary of the signal selection criteria, applied to particle-level objects, for defining the fiducial region.

For all processes except multijet production, the normalisations are initially estimated by using the simulated samples scaled to the theoretical cross-section predictions for pp collisions at $\sqrt{s} = 13\,\mathrm{TeV}$, discussed in Section 2. In the template fit and in the measurement of the angular differential cross-sections, described in Section 9 and Section 10, respectively, the MC predicted yields for the two major background processes ($t\bar{t}$ and W+jets) are normalised to the numbers of data events using the dedicated control regions defined in Section 4. The shape of the event distributions is taken from simulation.

The prediction for the normalisation and shape of any multijet distribution is obtained by using the purely data-driven anti-muon model for events containing a muon, and the mixed data–simulation jet-electron model for events containing an electron [114, 115]. In these methods, event distribution templates are derived from data (for the anti-muon method) or from dijet simulation (for the jet-electron method). For the jet-lepton model, a dedicated selection is imposed on the MC simulated dijet events, in order to enrich the sample with jets that are likely to resemble a lepton in the detector. The jet candidates are treated as a lepton henceforth. The anti-muon model imposes a dedicated selection on data to enrich the sample with events that contain fake muons. The templates are then used in a binned maximum-likelihood fit to the $E_{\mathrm{T}}^{\mathrm{miss}}$ distribution in the electron channel, or to the $m_{\mathrm{T}}(\ell, E_{\mathrm{T}}^{\mathrm{miss}})$ distribution in the muon channel, in multijet-enriched regions to extract the multijet normalisation. These two multijet-enriched regions are defined as the preselection region and the $t\bar{t}$ control region without applying the isolation requirement on the lepton p_{T} and without applying the $E_{\mathrm{T}}^{\mathrm{miss}}$ requirement for the electron channel and the $m_{\mathrm{T}}(\ell, E_{\mathrm{T}}^{\mathrm{miss}})$ requirement for the muon channel.

7 Signal and background event yields

Table 3 provides the predicted signal and background event yields for the combined electron and muon channels in the preselection, signal and control regions. The multijet background is normalised as explained in Section 6. Observed data yields are also shown. In addition, the S/B ratio and the ratio of the observed number to the expected number of events (Data/Prediction) are shown for each region.

Process	Preselection region	Signal region	$t\bar{t}$ control region	W+ jets control region
t-channel	219 000 ± 11 000	70 600 ± 3500	13 480 ± 680	148 200 ± 7400
$t\bar{t}$, tW, s-channel	736 000 ± 39 000	43 200 ± 2400	147 800 ± 8400	693 000 ± 37 000
W+ jets	590 000 ± 200 000	26 200 ± 8900	16 100 ± 5500	560 000 ± 190 000
Z + jets, diboson	52 900 ± 5100	2120 ± 350	2620 ± 360	50 800 ± 4900
Others	494 ± 38	30 ± 4	79 ± 6	464 ± 36
Multijet	52 000 ± 10 000	3500 ± 640	5500 ± 1800	48 500 ± 9400
Total expected	1 650 000 ± 210 000	145 600 ± 9900	186 000 ± 10 000	1 510 000 ± 200 000
Data	1 750 918	154 361	188 326	1 596 557
S/B	0.15 ± 0.02	0.94 ± 0.13	0.08 ± 0.01	0.11 ± 0.02
Data/Prediction	1.06 ± 0.13	1.06 ± 0.07	1.02 ± 0.06	1.06 ± 0.14

Table 3: Pre-fit event yields in the preselection and signal regions and in the $t\bar{t}$ and W+ jets control regions for the combined electron and muon channels. The predictions are derived from simulated event samples normalised to the theoretical cross-sections. For multijet production the normalisation is estimated using a data-driven likelihood fit. The label 'Others' represents $t\bar{t}Z$, $t\bar{t}W$, tZq, tHq, and tWZ production. The data-driven scale factors obtained for the top-quark and W+ jets background processes are not considered when computing these event yields. The uncertainties shown account for systematic effects and the uncertainty due to limited MC sample size. The expected S/B ratio and the ratio of the observed number to the expected number of events are also given.

8 Sources of systematic uncertainty

Various sources of systematic uncertainty affect the signal and background rates and the shape of the kinematic and angular distributions.

In the following, the procedures used to evaluate the systematic uncertainties are described. The systematic uncertainties are grouped into two main categories: experimental uncertainties and theoretical modelling uncertainties. The effect due to the limited size of the simulated event samples is also taken into account when evaluating the total uncertainty.

Experimental uncertainties: The uncertainty in the combined 2015–2018 integrated luminosity is 1.7% [39], obtained using the LUCID-2 detector [40] for the primary luminosity measurements. To account for the difference between the pile-up distributions in data and MC simulations, an uncertainty related to the scale factors used to adjust the MC pile-up to the data pile-up profile is applied.

For electrons and muons, the reconstruction, identification, isolation, and trigger performance can differ slightly between data and MC simulation. Scale factors are applied to simulated events to correct for these differences. These scale factors, estimated using the tag-and-probe method [97, 98], as well as the lepton momentum scale and resolution, are assessed using leptonic decays of Z bosons and J/ψ mesons. Corrections to the lepton momentum scale and resolution are applied to data. The associated systematic uncertainties are then propagated to the distributions used in this analysis.

To determine the jet energy scale (JES) uncertainty, information from test-beam data, LHC collision data, and simulation was used, as described in Ref. [100]. The JES uncertainty is decomposed into a set of 29 uncorrelated components, with contributions from pile-up, jet flavour composition, single-particle response, and effects of jets not contained within the calorimeter. The jet energy resolution (JER) is measured separately for data and MC simulation, using in situ techniques [100]. The measured relative JER ranges from 22% at 30 GeV to 6% at 300 GeV. Its uncertainty is represented by eight components accounting for jet-p_{T} and η-dependent differences between simulation and data. In the measurement of the three components of the polarisation vector, an additional uncertainty is considered in order to take into

account the kinematic and sample dependence of the JER uncertainty model. Further details are given in Section 9. The systematic uncertainty associated with the JVT is obtained by increasing and decreasing the scale factor used to correct the JVT efficiency in simulation within its uncertainties [101].

The b-tagging efficiency and mistagging rates are measured in data using the methods as described in Refs. [103, 105, 106], with the systematic uncertainties due to the b-tagging efficiency and the mistagging rates calculated separately. The impact of the uncertainties on the b-tagging calibration is evaluated separately for b-jets, c-jets and light-flavour jets.

The systematic uncertainties related to the modelling of the $E_{\mathrm{T}}^{\mathrm{miss}}$ in the simulation are estimated by propagating the uncertainties in the energy and momentum scales of electrons, muons and jets, as well as the uncertainties in the resolution and scale of the soft term [107].

Theoretical modelling uncertainties: Systematic uncertainties associated with the signal and background MC modelling are estimated by comparing event samples from different generators and by varying parameter values in the event generation.

To assess the uncertainty due to the choice of matching scheme in the t-channel single-top-quark signal and single-top-quark background ME generation, samples from the nominal MC generator Powheg Box are compared with those from MadGraph5_aMC@NLO, both interfaced to Pythia 8.

The uncertainty in the PS is estimated for all top-quark processes by comparing samples from Powheg Box interfaced to Pythia 8 with samples from Powheg Box interfaced to Herwig 7.

The uncertainty due to missing higher-order QCD corrections in the ME computation is estimated for all top-quark processes by independently varying the renormalisation and factorisation scales by factors of 0.5 and 2.0 from their central value. Additionally, uncertainties due to initial-state radiation from the PS are assessed by varying the corresponding parameter of the A14 parton shower tune `Var3c` [88]. For the $t\bar{t}$ process and just in the case of the upward variation, the h_{damp} parameter is also changed and set to $3\,m_t$ [116]. The uncertainties due to final-state radiation from the PS are assessed by varying the corresponding parameter of the A14 parton shower tune `Var2` [88] and by varying the renormalisation scale for QCD emission by factors of 0.5 and 2.0.

An additional uncertainty arising from the method used to handle the interference between tW and $t\bar{t}$ production is determined by comparing the tW simulated sample that uses the diagram-subtraction method with the nominal one based on the diagram-removal technique.

In the template fit, described in Section 9, an additional uncertainty due to t-channel modelling arises from the use of a LO generator (i.e. Protos) for the construction of templates in the signal region as detailed in Section 9, a choice which was motivated by the possibility of varying the polarisation in a straightforward way. This is determined by comparing the LO Protos prediction with the NLO Powheg Box prediction.

PDF uncertainties are evaluated using the PDF4LHC15 uncertainty set which consists of 30 eigenvector variations from multiple NLO PDF sets [62].

The event yields associated with the simulated signal and background processes are estimated using the selection acceptances and the theoretically predicted cross-sections as reported in Section 2. The uncertainties in these cross-sections are taken into account. However, for those processes whose normalisation is extracted from the data-driven fits, described in Sections 9 and 10, the effect is negligible. The multijet background is normalised through a data-driven analysis based on the techniques described in Section 6. A relative systematic uncertainty of 20% (40%) is assigned to this data-driven overall normalisation in the signal and W+jets-dominated ($t\bar{t}$-dominated) regions. It is estimated from fits, as

described in Section 6, using alternative kinematic variables (H_{T} and $\Delta\phi(p_{\mathrm{T}}(j_1), p_{\mathrm{T}}(\ell))$ in the electron channel and $\Delta\phi(p_{\mathrm{T}}(\ell), E_{\mathrm{T}}^{\mathrm{miss}})$ in the muon channel) and including modelling uncertainties for the main background processes.

To evaluate the impact of the systematic uncertainty in the shape of the W+jets simulated templates, an upward and downward variation of 30% is applied independently to the $W+b$-jets and $W+c$-jets samples [117]. No variation is considered for W+light-flavour jets production since its contribution is negligible. To evaluate the systematic uncertainty in the shape of the multijet templates, additional MC simulation and data-driven samples were produced, varying the fraction of the jet's energy that is deposited in the EM calorimeter (jet-electron model) and the ratio of the sum of the transverse momenta of tracks within a cone of maximum size $\Delta R = 0.4$ to the p_{T} of the muon (anti-muon model). These alternative multijet templates are normalised to the nominal yields and compared with the nominal multijet templates.

Statistical uncertainties: Statistical fluctuations in the MC simulated event samples contribute to the overall systematic uncertainty. These uncertainties arise from the finite number of simulated background and signal events. This uncertainty is discussed further in Sections 9 and 10.

9 Measurement of top-quark and top-antiquark polarisation vectors

The method used to measure the polarisation vector of an ensemble of top quarks or antiquarks that pass the event selection is discussed in this section. The unit vector of the reconstructed lepton momentum in the top-(anti)quark reference frame is first determined in the coordinate system described in Section 1.1. The variable Q (also called the *octant variable*) is constructed by slicing the tridimensional phase space into eight octants, in terms of the signs of three variables $\cos\theta_{\ell x'}$, $\cos\theta_{\ell y'}$, $\cos\theta_{\ell z'}$ of this unit vector as illustrated in Figure 3. An analysis of the coursely-binned fully differential top-quark decay distribution described in Ref. [23] is afforded by the variable Q. Mathematically, it is assigned a value zero through seven according to the equation $Q = 4 \cdot \Theta(\cos\theta_{\ell z'}) + 2 \cdot \Theta(\cos\theta_{\ell x'}) + \Theta(\cos\theta_{\ell y'})$ where $\Theta(\xi)$ is the Heaviside, or unit, step function of the variable ξ. The signal region is further divided by lepton charge for a total of 16 bins indexed by $Q_+ = 0, ..., 7$ for bins of positive lepton charge and $Q_- = 0, ..., 7$ for bins of negative lepton charge. Four bins of control data consisting of events with positive and negative leptons in the W+jets and the $t\bar{t}$ control regions, as described in Section 4, are also considered. These bins, related to the background control region, are indexed by $\mathcal{R}_\pm \in \{W\text{+jets}, t\bar{t}\}$ where the sign corresponds to the sign of the charged lepton's charge. This allows better control of these important backgrounds in the t-channel signal region. The event count in these 20 bins constitutes the twenty-bin input data distribution to a binned profile-likelihood fit which is designed to extract the polarisation vector of the top-quark and top-antiquark event sample.

A parameterised fitting function is constructed to describe the distribution in the variable $Q_\pm$ of the input data. Adjustable parameters of the function include $\vec{P} = \{P_{x'}, P_{y'}, P_{z'}\}$, separately for top quarks and top antiquarks (i.e. six parameters in total). Nuisance parameters (NPs) include the overall normalisation factors β_k for the production of the process $k \in (t\text{-channel}, t\bar{t}, W\text{+jets})$, as well as other NPs, collectively denoted by $\vec{\theta}$, corresponding to the systematic uncertainties described in Section 8. The fitting function in the variable $Q_\pm$ is determined by the projection of the joint probability density of the four-dimensional fully differential angular decay distribution for the top-(anti)quark decays [23] onto the octant variable $Q_\pm$. It is obtained from templates derived from histograms of quantities in events produced using a LO generator (i.e. Protos). These templates $\mathcal{T}_i(Q_\pm)$, with $i \in \{z'_+, z'_-, x', y'\}$, are produced using samples of

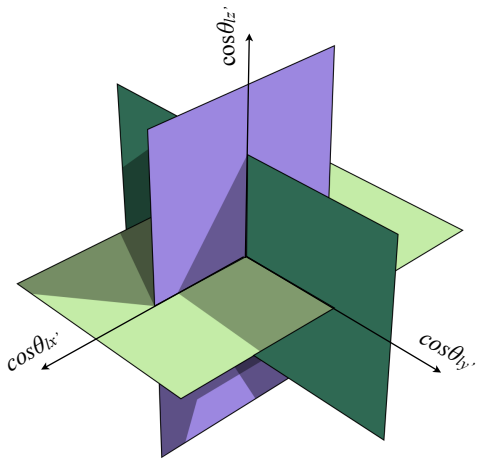

Figure 3: Representation of the octant variable Q constructed by slicing the tridimensional phase space into eight octants, according to the signs of the three variables $\cos\theta_{\ell x'}$, $\cos\theta_{\ell y'}$, $\cos\theta_{\ell z'}$.

fully simulated events in which the polarisation of the top (anti)quarks is manipulated to lie fully along the positive or negative x', y', or z' directions. The events are subjected to the same reconstruction procedures and event selection as the data.

The fitting function $\mu\left(Q_{\pm}\right)$ for the data is built from these templates plus an additional contribution from background events, also estimated from reconstructed quantities. It describes the expected number of signal events falling within a bin $Q_{\pm}$ and is written as

$$\mu\left(Q_{\pm};\vec{P},\vec{\beta},\vec{\theta}\right) = \beta_{t\text{-channel}}\cdot\left\{\frac{1+P_{z'}}{2}\mathcal{T}_{z'_{+}}\left(Q_{\pm}\right)+\frac{1-P_{z'}}{2}\mathcal{T}_{z'_{-}}\left(Q_{\pm}\right)+\frac{P_{x'}}{2}\mathcal{T}_{x'}\left(Q_{\pm}\right)+\frac{P_{y'}}{2}\mathcal{T}_{y'}\left(Q_{\pm}\right)\right\}+\mathcal{T}_{\text{bkg}}\left(Q_{\pm};\beta_{W+\text{jets}},\beta_{t\bar{t}}\right).$$

Here, $\mathcal{T}_{\text{bkg}}\left(Q_{\pm};\beta_{W+\text{jets}},\beta_{t\bar{t}}\right)$ is the template for the background, consisting of a sum over all sources of background. Likewise, the number of events in each of the four bins of control data is described by the function $\nu(\mathcal{R}_{\pm};\vec{\beta},\vec{\theta})$, also derived either from simulation or data-driven methods.

The fitting function is used to construct a likelihood function

$$\begin{aligned}\mathcal{L}\left(\vec{\mathcal{P}},\vec{\beta},\vec{\theta}\right) &= \prod_{Q_{+}=0}^{7}\mathcal{P}\left(N_{Q_{+}};\mu\left(Q_{+};\vec{P},\vec{\beta},\vec{\theta}\right)\right)\prod_{Q_{-}=0}^{7}\mathcal{P}\left(N_{Q_{-}};\mu\left(Q_{-};\vec{P},\vec{\beta},\vec{\theta}\right)\right)\\ &\times \prod_{\mathcal{R}_{+}\in\left\{W+\text{jets},t\bar{t}\right\}}\mathcal{P}\left(N_{\mathcal{R}_{+}};\nu\left(\mathcal{R}_{+};\vec{\beta},\vec{\theta}\right)\right)\prod_{\mathcal{R}_{-}\in\left\{W+\text{jets},t\bar{t}\right\}}\mathcal{P}\left(N_{\mathcal{R}_{-}};\nu\left(\mathcal{R}_{-};\vec{\beta},\vec{\theta}\right)\right)\\ &\times \prod_{l}\mathcal{G}(\theta_{l};0,1)\,,\end{aligned}$$

in which the first line refers to the octants, the second line refers to the control regions, and the third line refers to Gaussian constraints on the NPs $\vec{\theta}$, where $\mathcal{P}\left(N;\lambda\right)$ indicates a Poisson distribution for N events given expectation λ, and where $\mathcal{G}\left(m;m_0,\sigma\right)$ indicates a normal distribution in the variable m with mean m_0 and standard deviation σ. The full likelihood including all NPs is maximised to extract the six components of $\vec{P}^{t}=\{P^{t}_{x'},P^{t}_{y'},P^{t}_{z'}\}$ and $\vec{P}^{\bar{t}}=\{P^{\bar{t}}_{x'},P^{\bar{t}}_{y'},P^{\bar{t}}_{z'}\}$ for top quarks and antiquarks, respectively.

Nuisance parameters accounting for systematic uncertainties are not considered in the fit if they have an impact on either normalisation or shape which is below 0.5%.

The angular distributions studied in this paper are sensitive to the JER. The corrections and uncertainties in jet energy are p_{T} and η dependent and were determined with in situ techniques using dijet events. Poorer JER was observed in simulated single-top-quark t-channel events than in simulated dijet events. This increase in JER value, which may be attributed to different event kinematics, is also observed in the template fit.

In order to account for the difference, two JER uncertainty models are compared. The nominal fit model is used to obtain the central values for the polarisation. In this model, the JER is allowed to vary independently for each bin of the octant variable and for each control region. With this approach, the role of the single-top-quark t-channel events in constraining the JER is reduced. In the second model, t-channel events are allowed to have a larger impact on the JER. This is achieved by allowing each uncertainty affecting the JER to vary in a correlated way across all bins, leading to the larger JER value mentioned above. The polarisation is measured again in this second fit. The difference between the polarisations obtained with the two fit models is added in quadrature to the uncertainty obtained from the nominal model in order to get the overall uncertainty for the measurement. This additional uncertainty is more pronounced for $P_{x'}$, while $P_{z'}$ and $P_{y'}$ are much less affected. Figure 4 shows the observed and fitted numbers of events per octant Q for top quarks and top antiquarks, separately, after the nominal fit to data. In this figure, neighboring bins refer to pairs of quadrants lying on opposite sides of the production plane, i.e. differing by the sign of $\cos\theta_{\ell y'}$. The first four bins indicate leptons emitted opposite to the spectator-quark direction in the top-quark reference frame, while the last four bins refer to leptons emitted along the spectator-quark direction, i.e. differing by the sign of $\cos\theta_{\ell z'}$.

The extracted polarisations together with the normalisation factors of the t-channel, $t\bar{t}$ and W+jets processes are shown in Table 4. The column labelled 'extracted value' lists the result for the three normalisations and the six polarisation components, and the total uncertainty for each. In the column labelled '(stat.)' the statistical uncertainty is presented separately. These may be compared with parton-level predictions calculated at NNLO, based on Ref. [8], where stable single top quarks produced in the t-channel from pp collisions at $\sqrt{s} = 13$ TeV are considered. These predictions are $P^{t}_{x'} = -0.024 \pm 0.001\,(\mathrm{scale})^{+0.004}_{-0.007}\,(\mathrm{PDF}+\alpha_{\mathrm{s}})$ and $P^{t}_{z'} = 0.965 \pm 0.003\,(\mathrm{scale})^{+0.003}_{-0.004}\,(\mathrm{PDF}+\alpha_{\mathrm{s}})$ for top quarks and $P^{\bar{t}}_{x'} = -0.073 \pm 0.008\,(\mathrm{scale})^{+0.008}_{-0.004}\,(\mathrm{PDF}+\alpha_{\mathrm{s}})$ and $P^{\bar{t}}_{z'} = -0.957^{-0.003}_{+0.012}\,(\mathrm{scale})^{+0.004}_{-0.002}\,(\mathrm{PDF}+\alpha_{\mathrm{s}})$ for top antiquarks. Because of CP symmetry in top-quark production, $P^{t}_{y'}$ and $P^{\bar{t}}_{y'}$ are expected to be zero [7]; equivalently, the polarisation vector is expected to lie in the plane of production, as described in Section 1. The only non-zero SM contributions to $P^{t}_{y'}$ and $P^{\bar{t}}_{y'}$ come from absorptive parts of EW NLO diagrams, which are much smaller than the expected uncertainty of this measurement. These theoretical predictions and their uncertainties are calculated as detailed in Section 1.

A summary of the impact of the systematic uncertainties on the value of each polarisation parameter is shown in Table 5. The larger cross-section for top-quark versus top-antiquark production leads to smaller uncertainties for the measured polarisation for top quarks. Systematic effects tend to have symmetric impacts for either side of the production plane, leading to reduced impact on $P_{y'}$ versus the other directions. The uncertainties with the largest impact are those due to the JES and JER. This is because the polarisation depends on kinematic angles determined in the top-quark reference frame, and since jet energy and $E_{\mathrm{T}}^{\mathrm{miss}}$ are used to reconstruct that frame, uncertainties in the measurement of the jet energy are expected to contribute significantly to the total systematic uncertainty. The finite number of simulated events as well

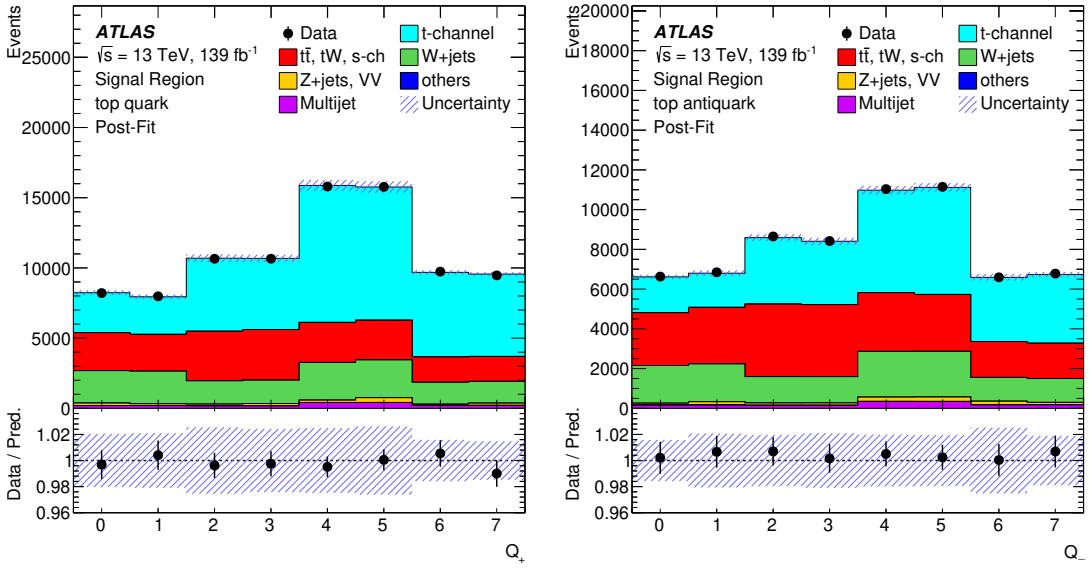

(a) (b)

Figure 4: Observed data and fitted distributions of the octant variable (a) Q_+ in the top-quark and (b) Q_- in the top-antiquark signal regions. The Q variable is assigned an integer value zero through seven according to $Q = 4 \cdot \Theta(\cos\theta_{\ell z'}) + 2 \cdot \Theta(\cos\theta_{\ell x'}) + \Theta(\cos\theta_{\ell y'})$ where $\Theta(\xi)$ is the Heaviside step function of the variable ξ. The label 'others' represents $t\bar{t}Z$, $t\bar{t}W$, tZq, tHq, and tWZ production. The uncertainty bands include both the statistical and systematic uncertainties. The lower panels show the ratio of data to prediction in each bin.

as the $t\bar{t}$ modelling are also important sources of uncertainty. The normalisation factor extracted for the t-channel signal contribution is compatible with results obtained in Ref. [118].

Parameter	Extracted value	(stat.)
t-channel norm.	$+1.045 \pm 0.022$	(± 0.006)
W+jets norm.	$+1.148 \pm 0.027$	(± 0.005)
$t\bar{t}$ norm.	$+1.005 \pm 0.016$	(± 0.004)
$P^{t}_{x'}$	$+0.01 \pm 0.18$	(± 0.02)
$P^{\bar{t}}_{x'}$	-0.02 ± 0.20	(± 0.03)
$P^{t}_{y'}$	-0.029 ± 0.027	(± 0.011)
$P^{\bar{t}}_{y'}$	-0.007 ± 0.051	(± 0.017)
$P^{t}_{z'}$	$+0.91 \pm 0.10$	(± 0.02)
$P^{\bar{t}}_{z'}$	-0.79 ± 0.16	(± 0.03)

Table 4: Normalisation factors of the t-channel, W+jets and $t\bar{t}$ processes together with the polarisation values as extracted from data, including total and statistical-only uncertainties in the fit.

Figure 5 shows the observed best-fit polarisation measurements of $P_{z'}$ and $P_{x'}$ in the two-dimensional polarisation parameter space. Contours for top quarks and top antiquarks are shown separately at 68% CL,

Uncertainty source	$\Delta P^{t}_{x'}$	$\Delta P^{\bar{t}}_{x'}$	$\Delta P^{t}_{y'}$	$\Delta P^{\bar{t}}_{y'}$	$\Delta P^{t}_{z'}$	$\Delta P^{\bar{t}}_{z'}$
Modelling						
Modelling (t-channel)	±0.037	±0.051	±0.010	±0.015	±0.061	±0.061
Modelling ($t\bar{t}$)	±0.016	±0.021	±0.004	±0.016	±0.003	±0.016
Modelling (other)	±0.013	±0.031	±0.003	±0.006	±0.026	±0.043
Experimental						
Jet energy scale	±0.045	±0.048	±0.005	±0.007	±0.033	±0.025
Jet energy resolution	±0.166	±0.185	±0.021	±0.040	±0.070	±0.130
Jet flavour tagging	±0.004	±0.002	<0.001	±0.001	±0.007	±0.009
Other experimental uncertainties	±0.015	±0.029	±0.002	±0.007	±0.014	±0.026
Multijet estimation	±0.008	±0.021	<0.001	±0.001	±0.008	±0.013
Luminosity	±0.001	±0.001	<0.001	<0.001	<0.001	<0.001
Simulation statistics	±0.020	±0.024	±0.008	±0.015	±0.017	±0.031
Total systematic uncertainty	±0.174	±0.199	±0.025	±0.048	±0.096	±0.153
Total statistical uncertainty	±0.017	±0.025	±0.011	±0.017	±0.022	±0.034

Table 5: Systematic and statistical uncertainties in the measurement of the polarisation vector $\vec{P}$ for top quarks and top antiquarks. The impact of each group of uncertainties is obtained by performing a fit where the NPs in the group are fixed to their best-fit values, subtracting the square of the resulting uncertainty in the parameter of interest (i.e. for each polarisation component) from the squared uncertainty from the nominal fit, and then taking the square root. An additional uncertainty from the JER is included, consisting of the difference between the central values of the nominal fit model and the alternative fit model in which JER variations are implemented coherently across all bins of the octant variable distribution. The total systematic uncertainty is calculated as the sum in quadrature of the individual grouped sources.

including statistical and systematic uncertainties.

From the present analysis one can conclude that a very high degree of polarisation is observed in t-channel production, primarily along the direction of the spectator quark (for top-quark events), or opposite to that direction (for top-antiquark events), in agreement with NNLO QCD predictions.

10 Angular differential cross-sections for top-quark production

Three angular differential cross-sections are obtained from the distribution of the charged-lepton momentum with respect to the i^{th} axis ($i = x', y', z'$), as defined in Section 1.1. These three distributions are associated with the three top-quark polarisation components ($\{P_{x'}, P_{y'}, P_{z'}\}$). The selection criteria for reconstructed events, defined in Section 4, are the same as the used for the measurement of top-quark and top-antiquark polarisation vectors in Section 9. These differential angular distributions are distorted by finite resolution of the detector and the trigger, reconstruction, and sculpted by the event selection criteria. The detector effects are corrected using an unfolding technique.

In the measurement of the angular differential cross-sections, the normalisation of the W+ jets and top-quark background (i.e. $t\bar{t}$, tW, and s-channel) contributions is estimated through a simultaneous maximum-likelihood fit to the numbers of data events observed in the signal region and the two control regions. All

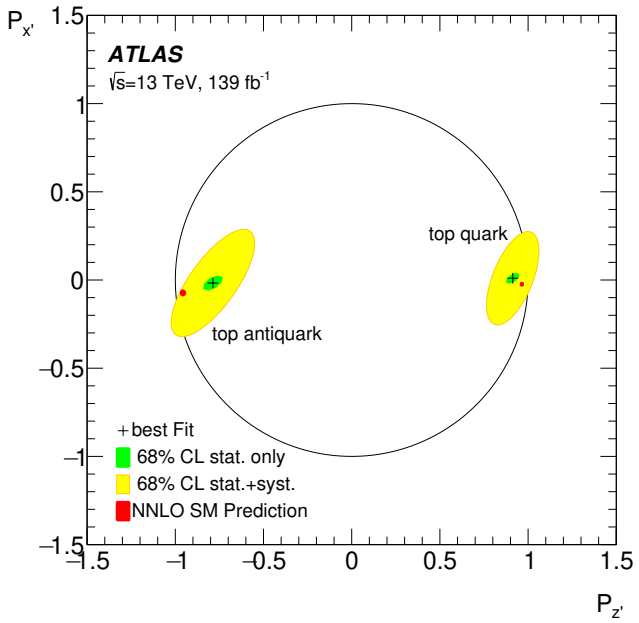

Figure 5: Summary of the observed best-fit polarisation measurements with their statistical-only (green) and statistical+systematic (yellow) contours at 68% CL, plotted on the two-dimensional polarisation parameter space ($P_{z'}$, $P_{x'}$). The interior of the black circle represents the physically allowed region of the parameter space, and the red point indicates the parton-level prediction at NNLO from a calculation based on Ref. [8]. The uncertainty in the theoretical prediction includes scale, α_s and PDF uncertainties. Correlations between the predictions of the polarisation parameters are not provided.

other backgrounds are fixed to their theoretical or data-driven predictions. The overall normalisation of the t-channel signal is treated as another free parameter in the fit. The likelihood function [119] is given by the product of Poisson probability terms associated with the three regions (signal region and $t\bar{t}$ and W+jets control regions). The fit is performed separately for the signal and control regions defined with positively (negatively) charged leptons for the measurement of top-quark (top-antiquark) events, as well as for the inclusive regions containing both lepton charges. These normalisation factors are compatible with those extracted in the template fit described in Section 9 and with the theoretical predictions.

The angular distributions observed at reconstruction level are shown in Figure 6 for the inclusive signal region. They are compared with the predicted signal and background distributions, normalised to the results of the maximum-likelihood fit. The selection requirements have a significant impact on the shapes of these distributions.

The measured angular distributions are unfolded to the particle level within the fiducial region. The particle-level selection criteria are discussed in Section 5. The unfolding corrections account for distortions due to detector resolution and efficiencies so as to allow direct comparison with theoretical predictions. In this analysis the same unfolding technique as in Ref. [120] is used. D'Agostini's iterative Bayesian approach [121] as implemented in `RooUnfold` [122] is used to unfold the distributions. The measured expectation value for the number of signal events at particle level in each bin k of the fiducial volume, ν_k^{particle}, is obtained from the observed number of events in each bin j of the reconstructed distribution

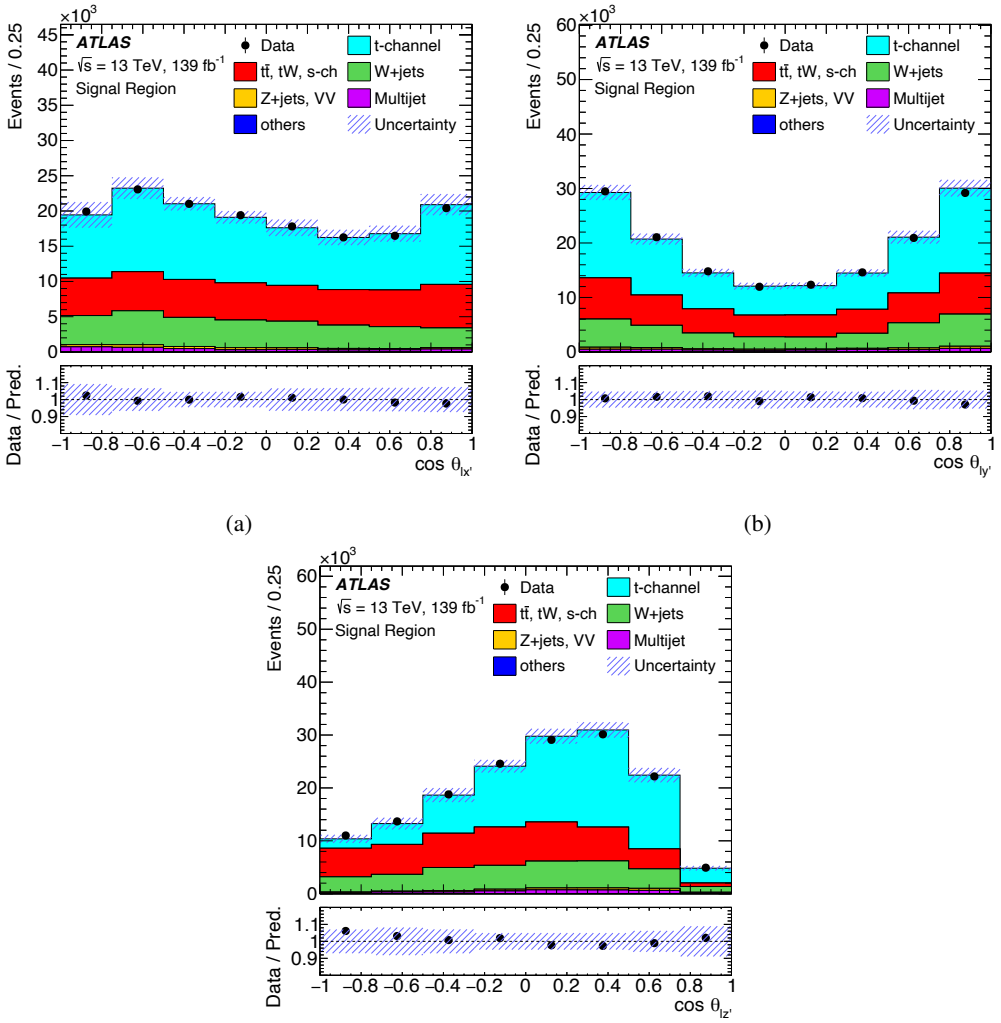

Figure 6: Post-fit distributions of (a) $\cos\theta_{\ell x'}$, (b) $\cos\theta_{\ell y'}$ and (c) $\cos\theta_{\ell z'}$ in the signal region. The data, shown as the black points with statistical uncertainties, are compared with SM signal and background predictions. The multijet background is estimated using MC and data-driven techniques, while contributions from simulated W+jets and top-quark background and t-channel signal event samples are normalised to the results of a maximum-likelihood fit to event yields in the signal and control regions. The label 'others' represents $t\bar{t}Z$, $t\bar{t}W$, tZq, tHq, and tWZ production. The uncertainty bands include both the statistical and systematic uncertainties. The lower panels show the ratio of data to prediction in each bin.

N_j^{data}, after subtracting the sum of all background contributions B_j, according to

$$\nu_k^{\text{particle}} = C_k^{\text{particle!reco}} \sum_j M_{jk}^{-1} C_j^{\text{reco!particle}} (N_j^{\text{data}} - B_j),$$

where M_{jk} is the migration matrix which relates the particle-level and reconstructed values, and $C_k^{\text{reco!particle}}$ is a correction factor that accounts for events that pass reconstruction selection but not particle-level

selection. It is defined as

$$C_j^{\text{reco!particle}} = \frac{S_j^{\text{reco}} - S_j^{\text{reco!particle}}}{S_j^{\text{reco}}},$$

where S_j^{reco} is the number of reconstructed signal events in bin j and $S_j^{\text{reco!particle}}$ is the number of events that pass the reconstruction-level selection but not the particle-level selection. Another correction factor, $C_j^{\text{particle!reco}}$, accounts for signal events that pass the particle-level selection but not the reconstruction-level selection:

$$C_k^{\text{particle!reco}} = \frac{1}{\epsilon_k} = \frac{S_k^{\text{particle}}}{S_k^{\text{particle}} - S_k^{\text{particle!reco}}},$$

where S_k^{particle} is the number of signal events at particle level and $S_k^{\text{particle!reco}}$ is the number of events that pass the particle-level selection but not the reconstruction-level selection. The factor $C_k^{\text{particle!reco}}$ is the inverse of the efficiency ϵ_k for signal events at particle level in bin k to pass the reconstruction-level requirements.

Each normalised differential cross-section is determined by dividing the obtained ν_k^{particle} value in each bin by the integral over all bins.

The migration matrix and the selection efficiency are computed using samples of t-channel signal events simulated with the Powheg Box+Pythia8 generator described in Section 2. They are calculated for the signal region defined with positively (negatively) charged leptons for the measurement of top-quark (top-antiquark) events, as well as for the inclusive signal region containing both lepton charges. The obtained $C_k^{\text{reco!particle}}$ correction factors are around 50% and the efficiencies ϵ_k around 20% for all bins.

The number of bins was chosen in order to have a stable unfolding response with at least 70% of the events in the diagonal elements of the migration matrix. This criterion results in eight bins for the $\cos\theta_{\ell x'}$ and $\cos\theta_{\ell y'}$ distributions and four bins for the $\cos\theta_{\ell z'}$ distribution for which larger migrations are observed. The number of iterations is chosen such that the absolute change between two successive steps becomes negligible (the difference must be smaller than 0.1% of the integral of the associated distribution) and when a convergent state is reached the difference between the results obtained with the chosen number of iterations and with 15 more iterations should not exceed 0.15% of the integral of the associated distribution for all bins. This stability criterion results in five iterations for the $\cos\theta_{\ell x'}$ distribution and three for both the $\cos\theta_{\ell y'}$ and $\cos\theta_{\ell z'}$ distributions.

The stability of the unfolding procedure was validated through convergence and closure tests performed by using template distributions constructed from the t-channel Powheg Box+Pythia8, Protos+Pythia8 and MadGraph5_aMC@NLO+Pythia8 samples. The closure tests showed that the residual bias induced by the unfolding method is negligible. By using template distributions given by the Protos+Pythia8 and MadGraph5_aMC@NLO+Pythia8 samples, generated including effects on the tWb vertex from anomalous couplings or additional EFT operators, it is shown that the unfolding method recovers the generated distributions at particle level within the fiducial region.

The statistical uncertainty of the data unfolded result is determined by running over an ensemble of 100 000 pseudo-experiments, varying the content of each bin according to its expected statistical uncertainty through Poisson fluctuations. For each pseudo-experiment a new background normalisation is extracted

using the procedure described above. After background subtraction, each pseudo-experiment is unfolded and normalised. The spread (RMS) of the result in each bin is taken as the measure of the statistical uncertainty.

The uncertainty associated with the finite size of the simulated samples is evaluated using 100 000 pseudo-experiments, varying for each process (excluding the data-driven multijet background) the total prediction in each bin according to the statistical uncertainty through Gaussian fluctuations. The same procedure as for the data statistical uncertainty is then used.

The impact of each source of systematic uncertainty is evaluated by unfolding template distributions resulting from simulated pseudo-data modified to reflect the effect of the given uncertainty source. In each case a new background normalisation estimation is performed before its subtraction from the pseudo-data, using the fitting procedure described above. For all sources of systematic uncertainty the nominal unfolding corrections are considered. Except for the signal modelling uncertainties affecting the unfolding corrections, the systematic uncertainty is evaluated as the difference between the nominal angular distribution values and the ones measured using the varied normalisations and shapes. For the signal modelling uncertainties, the unfolded varied distribution is compared with the corresponding particle-level spectra.

The resulting normalised angular differential cross-sections at particle level within the fiducial region are displayed in Figures 7–9 for the inclusive, top-quark and top-antiquark measurements. The measured cross-sections include both the statistical and systematic uncertainties, and are compared with the predictions given by the different generators. Among the different uncertainty sources, those related to JER and JES are dominant. The measured distributions are consistent with those obtained from a Protos simulation sample with the polarisations given by the template fit described in Section 9.

A global covariance matrix of size 20×20, corresponding to the 20 measured bins in Figures 7–9 and including the effects of all uncertainties and the correlations among the three angular distributions, is computed in order to perform quantitative comparisons with theoretical predictions.

An initial ensemble of 50 000 pseudo-experiments is used to compute the covariance matrix with the systematic uncertainties and the uncertainty associated with the limited size of the simulated samples. In each pseudo-experiment, Gaussian-distributed shifts are applied coherently for each detector-modelling systematic uncertainty by scaling each bin of the data distribution by the expected relative variation from the associated systematic uncertainty effect. For the uncertainty due to the limited size of the simulated samples the Gaussian-distributed shifts are computed independently for each bin. The varied distribution is unfolded with the nominal corrections after subtracting the backgrounds with the normalisation factors derived following the procedure described in Section 6. Additional Gaussian-distributed shifts are then applied coherently for each signal- and background-modelling systematic uncertainty. The modelling shifts are derived by using the expected relative variations from the associated systematic uncertainty to scale each bin of the data distribution unfolded with the nominal corrections. The resulting modified unfolded distributions are used to compute an initial matrix.

The statistical correlations between the three different angular distributions are evaluated using the bootstrap method [123], using a set of 1000 bootstrap samples. The global statistical matrix is calculated using the statistical error of each bin of the angular distributions and the correlation coefficients. This matrix is then added to the previous one to compute an unnormalised global covariance matrix.

Finally, a set of 100 000 additional pseudo-experiments is used to normalise the covariance matrix. For each additional pseudo-experiment, each element of the three angular distributions is fluctuated using

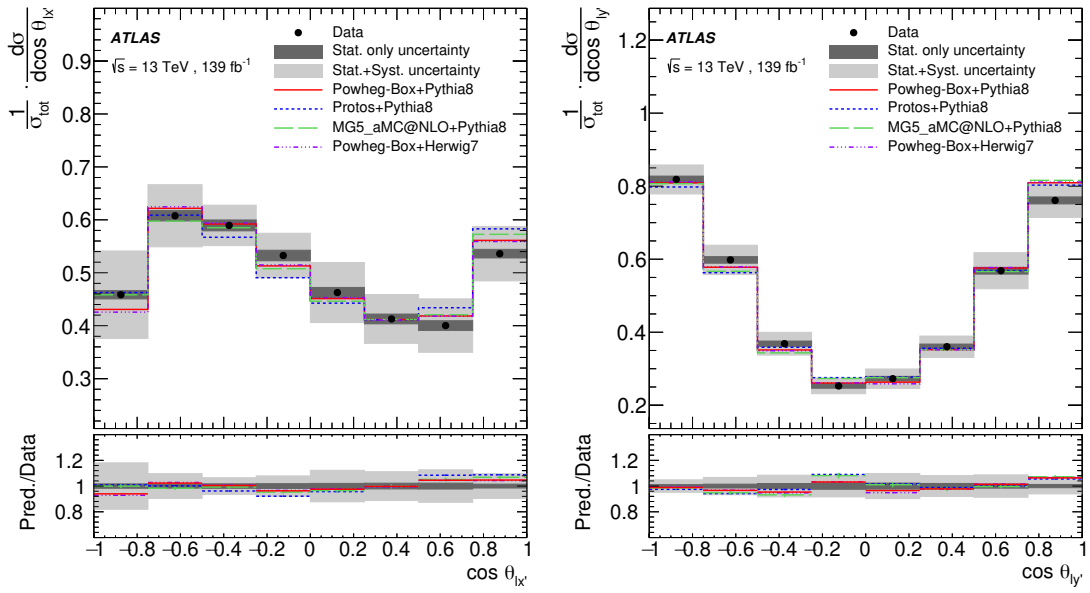

(a) (b)

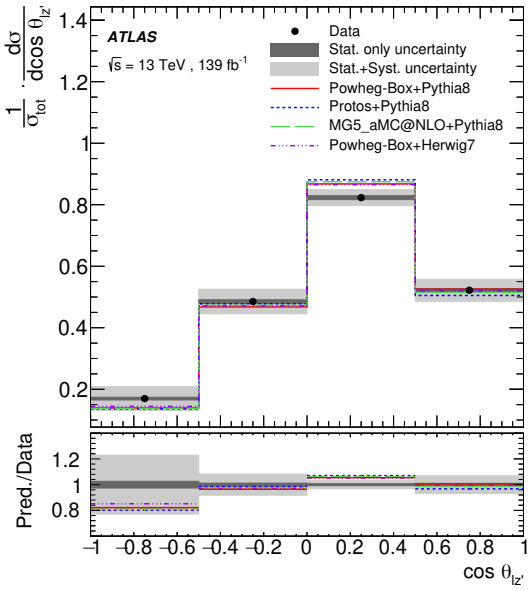

(c)

Figure 7: Particle-level normalised differential cross-sections as a function of (a) $\cos\theta_{\ell x'}$, (b) $\cos\theta_{\ell y'}$, and (c) $\cos\theta_{\ell z'}$, along with various SM MC predictions of the t-channel signal for both top quarks and top antiquarks. The data, shown as the black points with statistical uncertainties, are compared with predictions (lines) obtained by using the POWHEG BOX+PYTHIA8 (solid red), PROTOS+PYTHIA8 (dashed blue), MADGRAPH5_AMC@NLO+PYTHIA8 (long-dashed green) and POWHEG BOX+HERWIG7 (dot-dashed violet) generators. The uncertainty bands include both the statistical and systematic uncertainties. The data statistical uncertainty is too small to be visible. The lower panels show the ratio of prediction to data in each bin.

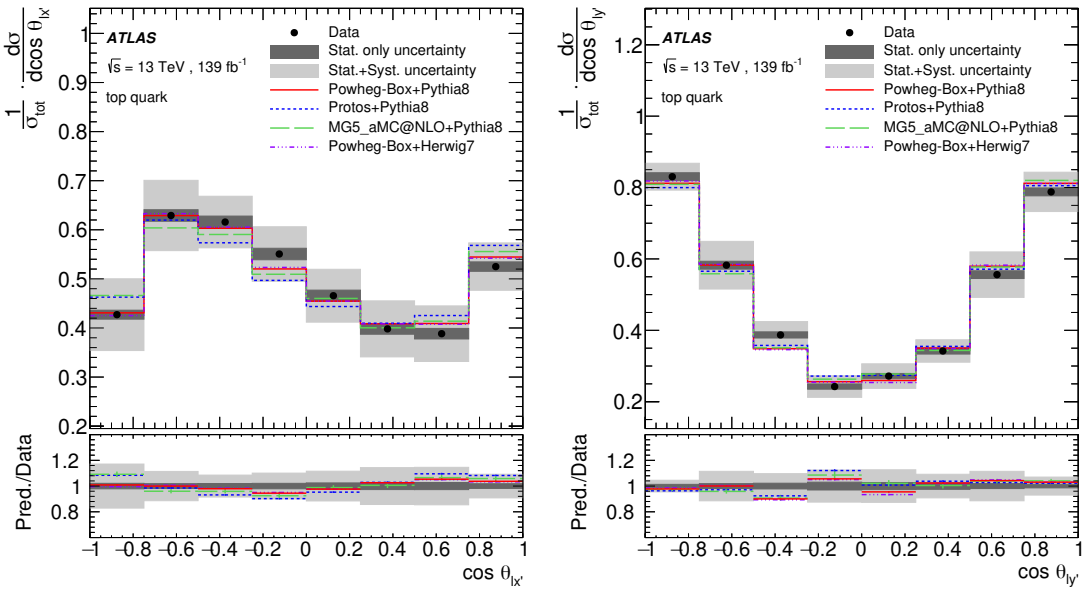

(a) (b)

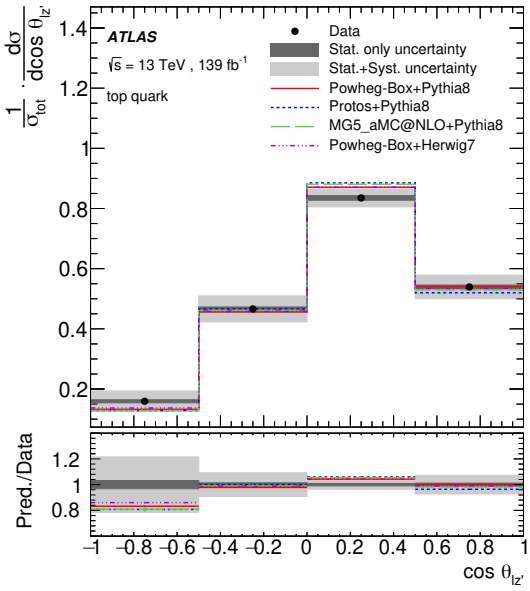

(c)

Figure 8: Particle-level normalised differential cross-sections as a function of (a) $\cos\theta_{\ell x'}$, (b) $\cos\theta_{\ell y'}$, and (c) $\cos\theta_{\ell z'}$, along with various SM MC predictions of the t-channel signal for top quarks. The data, shown as the black points with statistical uncertainties, are compared with predictions (lines) obtained by using the Powheg Box+Pythia8 (solid red), Protos+Pythia8 (dashed blue), MadGraph5_aMC@NLO+Pythia8 (long-dashed green) and Powheg Box+Herwig7 (dot-dashed violet) generators. The uncertainty bands include both the statistical and systematic uncertainties. The data statistical uncertainty is too small to be visible. The lower panels show the ratio of prediction to data in each bin.

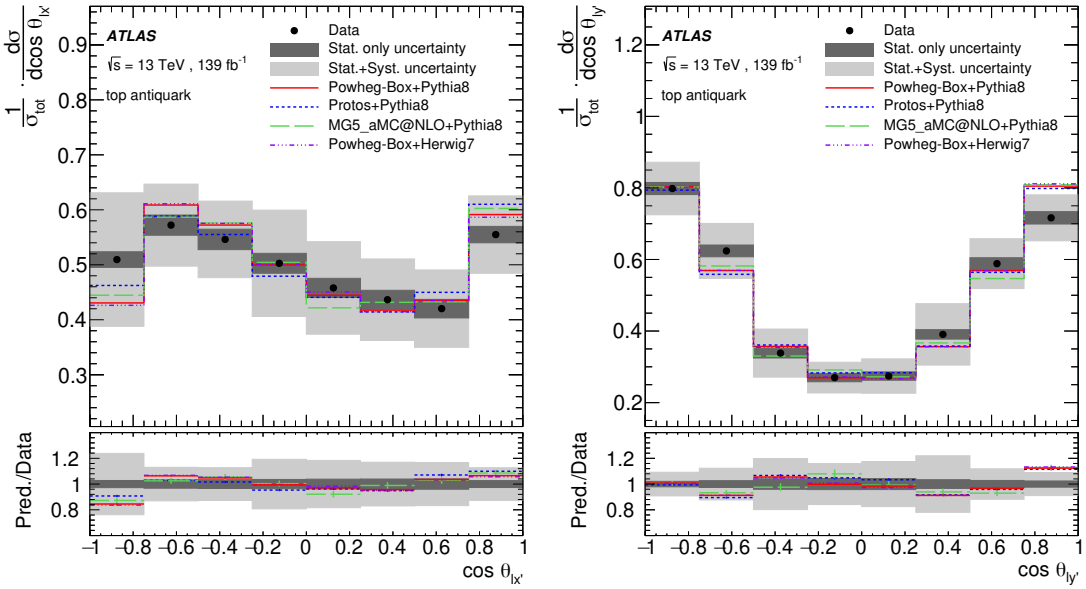

(a) (b)

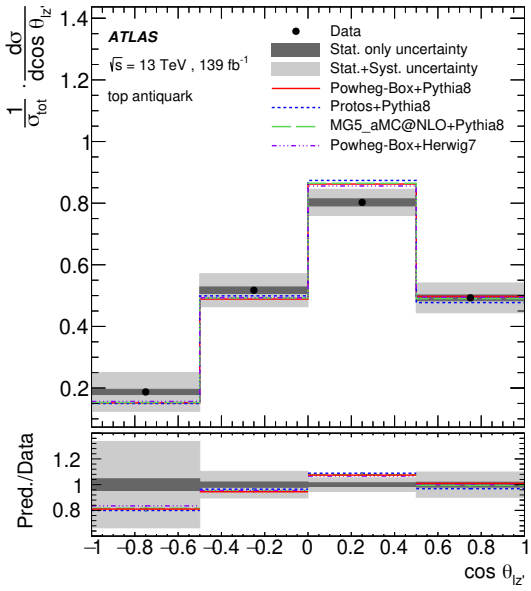

(c)

Figure 9: Particle-level normalised differential cross-sections as a function of (a) $\cos\theta_{\ell x'}$, (b) $\cos\theta_{\ell y'}$, and (c) $\cos\theta_{\ell z'}$, along with various SM MC predictions of the t-channel signal for top antiquarks. The data, shown as the black points with statistical uncertainties, are compared with predictions (lines) obtained by using the Powheg Box+Pythia8 (solid red), Protos+Pythia8 (dashed blue), MadGraph5_aMC@NLO+Pythia8 (long-dashed green) and Powheg Box+Herwig7 (dot-dashed violet) generators. The uncertainty bands include both the statistical and systematic uncertainties. The data statistical uncertainty is too small to be visible. The lower panels show the ratio of prediction to data in each bin.

a multivariate Gaussian distribution with the unnormalised global covariance matrix. The resulting pseudo-experiments are normalised and are used to calculate the normalised global covariance matrix.

To quantify the level of agreement between each of the measured normalised differential cross-sections and the theoretical predictions, χ^2 values are calculated according to the relation $\chi^2 = V^T_{N_b-1} \cdot \mathrm{Cov}^{-1}_{N_b-1} \cdot V_{N_b-1}$. Here N_b is the number of bins in the spectrum under consideration, V_{N_b-1} is a vector with the differences between the measured and the predicted cross-sections obtained by discarding one of the N_b elements, and Cov_{N_b-1} is the $(N_b-1)\times(N_b-1)$ sub-matrix derived from the relevant $N_b \times N_b$ part of the global covariance matrix by discarding the corresponding row and column. A global χ^2 value is also obtained using the full vector of differences for the three angular distributions and the full global covariance matrix. In this case, three elements of the vector and their corresponding rows and columns in the covariance matrix are discarded.

The p-values, relative to the Powheg Box+Pythia8 SM predictions, are then evaluated from the χ^2 values and the number of degrees of freedom (NDF) of each angular distribution, as shown in Table 6. Since these are normalised cross-sections, the NDF corresponds to the number of bins in each angular distribution minus one. The obtained values show good agreement of the SM prediction with the measured data. The high p-values for $\cos\theta_{\ell x'}$ distribution may indicate that the evaluation of systematics uncertainties is overly conservative.

	Top quark		Top antiquark		Top quark and antiquark	
Angular variable	χ^2/NDF	p-value	χ^2/NDF	p-value	χ^2/NDF	p-value
$\cos\theta_{\ell x'}$	1.35/7	0.99	0.94/7	1.00	1.32/7	0.99
$\cos\theta_{\ell y'}$	4.57/7	0.71	2.92/7	0.89	3.78/7	0.81
$\cos\theta_{\ell z'}$	1.55/3	0.67	2.04/3	0.56	2.26/3	0.52
Global	13.55/17	0.70	6.86/17	0.99	9.25/17	0.93

Table 6: The χ^2 and p-value of the three unfolded angular distributions for the top-quark, for the top-antiquark and for both the top-quark and top-antiquark measurements. The numbers are computed by comparing the observed data with the Powheg Box+Pythia8 SM predictions. The NDF corresponds to the number of bins of each angular distribution minus one. A global χ^2 and p-value for the three angular distributions are also included.

11 Bounds on EFT coefficients C_{tW} and C_{itW}

The unfolded and normalised distributions of $\cos\theta_{\ell x'}$ and $\cos\theta_{\ell y'}$ are used to set bounds on the complex Wilson coefficient of the dimension-six operator O_{tW}. The operator O_{tW} has only a small effect on the $\cos\theta_{\ell z'}$ distribution, which in contrast to the $\cos\theta_{\ell x'}$ and $\cos\theta_{\ell y'}$ distributions is sensitive to many additional EFT operators [124]. The $\cos\theta_{\ell z'}$ distribution is therefore ignored in this work. The data are compared with the effects of this dipole operator in a likelihood fit which requires a theoretical prediction in a parametric form. To describe the angular distributions as a function of C_{tW} and C_{itW}, a morphing technique [125, 126] is employed to interpolate from a set of 15 MC templates generated as described in Section 2. The O_{tW} operator contributes to the production and decay of the top quark. All orders of the EFT expansion parameter Λ are included in the parametric description, allowing studies of the effects from high-dimensional (up to $1/\Lambda^8$) terms, which are usually assumed negligible.

The EFT operator can contribute to both the production and decay of the top quark, which leads to 15 terms in the weight function:

$$\begin{aligned}\sigma(C_{tW}, C_{itW}) \propto & \left| O_{\text{SM}} + \frac{C_{tW}}{\Lambda^2} \cdot O_{tW} + \frac{C_{itW}}{\Lambda^2} \cdot O_{itW} \right|^2_{\text{production}} \cdot \left| O_{\text{SM}} + \frac{C_{tW}}{\Lambda^2} \cdot O_{tW} + \frac{C_{itW}}{\Lambda^2} \cdot O_{itW} \right|^2_{\text{decay}} \\ & = \sigma_1 + \left(C^1_{tW} \cdot \sigma_2 + C^1_{itW} \cdot \sigma_3 \right) / \Lambda^2 \\ & + \left(C^2_{tW} \cdot \sigma_4 + C^2_{itW} \cdot \sigma_5 + C^1_{tW} C^1_{itW} \cdot \sigma_6 \right) / \Lambda^4 \\ & + \left(C^3_{tW} \cdot \sigma_7 + C^3_{itW} \cdot \sigma_8 + C^2_{tW} C^1_{itW} \cdot \sigma_9 + C^1_{tW} C^2_{itW} \cdot \sigma_{10} \right) / \Lambda^6 \\ & + \left(C^4_{tW} \cdot \sigma_{11} + C^4_{itW} \cdot \sigma_{12} + C^3_{tW} C^1_{itW} \cdot \sigma_{13} + C^1_{tW} C^3_{itW} \cdot \sigma_{14} + C^2_{tW} C^2_{itW} \cdot \sigma_{15} \right) / \Lambda^8 .\end{aligned}$$

This expression includes all orders of the EFT expansion (Λ) with the numerical factors originating from the squaring absorbed in the σ_n terms, with $n = 1, ..., 15$. The positions in C_{tW} and C_{itW} of 15 simulated event samples was chosen such that the uncertainty in the weight function is a small contribution to the total uncertainty over the parameter-space region of interest. If the Lagrangian had not been truncated at dimension six, dimension-eight operators would also begin to contribute at $(1/\Lambda^4)$. In this work, Λ is set to 1 TeV.

The likelihood function has the form of a multivariate Gaussian distribution whose mean is set to the EFT prediction from the measured angular differential cross-section. The likelihood contains the uncertainties of the 15 σ_n terms, due to the limited size of the MC samples used to produce the templates, together with the uncertainty of the unfolded measurement contained in a covariance matrix.

The 16×16 covariance matrix for the 16 bins of the measured normalised $\cos\theta_{\ell x'}$ and $\cos\theta_{\ell y'}$ distributions is the corresponding sub-matrix of the global matrix described in Section 10. This matrix has two redundant dimensions caused by the fact that the angular distributions $\cos\theta_{\ell x'}$ and $\cos\theta_{\ell y'}$ are both normalised and are obtained from the same dataset. In the implementation of the fitting procedure, the covariance matrix is first diagonalised and the data is projected onto the eigenvectors with non-zero eigenvalues.

The robustness of the fit is tested in three ways. It was checked that the unfolding procedure which uses SM-derived corrections can correctly recover non-zero EFT coefficients over a range that spans the current bounds. Secondly, the effect of non-zero EFT coefficients on the background subtraction was proven to be smaller than the measurement uncertainties. Lastly, when applied to MC samples produced by the MadGraph5_aMC@NLO+Pythia8 generator with non-zero values for other EFT operator coefficients (C_{bW}, C_{ibW}, $C_{\varphi tb}$, C_{tg}), the stability of the fit for C_{tW} and C_{itW} was found to be well within the current experimental precision.

The result of fitting C_{tW} and C_{itW} simultaneously is shown in Figure 10, where good agreement between the model and the data is observed. Good agreement with the SM prediction from the NLO MadGraph5_aMC@NLO+Pythia8 generator is also seen. The best-fit values for the coefficients are $C_{tW} = 0.3 \pm 0.6$ (1.1) and $C_{itW} = -0.3 \pm 0.2$ (0.5) at 68% CL (95% CL), which is consistent with the SM prediction, as shown in Figure 11. The obtained limits for the coefficients at 68% CL and 95% CL are given in Table 7. The individual fit result for each coefficient is also obtained by fixing the other coefficient to zero, which results in $C_{tW} = 0.1 \pm 0.5$ (1.1) and $C_{itW} = -0.3 \pm 0.2$ (0.5) respectively, where the results are quoted for 68% CL (95% CL).

Among previous constraints on C_{tW}, the strongest come from measurements of the values of the W-boson helicity fractions in top-quark pair decays by ATLAS [127] and CMS [128], with the combined result [36]

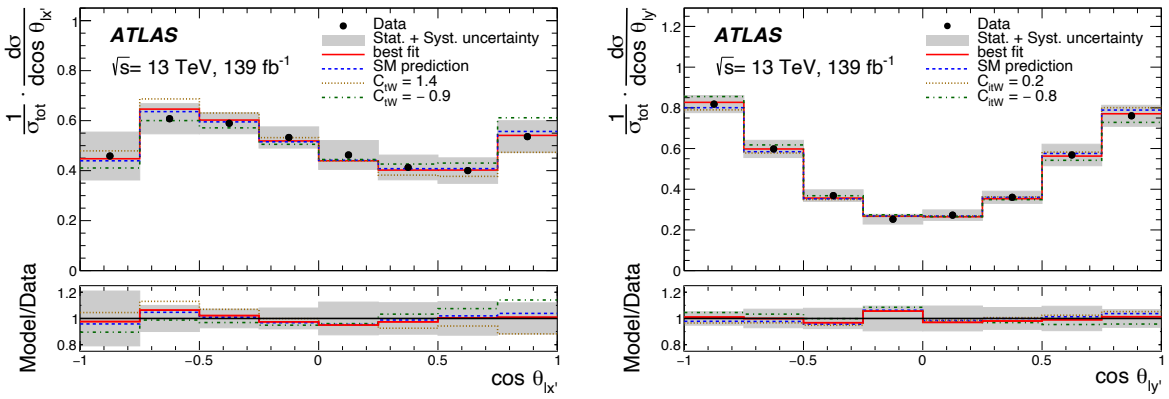

(a) (b)

Figure 10: Comparison of data and the result of the EFT fit for the polarisation angles (a) $\cos\theta_{\ell x'}$ and (b) $\cos\theta_{\ell y'}$. The solid points show the data, unfolded to particle level. The solid red line corresponds to the EFT prediction using the best-fit values for the Wilson coefficients $C_{tW} = 0.3$ and $C_{itW} = -0.3$. The blue dashed line represents the SM prediction obtained with the MadGraph5_aMC@NLO+Pythia8 generator. The brown dotted (green dash-dotted) line shows the model at its upper (lower) 95% CL bounds for (a) $C_{tW} = 1.4$ ($C_{tW} = -0.9$) and (b) $C_{itW} = 0.2$ ($C_{itW} = -0.8$) also obtained with the MadGraph5_aMC@NLO+Pythia8 generator. The uncertainty bands include both the statistical and systematic uncertainties. The lower panel gives the ratio of the model to the data.

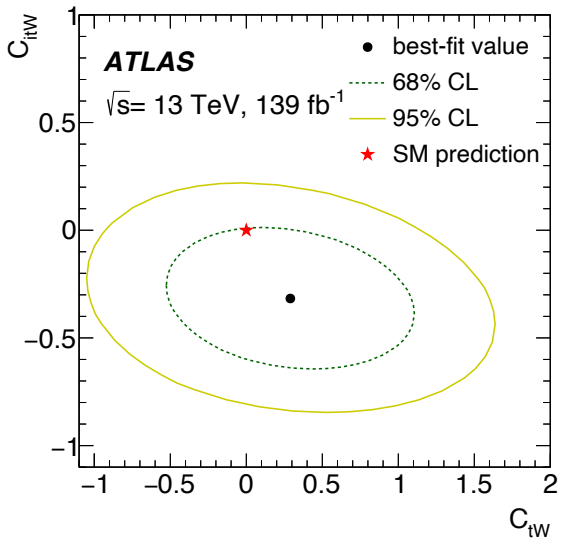

Figure 11: The observed best-fit value (dot) for the Wilson coefficients C_{tW} and C_{itW} with the uncertainty contours at 68% CL (dashed) and 95% CL (solid). The CLs are obtained in a simultaneous fit of the two parameters using the prediction obtained with the MadGraph5_aMC@NLO+Pythia8 generator. The red star indicates the SM prediction.

providing bounds of $[-0.48, 0.29]$ at 95% CL when only C_{tW} is allowed to vary. Comparable limits were also derived from EFT fits of the top-quark sector [31–34] that include those measurements. However, the

	C_{tW}		C_{itW}	
	68% CL	**95% CL**	**68% CL**	**95% CL**
All terms	$[-0.3, 0.8]$	$[-0.9, 1.4]$	$[-0.5, -0.1]$	$[-0.8, 0.2]$
Order $1/\Lambda^4$	$[-0.3, 0.8]$	$[-0.9, 1.4]$	$[-0.5, -0.1]$	$[-0.8, 0.2]$
Order $1/\Lambda^2$	$[-0.3, 0.8]$	$[-0.8, 1.5]$	$[-0.6, -0.1]$	$[-0.8, 0.2]$

Table 7: Obtained limits on the real (C_{tW}) and imaginary (C_{itW}) coefficient of the O_{tW} operator. Also shown are the limits when only the terms up to a specific order in Λ are taken into account.

constraints obtained in those analyses assume $C_{itW} = 0$, which is not assumed in the result presented here. Very stringent individual limits on C_{itW} were obtained from electric dipole moment analyses [129] when only C_{itW} is allowed to be non-zero, but these become much weaker when multiple EFT coefficients are allowed to vary simultaneously. In that case, the previous limits on C_{itW} were dominated by the input from ATLAS [18], which provides bounds on C_{itW} of $[-2.3, 3.0]$ at 95% CL. A global fit including real and imaginary parts of all *tWb* operators [35] gives $C_{tW} \in [-0.8, 0.7]$ and $C_{itW} \in [-2.3, 1.6]$, where the bound on C_{itW} is dominated by the ATLAS result [19]. A later ATLAS result [20] improved the 95% CL interval to $C_{itW} \in [-0.8, 0.7]$. The bounds on C_{itW} presented in this paper improve on all of these results.

Also given in Table 7 are the limits when a certain cut-off on the order of Λ is applied. It is observed that including terms up to $1/\Lambda^4$, which corresponds to the squared terms of a dimension-six coefficient, yields identical limits to retaining all 15 terms. The relatively small change in the result obtained with only $1/\Lambda^2$ terms indicates that there is only a modest dependence on $1/\Lambda^4$ terms. The usual assumption that terms beyond $1/\Lambda^4$ can be excluded is also validated.

12 Conclusions

The polarisation of single top quarks and antiquarks produced in the t-channel has been measured in 139 fb^{-1} of 13 TeV pp collision data collected with the ATLAS detector at the LHC. An analysis of the full polarisation vector of the top quarks (antiquarks) finds very high polarisation along (against) the direction of the spectator quark in the top-quark (top-antiquark) reference frame. The three components of polarisation are measured to be $P_{x'} = 0.01 \pm 0.18$, $P_{y'} = -0.029 \pm 0.027$, $P_{z'} = 0.91 \pm 0.10$ for top quarks and $P_{x'} = -0.02 \pm 0.20$, $P_{y'} = -0.007 \pm 0.051$, $P_{z'} = -0.79 \pm 0.16$ for top antiquarks. The results are consistent with NNLO QCD predictions and expectation of $P^{t}_{y'} = P^{\bar{t}}_{y'} = 0$ from the hypothesis of CP symmetry in the top-quark and top-antiquark decay.

Normalised differential cross-sections for top-quark production are measured at particle level as a function of the emission angle of the charged lepton resulting from the $t \to Wb \to \ell\nu b$ decay. They are provided for top quarks and antiquarks, both inclusively and separately. Such distributions are associated with the top-quark polarisation components. The measurements are consistent with SM predictions provided by various MC generators at LO and NLO in QCD.

An EFT prediction is fitted to the measured differential cross-sections to obtain exclusion limits simultaneously for the real and imaginary parts of the O_{tW} operator. Using a morphing technique, 95% CL intervals for these operators are found to be $C_{tW} \in [-0.9, 1.4]$ and $C_{itW} \in [-0.8, 0.2]$, compatible with

the SM predictions obtained with the NLO MadGraph5_aMC@NLO+Pythia8 generator. The bounds on C_{itW} presented in this paper improve on previous results from ATLAS.

Acknowledgements

We thank CERN for the very successful operation of the LHC, as well as the support staff from our institutions without whom ATLAS could not be operated efficiently.

We acknowledge the support of ANPCyT, Argentina; YerPhI, Armenia; ARC, Australia; BMWFW and FWF, Austria; ANAS, Azerbaijan; SSTC, Belarus; CNPq and FAPESP, Brazil; NSERC, NRC and CFI, Canada; CERN; ANID, Chile; CAS, MOST and NSFC, China; Minciencias, Colombia; MEYS CR, Czech Republic; DNRF and DNSRC, Denmark; IN2P3-CNRS and CEA-DRF/IRFU, France; SRNSFG, Georgia; BMBF, HGF and MPG, Germany; GSRI, Greece; RGC and Hong Kong SAR, China; ISF and Benoziyo Center, Israel; INFN, Italy; MEXT and JSPS, Japan; CNRST, Morocco; NWO, Netherlands; RCN, Norway; MEiN, Poland; FCT, Portugal; MNE/IFA, Romania; JINR; MES of Russia and NRC KI, Russian Federation; MESTD, Serbia; MSSR, Slovakia; ARRS and MIZŠ, Slovenia; DSI/NRF, South Africa; MICINN, Spain; SRC and Wallenberg Foundation, Sweden; SERI, SNSF and Cantons of Bern and Geneva, Switzerland; MOST, Taiwan; TENMAK, Türkiye; STFC, United Kingdom; DOE and NSF, United States of America. In addition, individual groups and members have received support from BCKDF, CANARIE, Compute Canada and CRC, Canada; COST, ERC, ERDF, Horizon 2020 and Marie Skłodowska-Curie Actions, European Union; Investissements d'Avenir Labex, Investissements d'Avenir Idex and ANR, France; DFG and AvH Foundation, Germany; Herakleitos, Thales and Aristeia programmes co-financed by EU-ESF and the Greek NSRF, Greece; BSF-NSF and GIF, Israel; Norwegian Financial Mechanism 2014-2021, Norway; NCN and NAWA, Poland; La Caixa Banking Foundation, CERCA Programme Generalitat de Catalunya and PROMETEO and GenT Programmes Generalitat Valenciana, Spain; Göran Gustafssons Stiftelse, Sweden; The Royal Society and Leverhulme Trust, United Kingdom.

The crucial computing support from all WLCG partners is acknowledged gratefully, in particular from CERN, the ATLAS Tier-1 facilities at TRIUMF (Canada), NDGF (Denmark, Norway, Sweden), CC-IN2P3 (France), KIT/GridKA (Germany), INFN-CNAF (Italy), NL-T1 (Netherlands), PIC (Spain), ASGC (Taiwan), RAL (UK) and BNL (USA), the Tier-2 facilities worldwide and large non-WLCG resource providers. Major contributors of computing resources are listed in Ref. [130].

References

[1] G. L. Kane, J. Pumplin and W. Repko, *Transverse Quark Polarization in Large-p_T Reactions, e^+e^- Jets, and Leptoproduction: A Test of Quantum Chromodynamics*, Phys. Rev. Lett. **41** (1978) 1689.

[2] A. DeVoto, J. Pumplin, W. W. Repko and G. L. Kane, *Polarization of gluon jets in photon-photon scattering*, Phys. Lett. B **90** (1980) 436.

[3] G. L. Kane, G. A. Ladinsky and C.-P. Yuan, *Using the top quark for testing standard-model polarization and* CP *predictions*, Phys. Rev. D **45** (1992) 124.

[4] G. Mahlon and S. J. Parke, *Angular correlations in top quark pair production and decay at hadron colliders*, Phys. Rev. D **53** (1996) 4886, arXiv: hep-ph/9512264.

[5] G. Mahlon and S. J. Parke, *Improved spin basis for angular correlation studies in single top quark production at the Fermilab Tevatron*, Phys. Rev. D **55** (1997) 7249, arXiv: hep-ph/9611367.

[6] G. Mahlon and S. J. Parke, *Single top quark production at the LHC: Understanding spin*, Phys. Lett. B **476** (2000) 323, arXiv: hep-ph/9912458.

[7] J. A. Aguilar-Saavedra and S. Amor Dos Santos, *New directions for top quark polarization in the t-channel process*, Phys. Rev. D **89** (2014) 114009, arXiv: 1404.1585 [hep-ph].

[8] E. L. Berger, J. Gao and H. X. Zhu, *Differential Distributions for t-channel Single Top-Quark Production and Decay at Next-to-Next-to-Leading Order in QCD*, JHEP **11** (2017) 158, arXiv: 1708.09405 [hep-ph].

[9] T.-J. Hou et al., *New CTEQ global analysis of quantum chromodynamics with high-precision data from the LHC*, Phys. Rev. D **103** (2021) 014013, arXiv: 1912.10053 [hep-ph].

[10] M. Cacciari, G. P. Salam and G. Soyez, *The anti-k_t jet clustering algorithm*, JHEP **04** (2008) 063, arXiv: 0802.1189 [hep-ph].

[11] R. Schwienhorst, C.-P. Yuan, C. Mueller and Q.-H. Cao, *Single top quark production and decay in the t channel at next-to-leading order at the LHC*, Phys. Rev. D **83** (2011) 034019, arXiv: 1012.5132 [hep-ph].

[12] H. S. Do, S. Groote, J. G. Körner and M. C. Mauser, *Electroweak and finite width corrections to top quark decays into transverse and longitudinal W bosons*, Phys. Rev. D **67** (2003) 091501, arXiv: hep-ph/0209185.

[13] G. A. González-Sprinberg, R. Martinez and J. Vidal, *Top quark tensor couplings*, JHEP **07** (2011) 094, arXiv: 1105.5601 [hep-ph], Erratum: JHEP **05** (2013) 117.

[14] G. A. González-Sprinberg and J. Vidal, *The top quark right coupling in the tbW-vertex*, Eur. Phys. J. C **75** (2015) 615, arXiv: 1510.02153 [hep-ph].

[15] A. Arhrib and A. Jueid, *tbW Anomalous Couplings in the Two Higgs Doublet Model*, JHEP **08** (2016) 082, arXiv: 1606.05270 [hep-ph].

[16] M. Fischer, S. Groote and J. G. Körner, *T-odd correlations in polarized top quark decays in the sequential decay $t(\uparrow) \to X_b + W^+(\to \ell^+ + \nu_\ell)$ and in the quasi-three-body decay $t(\uparrow) \to X_b + \ell^+ + \nu_\ell$*, Phys. Rev. D **97** (2018) 093001, arXiv: 1802.02492 [hep-ph].

[17] ATLAS Collaboration, *Measurements of top quark spin observables in $t\bar{t}$ events using dilepton final states in $\sqrt{s} = 8$ TeV pp collisions with the ATLAS detector*, JHEP **03** (2017) 113, arXiv: 1612.07004 [hep-ex].

[18] ATLAS Collaboration, *Search for anomalous couplings in the Wtb vertex from the measurement of double differential angular decay rates of single top quarks produced in the t-channel with the ATLAS detector*, JHEP **04** (2016) 023, arXiv: 1510.03764 [hep-ex].

[19] ATLAS Collaboration, *Probing the Wtb vertex structure in t-channel single-top-quark production and decay in pp collisions at $\sqrt{s} = 8$ TeV with the ATLAS detector*, JHEP **04** (2017) 124, arXiv: 1702.08309 [hep-ex].

[20] ATLAS Collaboration, *Analysis of the Wtb vertex from the measurement of triple-differential angular decay rates of single top quarks produced in the t-channel at $\sqrt{s} = 8$ TeV with the ATLAS detector*, JHEP **12** (2017) 017, arXiv: 1707.05393 [hep-ex].

[21] CMS Collaboration, *Measurement of differential cross sections and charge ratios for t-channel single top quark production in proton–proton collisions at* $\sqrt{s} = 13$ *TeV*, Eur. Phys. J. C **80** (2020) 370, arXiv: 1907.08330 [hep-ex].

[22] CMS Collaboration, *Measurement of top quark polarisation in t-channel single top quark production*, JHEP **04** (2016) 073, arXiv: 1511.02138 [hep-ex].

[23] J. A. Aguilar-Saavedra, J. Boudreau, C. Escobar and J. Mueller, *The fully differential top decay distribution*, Eur. Phys. J. C **77** (2017) 200, arXiv: 1702.03297 [hep-ph].

[24] J. A. Aguilar-Saavedra, *Single top quark production at LHC with anomalous Wtb couplings*, Nucl. Phys. B **804** (2008) 160, arXiv: 0803.3810 [hep-ph].

[25] M. Fischer, S. Groote, J. G. Körner and M. C. Mauser, *Complete angular analysis of polarized top decay at* $O(\alpha_s)$, Phys. Rev. D **65** (2002) 054036, arXiv: hep-ph/0101322.

[26] A. Czarnecki, J. G. Körner and J. H. Piclum, *Helicity fractions of W bosons from top quark decays at next-to-next-to-leading order in QCD*, Phys. Rev. D **81** (2010) 111503, arXiv: 1005.2625 [hep-ph].

[27] W. Buchmüller and D. Wyler, *Effective lagrangian analysis of new interactions and flavour conservation*, Nucl. Phys. B **268** (1986) 621.

[28] C. Zhang and S. Willenbrock, *Effective-field-theory approach to top-quark production and decay*, Phys. Rev. D **83** (2011) 034006, arXiv: 1008.3869 [hep-ph].

[29] M. de Beurs, E. Laenen, M. Vreeswijk and E. Vryonidou, *Effective operators in t-channel single top production and decay*, Eur. Phys. J. C **78** (2018) 919, arXiv: 1807.03576 [hep-ph].

[30] B. Grzadkowski, M. Iskrzyński, M. Misiak and J. Rosiek, *Dimension-six terms in the Standard Model Lagrangian*, JHEP **10** (2010) 085, arXiv: 1008.4884 [hep-ph].

[31] I. Brivio et al., *O new physics, where art thou? A global search in the top sector*, JHEP **02** (2020) 131, arXiv: 1910.03606 [hep-ph].

[32] N. P. Hartland et al., *A Monte Carlo global analysis of the Standard Model Effective Field Theory: the top quark sector*, JHEP **04** (2019) 100, arXiv: 1901.05965 [hep-ph].

[33] G. Durieux et al., *The electro-weak couplings of the top and bottom quarks — Global fit and future prospects*, JHEP **12** (2019) 98, arXiv: 1907.10619 [hep-ph], Erratum: JHEP **01** (2021) 195.

[34] J. J. Ethier et al., *Combined SMEFT interpretation of Higgs, diboson, and top quark data from the LHC*, JHEP **11** (2021) 089, arXiv: 2105.00006 [hep-ph].

[35] F. Déliot et al., *Global constraints on top quark anomalous couplings*, Phys. Rev. D **97** (2018) 013007, arXiv: 1711.04847 [hep-ph].

[36] ATLAS and CMS Collaborations, *Combination of the W boson polarization measurements in top quark decays using ATLAS and CMS data at* $\sqrt{s} = 8$ *TeV*, JHEP **08** (2020) 051, arXiv: 2005.03799 [hep-ex].

[37] ATLAS Collaboration, *The ATLAS Experiment at the CERN Large Hadron Collider*, JINST **3** (2008) S08003.

[38] ATLAS Collaboration, *ATLAS data quality operations and performance for 2015–2018 data-taking*, JINST **15** (2020) P04003, arXiv: 1911.04632 [physics.ins-det].

[39] ATLAS Collaboration, *Luminosity determination in pp collisions at* $\sqrt{s} = 13$ *TeV using the ATLAS detector at the LHC*, ATLAS-CONF-2019-021, 2019, URL: https://cds.cern.ch/record/2677054.

[40] G. Avoni et al., *The new LUCID-2 detector for luminosity measurement and monitoring in ATLAS*, JINST **13** (2018) P07017.

[41] ATLAS Collaboration, *Performance of electron and photon triggers in ATLAS during LHC Run 2*, Eur. Phys. J. C **80** (2020) 47, arXiv: 1909.00761 [hep-ex].

[42] ATLAS Collaboration, *Performance of the ATLAS muon triggers in Run 2*, JINST **15** (2020) P09015, arXiv: 2004.13447 [hep-ex].

[43] T. Sjöstrand, S. Mrenna and P. Skands, *A brief introduction to PYTHIA 8.1*, Comput. Phys. Commun. **178** (2008) 852, arXiv: 0710.3820 [hep-ph].

[44] T. Sjöstrand et al., *An introduction to PYTHIA 8.2*, Comput. Phys. Commun. **191** (2015) 159, arXiv: 1410.3012 [hep-ph].

[45] R. D. Ball et al., *Parton distributions with LHC data*, Nucl. Phys. B **867** (2013) 244, arXiv: 1207.1303 [hep-ph].

[46] ATLAS Collaboration, *The Pythia 8 A3 tune description of ATLAS minimum bias and inelastic measurements incorporating the Donnachie–Landshoff diffractive model*, ATL-PHYS-PUB-2016-017, 2016, URL: https://cds.cern.ch/record/2206965.

[47] R. Frederix, E. Re and P. Torrielli, *Single-top t-channel hadroproduction in the four-flavour scheme with POWHEG and aMC@NLO*, JHEP **09** (2012) 130, arXiv: 1207.5391 [hep-ph].

[48] P. Nason, *A new method for combining NLO QCD with shower Monte Carlo algorithms*, JHEP **11** (2004) 040, arXiv: hep-ph/0409146.

[49] S. Frixione, P. Nason and C. Oleari, *Matching NLO QCD computations with parton shower simulations: the POWHEG method*, JHEP **11** (2007) 070, arXiv: 0709.2092 [hep-ph].

[50] S. Alioli, P. Nason, C. Oleari and E. Re, *A general framework for implementing NLO calculations in shower Monte Carlo programs: the POWHEG BOX*, JHEP **06** (2010) 043, arXiv: 1002.2581 [hep-ph].

[51] R. D. Ball et al., *Parton distributions for the LHC run II*, JHEP **04** (2015) 040, arXiv: 1410.8849 [hep-ph].

[52] J. Pumplin et al., *New Generation of Parton Distributions with Uncertainties from Global QCD Analysis*, JHEP **07** (2002) 012, arXiv: hep-ph/0201195.

[53] T. Stelzer, Z. Sullivan and S. Willenbrock, *Single-top-quark production via W-gluon fusion at next-to-leading order*, Phys. Rev. D **56** (1997) 5919, arXiv: hep-ph/9705398.

[54] E. Boos, L. Dudko and T. Ohl, *Complete calculations of $Wb\bar{b}$ and $Wb\bar{b}$ + jet production at Tevatron and LHC: Probing anomalous Wtb couplings in single top production*, Eur. Phys. J. C **11** (1999) 473, arXiv: hep-ph/9903215.

[55] C.-R. Chen, F. Larios and C.-P. Yuan, *General analysis of single top production and W helicity in top decay*, Phys. Lett. B **631** (2005) 126, arXiv: hep-ph/0503040.

[56] J. A. Aguilar-Saavedra, *A Minimal set of top anomalous couplings*, Nucl. Phys. B **812** (2009) 181, arXiv: 0811.3842 [hep-ph].

[57] J. Alwall et al., *The automated computation of tree-level and next-to-leading order differential cross sections, and their matching to parton shower simulations*, JHEP **07** (2014) 079, arXiv: 1405.0301 [hep-ph].

[58] C. Zhang, *Single Top Production at Next-to-Leading Order in the Standard Model Effective Field Theory*, Phys. Rev. Lett. **116** (2016) 162002, arXiv: 1601.06163 [hep-ph].

[59] J. M. Campbell, R. Frederix, F. Maltoni and F. Tramontano, *Next-to-Leading-Order Predictions for t-Channel Single-Top Production at Hadron Colliders*, Phys. Rev. Lett. **102** (18 2009) 182003.

[60] M. Aliev et al., *HATHOR – HAdronic Top and Heavy quarks crOss section calculatoR*, Comput. Phys. Commun. **182** (2011) 1034, arXiv: 1007.1327 [hep-ph].

[61] P. Kant et al., *HatHor for single top-quark production: Updated predictions and uncertainty estimates for single top-quark production in hadronic collisions*, Comput. Phys. Commun. **191** (2015) 74, arXiv: 1406.4403 [hep-ph].

[62] J. Butterworth et al., *PDF4LHC recommendations for LHC Run II*, J. Phys. G **43** (2016) 023001, arXiv: 1510.03865 [hep-ph].

[63] A. D. Martin, W. J. Stirling, R. S. Thorne and G. Watt, *Parton distributions for the LHC*, Eur. Phys. J. C **63** (2009) 189, arXiv: 0901.0002 [hep-ph].

[64] A. D. Martin, W. J. Stirling, R. S. Thorne and G. Watt, *Uncertainties on α_S in global PDF analyses and implications for predicted hadronic cross sections*, Eur. Phys. J. C **64** (2009) 653, arXiv: 0905.3531 [hep-ph].

[65] J. Gao et al., *CT10 next-to-next-to-leading order global analysis of QCD*, Phys. Rev. D **89** (2014) 033009, arXiv: 1302.6246 [hep-ph].

[66] ATLAS Collaboration, *Studies on top-quark Monte Carlo modelling for Top2016*, ATL-PHYS-PUB-2016-020, 2016, URL: https://cds.cern.ch/record/2216168.

[67] S. Frixione, E. Laenen, P. Motylinski, C. White and B. R. Webber, *Single-top hadroproduction in association with a W boson*, JHEP **07** (2008) 029, arXiv: 0805.3067 [hep-ph].

[68] P. Bärnreuther, M. Czakon and A. Mitov, *Percent-Level-Precision Physics at the Tevatron: Next-to-Next-to-Leading Order QCD Corrections to $q\bar{q} \to t\bar{t} + X$*, Phys. Rev. Lett. **109** (2012) 132001, arXiv: 1204.5201 [hep-ph].

[69] M. Czakon and A. Mitov, *Top++: A program for the calculation of the top-pair cross-section at hadron colliders*, Comput. Phys. Commun. **185** (2014) 2930, arXiv: 1112.5675 [hep-ph].

[70] M. Czakon and A. Mitov, *NNLO corrections to top-pair production at hadron colliders: the all-fermionic scattering channels*, JHEP **12** (2012) 054, arXiv: 1207.0236 [hep-ph].

[71] M. Czakon and A. Mitov, *NNLO corrections to top pair production at hadron colliders: the quark-gluon reaction*, JHEP **01** (2013) 080, arXiv: 1210.6832 [hep-ph].

[72] M. Czakon, P. Fiedler and A. Mitov, *Total Top-Quark Pair-Production Cross Section at Hadron Colliders Through $O(\alpha_S^4)$*, Phys. Rev. Lett. **110** (2013) 252004, arXiv: 1303.6254 [hep-ph].

[73] M. Cacciari, M. Czakon, M. Mangano, A. Mitov and P. Nason, *Top-pair production at hadron colliders with next-to-next-to-leading logarithmic soft-gluon resummation*, Phys. Lett. B **710** (2012) 612, arXiv: 1111.5869 [hep-ph].

[74] H.-L. Lai et al., *New parton distributions for collider physics*, Phys. Rev. D **82** (2010) 074024, arXiv: 1007.2241 [hep-ph].

[75] N. Kidonakis, *Two-loop soft anomalous dimensions for single top quark associated production with a W^- or H^-*, Phys. Rev. D **82** (2010) 054018, arXiv: 1005.4451 [hep-ph].

[76] E. Bothmann et al., *Event generation with Sherpa 2.2*, SciPost Phys. **7** (2019) 034, arXiv: 1905.09127 [hep-ph].

[77] S. Höche, F. Krauss, M. Schönherr and F. Siegert, *A critical appraisal of NLO+PS matching methods*, JHEP **09** (2012) 049, arXiv: 1111.1220 [hep-ph].

[78] S. Catani, F. Krauss, B. R. Webber and R. Kuhn, *QCD Matrix Elements + Parton Showers*, JHEP **11** (2001) 063, arXiv: hep-ph/0109231.

[79] S. Höche, F. Krauss, S. Schumann and F. Siegert, *QCD matrix elements and truncated showers*, JHEP **05** (2009) 053, arXiv: 0903.1219 [hep-ph].

[80] S. Höche, F. Krauss, M. Schönherr and F. Siegert, *QCD matrix elements + parton showers. The NLO case*, JHEP **04** (2013) 027, arXiv: 1207.5030 [hep-ph].

[81] F. Cascioli, P. Maierhöfer and S. Pozzorini, *Scattering Amplitudes with Open Loops*, Phys. Rev. Lett. **108** (2012) 111601, arXiv: 1111.5206 [hep-ph].

[82] A. Denner, S. Dittmaier and L. Hofer, *Collier: A fortran-based complex one-loop library in extended regularizations*, Comput. Phys. Commun. **212** (2017) 220, arXiv: 1604.06792 [hep-ph].

[83] ATLAS Collaboration, *ATLAS simulation of boson plus jets processes in Run 2*, ATL-PHYS-PUB-2017-006, 2017, URL: https://cds.cern.ch/record/2261937.

[84] C. Anastasiou, L. Dixon, K. Melnikov and F. Petriello, *High-precision QCD at hadron colliders: Electroweak gauge boson rapidity distributions at next-to-next-to leading order*, Phys. Rev. D **69** (2004) 094008, arXiv: hep-ph/0312266.

[85] F. A. Berends, H. Kuijf, B. Tausk and W. T. Giele, *On the production of a W and jets at hadron colliders*, Nucl. Phys. B **357** (1991) 32.

[86] S. Frixione, E. Laenen, P. Motylinski and B. R. Webber, *Angular correlations of lepton pairs from vector boson and top quark decays in Monte Carlo simulations*, JHEP **04** (2007) 081, arXiv: hep-ph/0702198.

[87] P. Artoisenet, R. Frederix, O. Mattelaer and R. Rietkerk, *Automatic spin-entangled decays of heavy resonances in Monte Carlo simulations*, JHEP **03** (2013) 015, arXiv: 1212.3460 [hep-ph].

[88] ATLAS Collaboration, *ATLAS Pythia 8 tunes to 7 TeV data*, ATL-PHYS-PUB-2014-021, 2014, URL: https://cds.cern.ch/record/1966419.

[89] D. J. Lange, *The EvtGen particle decay simulation package*, Nucl. Instrum. Meth. A **462** (2001) 152.

[90] M. Bähr et al., *Herwig++ physics and manual*, Eur. Phys. J. C **58** (2008) 639, arXiv: 0803.0883 [hep-ph].

[91] J. Bellm et al., *Herwig 7.0/Herwig++ 3.0 release note*, Eur. Phys. J. C **76** (2016) 196, arXiv: 1512.01178 [hep-ph].

[92] L. A. Harland-Lang, A. D. Martin, P. Motylinski and R. S. Thorne, *Parton distributions in the LHC era: MMHT 2014 PDFs*, Eur. Phys. J. C **75** (2015) 204, arXiv: 1412.3989 [hep-ph].

[93] ATLAS Collaboration, *The ATLAS Simulation Infrastructure*, Eur. Phys. J. C **70** (2010) 823, arXiv: 1005.4568 [physics.ins-det].

[94] GEANT4 Collaboration, S. Agostinelli et al., *Geant4 – a simulation toolkit*, Nucl. Instrum. Meth. A **506** (2003) 250.

[95] ATLAS Collaboration, *The simulation principle and performance of the ATLAS fast calorimeter simulation FastCaloSim*, ATL-PHYS-PUB-2010-013, 2010, URL: https://cds.cern.ch/record/1300517.

[96] ATLAS Collaboration, *The ATLAS Collaboration Software and Firmware*, ATL-SOFT-PUB-2021-001, 2021, URL: https://cds.cern.ch/record/2767187.

[97] ATLAS Collaboration, *Electron and photon performance measurements with the ATLAS detector using the 2015–2017 LHC proton–proton collision data*, JINST **14** (2019) P12006, arXiv: 1908.00005 [hep-ex].

[98] ATLAS Collaboration, *Muon reconstruction and identification efficiency in ATLAS using the full Run 2 pp collision data set at* $\sqrt{s} = 13$ *TeV*, Eur. Phys. J. C **81** (2021) 578, arXiv: 2012.00578 [hep-ex].

[99] ATLAS Collaboration, *Topological cell clustering in the ATLAS calorimeters and its performance in LHC Run 1*, Eur. Phys. J. C **77** (2017) 490, arXiv: 1603.02934 [hep-ex].

[100] ATLAS Collaboration, *Jet energy scale and resolution measured in proton–proton collisions at* $\sqrt{s} = 13$ *TeV with the ATLAS detector*, Eur. Phys. J. C **81** (2020) 689, arXiv: 2007.02645 [hep-ex].

[101] ATLAS Collaboration, *Performance of pile-up mitigation techniques for jets in pp collisions at* $\sqrt{s} = 8$ *TeV using the ATLAS detector*, Eur. Phys. J. C **76** (2016) 581, arXiv: 1510.03823 [hep-ex].

[102] ATLAS Collaboration, *Optimisation and performance studies of the ATLAS b-tagging algorithms for the 2017-18 LHC run*, ATL-PHYS-PUB-2017-013, 2017, URL: https://cds.cern.ch/record/2273281.

[103] ATLAS Collaboration, *ATLAS b-jet identification performance and efficiency measurement with* $t\bar{t}$ *events in pp collisions at* $\sqrt{s} = 13$ *TeV*, Eur. Phys. J. C **79** (2019) 970, arXiv: 1907.05120 [hep-ex].

[104] ATLAS Collaboration, *Measurements of b-jet tagging efficiency with the ATLAS detector using* $t\bar{t}$ *events at* $\sqrt{s} = 13$ *TeV*, JHEP **08** (2018) 089, arXiv: 1805.01845 [hep-ex].

[105] ATLAS Collaboration, *Measurement of b-tagging efficiency of c-jets in* $t\bar{t}$ *events using a likelihood approach with the ATLAS detector*, ATLAS-CONF-2018-001, 2018, URL: https://cds.cern.ch/record/2306649.

[106] ATLAS Collaboration, *Calibration of light-flavour b-jet mistagging rates using ATLAS proton–proton collision data at* $\sqrt{s} = 13$ *TeV*, ATLAS-CONF-2018-006, 2018, URL: https://cds.cern.ch/record/2314418.

[107] ATLAS Collaboration, *Performance of missing transverse momentum reconstruction with the ATLAS detector using proton–proton collisions at* $\sqrt{s} = 13$ *TeV*, Eur. Phys. J. C **78** (2018) 903, arXiv: 1802.08168 [hep-ex].

[108] ATLAS Collaboration, E_T^{miss} *performance in the ATLAS detector using 2015–2016 LHC pp collisions*, ATLAS-CONF-2018-023, 2018, URL: https://cds.cern.ch/record/2625233.

[109] ATLAS Collaboration, *Vertex Reconstruction Performance of the ATLAS Detector at* $\sqrt{s} = 13$ *TeV*, ATL-PHYS-PUB-2015-026, 2015, URL: https://cds.cern.ch/record/2037717.

[110] ATLAS Collaboration, *Electron identification measurements in ATLAS using* $\sqrt{s} = 13$ *TeV data with 50 ns bunch spacing*, ATL-PHYS-PUB-2015-041, 2015, URL: https://cds.cern.ch/record/2048202.

[111] ATLAS Collaboration, *Electron and photon energy calibration with the ATLAS detector using data collected in 2015 at $\sqrt{s}$ = 13 TeV*, ATL-PHYS-PUB-2016-015, 2016, URL: https://cds.cern.ch/record/2203514.

[112] ATLAS Collaboration, *Fiducial, total and differential cross-section measurements of t-channel single top-quark production in pp collisions at 8 TeV using data collected by the ATLAS detector*, Eur. Phys. J. C **77** (2017) 531, arXiv: 1702.02859 [hep-ex].

[113] M. Cacciari, G. P. Salam and G. Soyez, *The catchment area of jets*, JHEP **04** (2008) 005, arXiv: 0802.1188 [hep-ph].

[114] ATLAS Collaboration, *Estimation of non-prompt and fake lepton backgrounds in final states with top quarks produced in proton–proton collisions at $\sqrt{s}$ = 8 TeV with the ATLAS Detector*, ATLAS-CONF-2014-058, 2014, URL: https://cds.cern.ch/record/1951336.

[115] ATLAS Collaboration, *Measurement of the top quark pair production cross-section with ATLAS in the single lepton channel*, Phys. Lett. B **711** (2012) 244, arXiv: 1201.1889 [hep-ex].

[116] ATLAS Collaboration, *Study of top-quark pair modelling and uncertainties using ATLAS measurements at $\sqrt{s}$ = 13 TeV*, ATL-PHYS-PUB-2020-023, 2020, URL: https://cds.cern.ch/record/2730443.

[117] ATLAS Collaboration, *Evidence for the $H \to b\bar{b}$ decay with the ATLAS detector*, JHEP **12** (2017) 024, arXiv: 1708.03299 [hep-ex].

[118] ATLAS Collaboration, *Measurement of the inclusive cross-sections of single top-quark and top-antiquark t-channel production in pp collisions at $\sqrt{s}$ = 13 TeV with the ATLAS detector*, JHEP **04** (2017) 086, arXiv: 1609.03920 [hep-ex].

[119] ATLAS Collaboration, *Measurement of the t-channel single top-quark production cross section in pp collisions at $\sqrt{s}$ = 7 TeV with the ATLAS detector*, Phys. Lett. B **717** (2012) 330, arXiv: 1205.3130 [hep-ex].

[120] ATLAS Collaboration, *Fiducial, total and differential cross-section measurements of t-channel single top-quark production in pp collisions at 8 TeV using data collected by the ATLAS detector*, Eur. Phys. J. C **77** (2017) 531, arXiv: 1702.02859 [hep-ex].

[121] G. D'Agostini, *A Multidimensional unfolding method based on Bayes' theorem*, Nucl. Instrum. Meth. A **362** (1995) 487.

[122] T. Adye, 'Unfolding algorithms and tests using RooUnfold', *Proceedings, 2011 Workshop on Statistical Issues Related to Discovery Claims in Search Experiments and Unfolding (PHYSTAT 2011)* (CERN, Geneva, Switzerland, 17th–20th Jan. 2011) 313, arXiv: 1105.1160 [physics.data-an].

[123] G. Bohm and G. Zech, *Introduction to Statistics and Data Analysis for Physicists; 3rd revised*, Hamburg: Verlag Deutsches Elektronen-Synchrotron, 2017, ISBN: 978-3-945931-13-4, URL: https://bib-pubdb1.desy.de/record/389738.

[124] J. A. Aguilar-Saavedra, C. Degrande and S. Khatibi, *Single top polarisation as a window to new physics*, Phys. Lett. B **769** (2017) 498, arXiv: 1701.05900 [hep-ph].

[125] M. Baak, S. Gadatsch, R. Harrington and W. Verkerke, *Interpolation between multi-dimensional histograms using a new non-linear moment morphing method*, Nucl. Instrum. Meth. A **771** (2015) 39, arXiv: 1410.7388 [physics.data-an].

[126] ATLAS Collaboration, *A morphing technique for signal modelling in a multidimensional space of coupling parameters*, ATL-PHYS-PUB-2015-047, 2015, URL: https://cds.cern.ch/record/2066980.

[127] ATLAS Collaboration, *Measurement of the W boson polarisation in $t\bar{t}$ events from pp collisions at $\sqrt{s}$ = 8 TeV in the lepton+jets channel with ATLAS*, Eur. Phys. J. C **77** (2017) 264, arXiv: 1612.02577 [hep-ex], Erratum: Eur. Phys. J. C **79** (2019) 19.

[128] CMS Collaboration, *Measurement of the W boson helicity fractions in the decays of top quark pairs to lepton+jets final states produced in pp collisions at $\sqrt{s}$ = 8 TeV*, Phys. Lett. B **762** (2016) 512, arXiv: 1605.09047 [hep-ex].

[129] V. Cirigliano, W. Dekens, J. de Vries and E. Mereghetti, *Constraining the top-Higgs sector of the Standard Model Effective Field Theory*, Phys. Rev. D **94** (2016) 034031, arXiv: 1605.04311 [hep-ph].

[130] ATLAS Collaboration, *ATLAS Computing Acknowledgements*, ATL-SOFT-PUB-2021-003, URL: https://cds.cern.ch/record/2776662.

The ATLAS Collaboration

G. Aad[99], B. Abbott[124], D.C. Abbott[100], A. Abed Abud[34], K. Abeling[51], D.K. Abhayasinghe[91], S.H. Abidi[27], H. Abramowicz[157], H. Abreu[156], Y. Abulaiti[5], A.C. Abusleme Hoffman[142a], B.S. Acharya[64a,64b,p], B. Achkar[51], L. Adam[97], C. Adam Bourdarios[4], L. Adamczyk[81a], L. Adamek[162], S.V. Addepalli[24], J. Adelman[117], A. Adiguzel[11c,ae], S. Adorni[52], T. Adye[139], A.A. Affolder[141], Y. Afik[156], C. Agapopoulou[62], M.N. Agaras[12], J. Agarwala[68a,68b], A. Aggarwal[115], C. Agheorghiesei[25c], J.A. Aguilar-Saavedra[135f,135a,ad], A. Ahmad[34], F. Ahmadov[77,ab], W.S. Ahmed[101], X. Ai[44], G. Aielli[71a,71b], I. Aizenberg[175], S. Akatsuka[83], M. Akbiyik[97], T.P.A. Åkesson[94], A.V. Akimov[108], K. Al Khoury[37], G.L. Alberghi[21b], J. Albert[171], P. Albicocco[49], M.J. Alconada Verzini[86], S. Alderweireldt[48], M. Aleksa[34], I.N. Aleksandrov[77], C. Alexa[25b], T. Alexopoulos[9], A. Alfonsi[116], F. Alfonsi[21b], M. Alhroob[124], B. Ali[137], S. Ali[154], M. Aliev[161], G. Alimonti[66a], C. Allaire[34], B.M.M. Allbrooke[152], P.P. Allport[19], A. Aloisio[67a,67b], F. Alonso[86], C. Alpigiani[144], E. Alunno Camelia[71a,71b], M. Alvarez Estevez[96], M.G. Alviggi[67a,67b], Y. Amaral Coutinho[78b], A. Ambler[101], L. Ambroz[130], C. Amelung[34], D. Amidei[103], S.P. Amor Dos Santos[135a], S. Amoroso[44], C.S. Amrouche[52], C. Anastopoulos[145], N. Andari[140], T. Andeen[10], J.K. Anders[18], S.Y. Andrean[43a,43b], A. Andreazza[66a,66b], S. Angelidakis[8], A. Angerami[37], A.V. Anisenkov[118b,118a], A. Annovi[69a], C. Antel[52], M.T. Anthony[145], E. Antipov[125], M. Antonelli[49], D.J.A. Antrim[16], F. Anulli[70a], M. Aoki[79], J.A. Aparisi Pozo[169], M.A. Aparo[152], L. Aperio Bella[44], N. Aranzabal[34], V. Araujo Ferraz[78a], C. Arcangeletti[49], A.T.H. Arce[47], E. Arena[88], J-F. Arguin[107], S. Argyropoulos[50], J.-H. Arling[44], A.J. Armbruster[34], A. Armstrong[166], O. Arnaez[162], H. Arnold[34], Z.P. Arrubarrena Tame[111], G. Artoni[130], H. Asada[113], K. Asai[122], S. Asai[159], N.A. Asbah[57], E.M. Asimakopoulou[167], L. Asquith[152], J. Assahsah[33d], K. Assamagan[27], R. Astalos[26a], R.J. Atkin[31a], M. Atkinson[168], N.B. Atlay[17], H. Atmani[58b], P.A. Atmasiddha[103], K. Augsten[137], S. Auricchio[67a,67b], V.A. Austrup[177], G. Avner[156], G. Avolio[34], M.K. Ayoub[13c], G. Azuelos[107,al], D. Babal[26a], H. Bachacou[140], K. Bachas[158], A. Bachiu[32], F. Backman[43a,43b], A. Badea[57], P. Bagnaia[70a,70b], H. Bahrasemani[148], A.J. Bailey[169], V.R. Bailey[168], J.T. Baines[139], C. Bakalis[9], O.K. Baker[178], P.J. Bakker[116], E. Bakos[14], D. Bakshi Gupta[7], S. Balaji[153], R. Balasubramanian[116], E.M. Baldin[118b,118a], P. Balek[138], E. Ballabene[66a,66b], F. Balli[140], W.K. Balunas[130], J. Balz[97], E. Banas[82], M. Bandieramonte[134], A. Bandyopadhyay[17], S. Bansal[22], L. Barak[157], E.L. Barberio[102], D. Barberis[53b,53a], M. Barbero[99], G. Barbour[92], K.N. Barends[31a], T. Barillari[112], M-S. Barisits[34], J. Barkeloo[127], T. Barklow[149], B.M. Barnett[139], R.M. Barnett[16], A. Baroncelli[58a], G. Barone[27], A.J. Barr[130], L. Barranco Navarro[43a,43b], F. Barreiro[96], J. Barreiro Guimarães da Costa[13a], U. Barron[157], S. Barsov[133], F. Bartels[59a], R. Bartoldus[149], G. Bartolini[99], A.E. Barton[87], P. Bartos[26a], A. Basalaev[44], A. Basan[97], I. Bashta[72a,72b], A. Bassalat[62,ai], M.J. Basso[162], C.R. Basson[98], R.L. Bates[55], S. Batlamous[33e], J.R. Batley[30], B. Batool[147], M. Battaglia[141], M. Bauce[70a,70b], F. Bauer[140,*], P. Bauer[22], H.S. Bawa[29], A. Bayirli[11c], J.B. Beacham[47], T. Beau[131], P.H. Beauchemin[165], F. Becherer[50], P. Bechtle[22], H.P. Beck[18,r], K. Becker[173], C. Becot[44], A.J. Beddall[11a], V.A. Bednyakov[77], C.P. Bee[151], T.A. Beermann[177], M. Begalli[78b], M. Begel[27], A. Behera[151], J.K. Behr[44], C. Beirao Da Cruz E Silva[34], J.F. Beirer[51,34], F. Beisiegel[22], M. Belfkir[4], G. Bella[157], L. Bellagamba[21b], A. Bellerive[32], P. Bellos[19], K. Beloborodov[118b,118a], K. Belotskiy[109], N.L. Belyaev[109], D. Benchekroun[33a], Y. Benhammou[157], D.P. Benjamin[27], M. Benoit[27], J.R. Bensinger[24], S. Bentvelsen[116], L. Beresford[34], M. Beretta[49], D. Berge[17], E. Bergeaas Kuutmann[167], N. Berger[4], B. Bergmann[137], L.J. Bergsten[24], J. Beringer[16], S. Berlendis[6], G. Bernardi[131], C. Bernius[149], F.U. Bernlochner[22], T. Berry[91], P. Berta[138], A. Berthold[46], I.A. Bertram[87], O. Bessidskaia Bylund[177], S. Bethke[112], A. Betti[40], A.J. Bevan[90], S. Bhatta[151], D.S. Bhattacharya[172], P. Bhattarai[24], V.S. Bhopatkar[5], R. Bi[134], R.M. Bianchi[134], O. Biebel[111], R. Bielski[127], N.V. Biesuz[69a,69b], M. Biglietti[72a], T.R.V. Billoud[137], M. Bindi[51], A. Bingul[11d], C. Bini[70a,70b], S. Biondi[21b,21a], A. Biondini[88], C.J. Birch-sykes[98], G.A. Bird[19,139], M. Birman[175],

T. Bisanz[34], J.P. Biswal[2], D. Biswas[176,k], A. Bitadze[98], C. Bittrich[46], K. Bjørke[129], I. Bloch[44], C. Blocker[24], A. Blue[55], U. Blumenschein[90], J. Blumenthal[97], G.J. Bobbink[116], V.S. Bobrovnikov[118b,118a], M. Boehler[50], D. Bogavac[12], A.G. Bogdanchikov[118b,118a], C. Bohm[43a], V. Boisvert[91], P. Bokan[44], T. Bold[81a], M. Bomben[131], M. Bona[90], M. Boonekamp[140], C.D. Booth[91], A.G. Borbély[55], H.M. Borecka-Bielska[107], L.S. Borgna[92], G. Borissov[87], D. Bortoletto[130], D. Boscherini[21b], M. Bosman[12], J.D. Bossio Sola[34], K. Bouaouda[33a], J. Boudreau[134], E.V. Bouhova-Thacker[87], D. Boumediene[36], R. Bouquet[131], A. Boveia[123], J. Boyd[34], D. Boye[27], I.R. Boyko[77], A.J. Bozson[91], J. Bracinik[19], N. Brahimi[58d,58c], G. Brandt[177], O. Brandt[30], F. Braren[44], B. Brau[100], J.E. Brau[127], W.D. Breaden Madden[55], K. Brendlinger[44], R. Brener[175], L. Brenner[34], R. Brenner[167], S. Bressler[175], B. Brickwedde[97], D.L. Briglin[19], D. Britton[55], D. Britzger[112], I. Brock[22], R. Brock[104], G. Brooijmans[37], W.K. Brooks[142d], E. Brost[27], P.A. Bruckman de Renstrom[82], B. Brüers[44], D. Bruncko[26b], A. Bruni[21b], G. Bruni[21b], M. Bruschi[21b], N. Bruscino[70a,70b], L. Bryngemark[149], T. Buanes[15], Q. Buat[151], P. Buchholz[147], A.G. Buckley[55], I.A. Budagov[77], M.K. Bugge[129], O. Bulekov[109], B.A. Bullard[57], T.J. Burch[117], S. Burdin[88], C.D. Burgard[44], A.M. Burger[125], B. Burghgrave[7], J.T.P. Burr[44], C.D. Burton[10], J.C. Burzynski[100], V. Büscher[97], P.J. Bussey[55], J.M. Butler[23], C.M. Buttar[55], J.M. Butterworth[92], W. Buttinger[139], C.J. Buxo Vazquez[104], A.R. Buzykaev[118b,118a], G. Cabras[21b], S. Cabrera Urbán[169], D. Caforio[54], H. Cai[134], V.M.M. Cairo[149], O. Cakir[3a], N. Calace[34], P. Calafiura[16], G. Calderini[131], P. Calfayan[63], G. Callea[55], L.P. Caloba[78b], S. Calvente Lopez[96], D. Calvet[36], S. Calvet[36], T.P. Calvet[99], M. Calvetti[69a,69b], R. Camacho Toro[131], S. Camarda[34], D. Camarero Munoz[96], P. Camarri[71a,71b], M.T. Camerlingo[72a,72b], D. Cameron[129], C. Camincher[171], M. Campanelli[92], A. Camplani[38], V. Canale[67a,67b], A. Canesse[101], M. Cano Bret[75], J. Cantero[125], Y. Cao[168], F. Capocasa[24], M. Capua[39b,39a], A. Carbone[66a,66b], R. Cardarelli[71a], J.C.J. Cardenas[7], F. Cardillo[169], G. Carducci[39b,39a], T. Carli[34], G. Carlino[67a], B.T. Carlson[134], E.M. Carlson[171,163a], L. Carminati[66a,66b], M. Carnesale[70a,70b], R.M.D. Carney[149], S. Caron[115], E. Carquin[142d], S. Carrá[44], G. Carratta[21b,21a], J.W.S. Carter[162], T.M. Carter[48], D. Casadei[31c], M.P. Casado[12,h], A.F. Casha[162], E.G. Castiglia[178], F.L. Castillo[59a], L. Castillo Garcia[12], V. Castillo Gimenez[169], N.F. Castro[135a,135e], A. Catinaccio[34], J.R. Catmore[129], A. Cattai[34], V. Cavaliere[27], N. Cavalli[21b,21a], V. Cavasinni[69a,69b], E. Celebi[11b], F. Celli[130], M.S. Centonze[65a,65b], K. Cerny[126], A.S. Cerqueira[78a], A. Cerri[152], L. Cerrito[71a,71b], F. Cerutti[16], A. Cervelli[21b], S.A. Cetin[11b], Z. Chadi[33a], D. Chakraborty[117], M. Chala[135f], J. Chan[176], W.S. Chan[116], W.Y. Chan[88], J.D. Chapman[30], B. Chargeishvili[155b], D.G. Charlton[19], T.P. Charman[90], M. Chatterjee[18], S. Chekanov[5], S.V. Chekulaev[163a], G.A. Chelkov[77,ag], A. Chen[103], B. Chen[157], C. Chen[58a], C.H. Chen[76], H. Chen[13c], H. Chen[27], J. Chen[58c], J. Chen[24], S. Chen[132], S.J. Chen[13c], X. Chen[58c], X. Chen[13b], Y. Chen[58a], Y-H. Chen[44], C.L. Cheng[176], H.C. Cheng[60a], A. Cheplakov[77], E. Cheremushkina[44], E. Cherepanova[77], R. Cherkaoui El Moursli[33e], E. Cheu[6], K. Cheung[61], L. Chevalier[140], V. Chiarella[49], G. Chiarelli[69a], G. Chiodini[65a], A.S. Chisholm[19], A. Chitan[25b], Y.H. Chiu[171], M.V. Chizhov[77,t], K. Choi[10], A.R. Chomont[70a,70b], Y. Chou[100], E.Y.S. Chow[116], L.D. Christopher[31f], M.C. Chu[60a], X. Chu[13a,13d], J. Chudoba[136], J.J. Chwastowski[82], D. Cieri[112], K.M. Ciesla[82], V. Cindro[89], I.A. Cioară[25b], A. Ciocio[16], F. Cirotto[67a,67b], Z.H. Citron[175,l], M. Citterio[66a], D.A. Ciubotaru[25b], B.M. Ciungu[162], A. Clark[52], P.J. Clark[48], J.M. Clavijo Columbie[44], S.E. Clawson[98], C. Clement[43a,43b], L. Clissa[21b,21a], Y. Coadou[99], M. Cobal[64a,64c], A. Coccaro[53b], J. Cochran[76], R.F. Coelho Barrue[135a], R. Coelho Lopes De Sa[100], S. Coelli[66a], H. Cohen[157], A.E.C. Coimbra[34], B. Cole[37], J. Collot[56], P. Conde Muiño[135a,135h], S.H. Connell[31c], I.A. Connelly[55], E.I. Conroy[130], F. Conventi[67a,am], H.G. Cooke[19], A.M. Cooper-Sarkar[130], F. Cormier[170], L.D. Corpe[34], M. Corradi[70a,70b], E.E. Corrigan[94], F. Corriveau[101,aa], M.J. Costa[169], F. Costanza[4], D. Costanzo[145], B.M. Cote[123], G. Cowan[91], J.W. Cowley[30], K. Cranmer[121], S. Crépé-Renaudin[56], F. Crescioli[131], M. Cristinziani[147], M. Cristoforetti[73a,73b,b], V. Croft[165], G. Crosetti[39b,39a], A. Cueto[34], T. Cuhadar Donszelmann[166], H. Cui[13a,13d], A.R. Cukierman[149], W.R. Cunningham[55], P. Czodrowski[34], M.M. Czurylo[59b], M.J. Da Cunha Sargedas De Sousa[58a], J.V. Da Fonseca Pinto[78b], C. Da Via[98],

W. Dabrowski[81a], T. Dado[45], S. Dahbi[31f], T. Dai[103], C. Dallapiccola[100], M. Dam[38], G. D'amen[27], V. D'Amico[72a,72b], J. Damp[97], J.R. Dandoy[132], M.F. Daneri[28], M. Danninger[148], V. Dao[34], G. Darbo[53b], S. Darmora[5], A. Dattagupta[127], S. D'Auria[66a,66b], C. David[163b], T. Davidek[138], D.R. Davis[47], B. Davis-Purcell[32], I. Dawson[90], K. De[7], R. De Asmundis[67a], M. De Beurs[116], S. De Castro[21b,21a], N. De Groot[115], P. de Jong[116], H. De la Torre[104], A. De Maria[13c], D. De Pedis[70a], A. De Salvo[70a], U. De Sanctis[71a,71b], M. De Santis[71a,71b], A. De Santo[152], J.B. De Vivie De Regie[56], D.V. Dedovich[77], J. Degens[116], A.M. Deiana[40], J. Del Peso[96], Y. Delabat Diaz[44], F. Deliot[140], C.M. Delitzsch[6], M. Della Pietra[67a,67b], D. Della Volpe[52], A. Dell'Acqua[34], L. Dell'Asta[66a,66b], M. Delmastro[4], P.A. Delsart[56], S. Demers[178], M. Demichev[77], S.P. Denisov[119], L. D'Eramo[117], D. Derendarz[82], J.E. Derkaoui[33d], F. Derue[131], P. Dervan[88], K. Desch[22], K. Dette[162], C. Deutsch[22], P.O. Deviveiros[34], F.A. Di Bello[70a,70b], A. Di Ciaccio[71a,71b], L. Di Ciaccio[4], C. Di Donato[67a,67b], A. Di Girolamo[34], G. Di Gregorio[69a,69b], A. Di Luca[73a,73b], B. Di Micco[72a,72b], R. Di Nardo[72a,72b], C. Diaconu[99], F.A. Dias[116], T. Dias Do Vale[135a], M.A. Diaz[142a], F.G. Diaz Capriles[22], J. Dickinson[16], M. Didenko[169], E.B. Diehl[103], J. Dietrich[17], S. Díez Cornell[44], C. Diez Pardos[147], A. Dimitrievska[16], W. Ding[13b], J. Dingfelder[22], I-M. Dinu[25b], S.J. Dittmeier[59b], F. Dittus[34], F. Djama[99], T. Djobava[155b], J.I. Djuvsland[15], M.A.B. Do Vale[143], D. Dodsworth[24], C. Doglioni[94], J. Dolejsi[138], Z. Dolezal[138], M. Donadelli[78c], B. Dong[58c], J. Donini[36], A. D'onofrio[13c], M. D'Onofrio[88], J. Dopke[139], A. Doria[67a], M.T. Dova[86], A.T. Doyle[55], E. Drechsler[148], E. Dreyer[148], T. Dreyer[51], A.S. Drobac[165], D. Du[58b], T.A. du Pree[116], F. Dubinin[108], M. Dubovsky[26a], A. Dubreuil[52], E. Duchovni[175], G. Duckeck[111], O.A. Ducu[34,25b], D. Duda[112], A. Dudarev[34], M. D'uffizi[98], L. Duflot[62], M. Dührssen[34], C. Dülsen[177], A.E. Dumitriu[25b], M. Dunford[59a], S. Dungs[45], K. Dunne[43a,43b], A. Duperrin[99], H. Duran Yildiz[3a], M. Düren[54], A. Durglishvili[155b], B. Dutta[44], B.L. Dwyer[117], G.I. Dyckes[132], M. Dyndal[81a], S. Dysch[98], B.S. Dziedzic[82], B. Eckerova[26a], M.G. Eggleston[47], E. Egidio Purcino De Souza[78b], L.F. Ehrke[52], T. Eifert[7], G. Eigen[15], K. Einsweiler[16], T. Ekelof[167], Y. El Ghazali[33b], H. El Jarrari[33e], A. El Moussaouy[33a], V. Ellajosyula[167], M. Ellert[167], F. Ellinghaus[177], A.A. Elliot[90], N. Ellis[34], J. Elmsheuser[27], M. Elsing[34], D. Emeliyanov[139], A. Emerman[37], Y. Enari[159], J. Erdmann[45], A. Ereditato[18], P.A. Erland[82], M. Errenst[177], M. Escalier[62], C. Escobar[169], O. Estrada Pastor[169], E. Etzion[157], G. Evans[135a], H. Evans[63], M.O. Evans[152], A. Ezhilov[133], F. Fabbri[55], L. Fabbri[21b,21a], V. Fabiani[115], G. Facini[173], V. Fadeyev[141], R.M. Fakhrutdinov[119], S. Falciano[70a], P.J. Falke[22], S. Falke[34], J. Faltova[138], Y. Fan[13a], Y. Fang[13a], Y. Fang[13a], G. Fanourakis[42], M. Fanti[66a,66b], M. Faraj[58c], A. Farbin[7], A. Farilla[72a], E.M. Farina[68a,68b], T. Farooque[104], S.M. Farrington[48], P. Farthouat[34], F. Fassi[33e], D. Fassouliotis[8], M. Faucci Giannelli[71a,71b], W.J. Fawcett[30], L. Fayard[62], O.L. Fedin[133,q], M. Feickert[168], L. Feligioni[99], A. Fell[145], C. Feng[58b], M. Feng[13b], M.J. Fenton[166], A.B. Fenyuk[119], S.W. Ferguson[41], J. Ferrando[44], A. Ferrari[167], P. Ferrari[116], R. Ferrari[68a], D. Ferrere[52], C. Ferretti[103], F. Fiedler[97], A. Filipčič[89], F. Filthaut[115], M.C.N. Fiolhais[135a,135c,a], L. Fiorini[169], F. Fischer[147], W.C. Fisher[104], T. Fitschen[19], I. Fleck[147], P. Fleischmann[103], T. Flick[177], B.M. Flierl[111], L. Flores[132], L.R. Flores Castillo[60a], F.M. Follega[73a,73b], N. Fomin[15], J.H. Foo[162], B.C. Forland[63], A. Formica[140], F.A. Förster[12], A.C. Forti[98], E. Fortin[99], M.G. Foti[130], L. Fountas[8], D. Fournier[62], H. Fox[87], P. Francavilla[69a,69b], S. Francescato[57], M. Franchini[21b,21a], S. Franchino[59a], D. Francis[34], L. Franco[4], L. Franconi[18], M. Franklin[57], G. Frattari[70a,70b], A.C. Freegard[90], P.M. Freeman[19], W.S. Freund[78b], E.M. Freundlich[45], D. Froidevaux[34], J.A. Frost[130], Y. Fu[58a], M. Fujimoto[122], E. Fullana Torregrosa[169], J. Fuster[169], A. Gabrielli[21b,21a], A. Gabrielli[34], P. Gadow[44], G. Gagliardi[53b,53a], L.G. Gagnon[16], G.E. Gallardo[130], E.J. Gallas[130], B.J. Gallop[139], R. Gamboa Goni[90], K.K. Gan[123], S. Ganguly[175], J. Gao[58a], Y. Gao[48], Y.S. Gao[29,n], F.M. Garay Walls[142a], C. García[169], J.E. García Navarro[169], J.A. García Pascual[13a], M. Garcia-Sciveres[16], R.W. Gardner[35], D. Garg[75], S. Gargiulo[50], C.A. Garner[162], V. Garonne[129], S.J. Gasiorowski[144], P. Gaspar[78b], G. Gaudio[68a], P. Gauzzi[70a,70b], I.L. Gavrilenko[108], A. Gavrilyuk[120], C. Gay[170], G. Gaycken[44], E.N. Gazis[9], A.A. Geanta[25b], C.M. Gee[141], C.N.P. Gee[139], J. Geisen[94], M. Geisen[97], C. Gemme[53b], M.H. Genest[56],

S. Gentile[70a,70b], S. George[91], W.F. George[19], T. Geralis[42], L.O. Gerlach[51], P. Gessinger-Befurt[34], M. Ghasemi Bostanabad[171], M. Ghneimat[147], A. Ghosh[166], A. Ghosh[75], B. Giacobbe[21b], S. Giagu[70a,70b], N. Giangiacomi[162], P. Giannetti[69a], A. Giannini[67a,67b], S.M. Gibson[91], M. Gignac[141], D.T. Gil[81b], B.J. Gilbert[37], D. Gillberg[32], G. Gilles[116], N.E.K. Gillwald[44], D.M. Gingrich[2,al], M.P. Giordani[64a,64c], P.F. Giraud[140], G. Giugliarelli[64a,64c], D. Giugni[66a], F. Giuli[71a,71b], I. Gkialas[8,i], P. Gkountoumis[9], L.K. Gladilin[110], C. Glasman[96], G.R. Gledhill[127], M. Glisic[127], I. Gnesi[39b,d], M. Goblirsch-Kolb[24], D. Godin[107], S. Goldfarb[102], T. Golling[52], D. Golubkov[119], J.P. Gombas[104], A. Gomes[135a,135b], R. Goncalves Gama[51], R. Gonçalo[135a,135c], G. Gonella[127], L. Gonella[19], A. Gongadze[77], F. Gonnella[19], J.L. Gonski[37], S. González de la Hoz[169], S. Gonzalez Fernandez[12], R. Gonzalez Lopez[88], C. Gonzalez Renteria[16], R. Gonzalez Suarez[167], S. Gonzalez-Sevilla[52], G.R. Gonzalvo Rodriguez[169], R.Y. González Andana[142a], L. Goossens[34], N.A. Gorasia[19], P.A. Gorbounov[120], H.A. Gordon[27], B. Gorini[34], E. Gorini[65a,65b], A. Gorišek[89], A.T. Goshaw[47], M.I. Gostkin[77], C.A. Gottardo[115], M. Gouighri[33b], V. Goumarre[44], A.G. Goussiou[144], N. Govender[31c], C. Goy[4], I. Grabowska-Bold[81a], K. Graham[32], E. Gramstad[129], S. Grancagnolo[17], M. Grandi[152], V. Gratchev[133], P.M. Gravila[25f], F.G. Gravili[65a,65b], H.M. Gray[16], C. Grefe[22], I.M. Gregor[44], P. Grenier[149], K. Grevtsov[44], C. Grieco[12], N.A. Grieser[124], A.A. Grillo[141], K. Grimm[29,m], S. Grinstein[12,x], J.-F. Grivaz[62], S. Groh[97], E. Gross[175], J. Grosse-Knetter[51], C. Grud[103], A. Grummer[114], J.C. Grundy[130], L. Guan[103], W. Guan[176], C. Gubbels[170], J. Guenther[34], J.G.R. Guerrero Rojas[169], F. Guescini[112], D. Guest[17], R. Gugel[97], A. Guida[44], T. Guillemin[4], S. Guindon[34], J. Guo[58c], L. Guo[62], Y. Guo[103], R. Gupta[44], S. Gurbuz[22], G. Gustavino[124], M. Guth[52], P. Gutierrez[124], L.F. Gutierrez Zagazeta[132], C. Gutschow[92], C. Guyot[140], C. Gwenlan[130], C.B. Gwilliam[88], E.S. Haaland[129], A. Haas[121], M. Habedank[17], C. Haber[16], H.K. Hadavand[7], A. Hadef[97], S. Hadzic[112], M. Haleem[172], J. Haley[125], J.J. Hall[145], G. Halladjian[104], G.D. Hallewell[99], L. Halser[18], K. Hamano[171], H. Hamdaoui[33e], M. Hamer[22], G.N. Hamity[48], K. Han[58a], L. Han[13c], L. Han[58a], S. Han[16], Y.F. Han[162], K. Hanagaki[79,v], M. Hance[141], M.D. Hank[35], R. Hankache[98], E. Hansen[94], J.B. Hansen[38], J.D. Hansen[38], M.C. Hansen[22], P.H. Hansen[38], K. Hara[164], T. Harenberg[177], S. Harkusha[105], Y.T. Harris[130], P.F. Harrison[173], N.M. Hartman[149], N.M. Hartmann[111], Y. Hasegawa[146], A. Hasib[48], S. Hassani[140], S. Haug[18], R. Hauser[104], M. Havranek[137], C.M. Hawkes[19], R.J. Hawkings[34], S. Hayashida[113], D. Hayden[104], C. Hayes[103], R.L. Hayes[170], C.P. Hays[130], J.M. Hays[90], H.S. Hayward[88], S.J. Haywood[139], F. He[58a], Y. He[160], Y. He[131], M.P. Heath[48], V. Hedberg[94], A.L. Heggelund[129], N.D. Hehir[90], C. Heidegger[50], K.K. Heidegger[50], W.D. Heidorn[76], J. Heilman[32], S. Heim[44], T. Heim[16], B. Heinemann[44,aj], J.G. Heinlein[132], J.J. Heinrich[127], L. Heinrich[34], J. Hejbal[136], L. Helary[44], A. Held[121], S. Hellesund[129], C.M. Helling[141], S. Hellman[43a,43b], C. Helsens[34], R.C.W. Henderson[87], L. Henkelmann[30], A.M. Henriques Correia[34], H. Herde[149], Y. Hernández Jiménez[151], H. Herr[97], M.G. Herrmann[111], T. Herrmann[46], G. Herten[50], R. Hertenberger[111], L. Hervas[34], N.P. Hessey[163a], H. Hibi[80], S. Higashino[79], E. Higón-Rodriguez[169], K.K. Hill[27], K.H. Hiller[44], S.J. Hillier[19], M. Hils[46], I. Hinchliffe[16], F. Hinterkeuser[22], M. Hirose[128], S. Hirose[164], D. Hirschbuehl[177], B. Hiti[89], O. Hladik[136], J. Hobbs[151], R. Hobincu[25e], N. Hod[175], M.C. Hodgkinson[145], B.H. Hodkinson[30], A. Hoecker[34], J. Hofer[44], D. Hohn[50], T. Holm[22], T.R. Holmes[35], M. Holzbock[112], L.B.A.H. Hommels[30], B.P. Honan[98], J. Hong[58c], T.M. Hong[134], J.C. Honig[50], A. Hönle[112], B.H. Hooberman[168], W.H. Hopkins[5], Y. Horii[113], L.A. Horyn[35], S. Hou[154], J. Howarth[55], J. Hoya[86], M. Hrabovsky[126], A. Hrynevich[106], T. Hryn'ova[4], P.J. Hsu[61], S.-C. Hsu[144], Q. Hu[37], S. Hu[58c], Y.F. Hu[13a,13d,an], D.P. Huang[92], X. Huang[13c], Y. Huang[58a], Y. Huang[13a], Z. Hubacek[137], F. Hubaut[99], M. Huebner[22], F. Huegging[22], T.B. Huffman[130], M. Huhtinen[34], R. Hulsken[56], N. Huseynov[77,ab], J. Huston[104], J. Huth[57], R. Hyneman[149], S. Hyrych[26a], G. Iacobucci[52], G. Iakovidis[27], I. Ibragimov[147], L. Iconomidou-Fayard[62], P. Iengo[34], R. Iguchi[159], T. Iizawa[52], Y. Ikegami[79], A. Ilg[18], N. Ilic[162], H. Imam[33a], T. Ingebretsen Carlson[43a,43b], G. Introzzi[68a,68b], M. Iodice[72a], V. Ippolito[70a,70b], M. Ishino[159], W. Islam[125], C. Issever[17,44], S. Istin[11c,ao], J.M. Iturbe Ponce[60a], R. Iuppa[73a,73b], A. Ivina[175], J.M. Izen[41], V. Izzo[67a], P. Jacka[136], P. Jackson[1], R.M. Jacobs[44], B.P. Jaeger[148], C.S. Jagfeld[111], G. Jäkel[177],

K. Jakobs[50], T. Jakoubek[175], J. Jamieson[55], K.W. Janas[81a], G. Jarlskog[94], A.E. Jaspan[88], N. Javadov[77,ab], T. Javůrek[34], M. Javurkova[100], F. Jeanneau[140], L. Jeanty[127], J. Jejelava[155a,ac], P. Jenni[50,e], S. Jézéquel[4], J. Jia[151], Z. Jia[13c], Y. Jiang[58a], S. Jiggins[50], J. Jimenez Pena[112], S. Jin[13c], A. Jinaru[25b], O. Jinnouchi[160], H. Jivan[31f], P. Johansson[145], K.A. Johns[6], C.A. Johnson[63], D.M. Jones[30], E. Jones[173], R.W.L. Jones[87], T.J. Jones[88], J. Jovicevic[51], X. Ju[16], J.J. Junggeburth[34], A. Juste Rozas[12,x], S. Kabana[142c], A. Kaczmarska[82], M. Kado[70a,70b], H. Kagan[123], M. Kagan[149], A. Kahn[37], C. Kahra[97], T. Kaji[174], E. Kajomovitz[156], C.W. Kalderon[27], A. Kamenshchikov[119], M. Kaneda[159], N.J. Kang[141], S. Kang[76], Y. Kano[113], J. Kanzaki[79], D. Kar[31f], K. Karava[130], M.J. Kareem[163b], I. Karkanias[158], S.N. Karpov[77], Z.M. Karpova[77], V. Kartvelishvili[87], A.N. Karyukhin[119], E. Kasimi[158], C. Kato[58d], J. Katzy[44], K. Kawade[146], K. Kawagoe[85], T. Kawaguchi[113], T. Kawamoto[140], G. Kawamura[51], E.F. Kay[171], F.I. Kaya[165], S. Kazakos[12], V.F. Kazanin[118b,118a], Y. Ke[151], J.M. Keaveney[31a], R. Keeler[171], J.S. Keller[32], D. Kelsey[152], J.J. Kempster[19], J. Kendrick[19], K.E. Kennedy[37], O. Kepka[136], S. Kersten[177], B.P. Kerševan[89], S. Ketabchi Haghighat[162], M. Khandoga[131], A. Khanov[125], A.G. Kharlamov[118b,118a], T. Kharlamova[118b,118a], E.E. Khoda[144], T.J. Khoo[17], G. Khoriauli[172], E. Khramov[77], J. Khubua[155b], S. Kido[80], M. Kiehn[34], A. Kilgallon[127], E. Kim[160], Y.K. Kim[35], N. Kimura[92], A. Kirchhoff[51], D. Kirchmeier[46], C. Kirfel[22], J. Kirk[139], A.E. Kiryunin[112], T. Kishimoto[159], D.P. Kisliuk[162], V. Kitali[44], C. Kitsaki[9], O. Kivernyk[22], T. Klapdor-Kleingrothaus[50], M. Klassen[59a], C. Klein[32], L. Klein[172], M.H. Klein[103], M. Klein[88], U. Klein[88], P. Klimek[34], A. Klimentov[27], F. Klimpel[34], T. Klingl[22], T. Klioutchnikova[34], F.F. Klitzner[111], P. Kluit[116], S. Kluth[112], E. Kneringer[74], T.M. Knight[162], A. Knue[50], D. Kobayashi[85], M. Kobel[46], M. Kocian[149], T. Kodama[159], P. Kodys[138], D.M. Koeck[152], P.T. Koenig[22], T. Koffas[32], N.M. Köhler[34], M. Kolb[140], I. Koletsou[4], T. Komarek[126], K. Köneke[50], A.X.Y. Kong[1], T. Kono[122], V. Konstantinides[92], N. Konstantinidis[92], B. Konya[94], R. Kopeliansky[63], S. Koperny[81a], K. Korcyl[82], K. Kordas[158], G. Koren[157], A. Korn[92], S. Korn[51], I. Korolkov[12], E.V. Korolkova[145], N. Korotkova[110], B. Kortman[116], O. Kortner[112], S. Kortner[112], W.H. Kostecka[117], V.V. Kostyukhin[145,161], A. Kotsokechagia[62], A. Kotwal[47], A. Koulouris[34], A. Kourkoumeli-Charalampidi[68a,68b], C. Kourkoumelis[8], E. Kourlitis[5], O. Kovanda[152], R. Kowalewski[171], W. Kozanecki[140], A.S. Kozhin[119], V.A. Kramarenko[110], G. Kramberger[89], D. Krasnopevtsev[58a], M.W. Krasny[131], A. Krasznahorkay[34], J.A. Kremer[97], J. Kretzschmar[88], K. Kreul[17], P. Krieger[162], F. Krieter[111], S. Krishnamurthy[100], A. Krishnan[59b], M. Krivos[138], K. Krizka[16], K. Kroeninger[45], H. Kroha[112], J. Kroll[136], J. Kroll[132], K.S. Krowpman[104], U. Kruchonak[77], H. Krüger[22], N. Krumnack[76], M.C. Kruse[47], J.A. Krzysiak[82], A. Kubota[160], O. Kuchinskaia[161], S. Kuday[3b], D. Kuechler[44], J.T. Kuechler[44], S. Kuehn[34], T. Kuhl[44], V. Kukhtin[77], Y. Kulchitsky[105,af], S. Kuleshov[142b], M. Kumar[31f], N. Kumari[99], M. Kuna[56], A. Kupco[136], T. Kupfer[45], O. Kuprash[50], H. Kurashige[80], L.L. Kurchaninov[163a], Y.A. Kurochkin[105], A. Kurova[109], M.G. Kurth[13a,13d], E.S. Kuwertz[34], M. Kuze[160], A.K. Kvam[144], J. Kvita[126], T. Kwan[101], K.W. Kwok[60a], C. Lacasta[169], F. Lacava[70a,70b], H. Lacker[17], D. Lacour[131], N.N. Lad[92], E. Ladygin[77], R. Lafaye[4], B. Laforge[131], T. Lagouri[142c], S. Lai[51], I.K. Lakomiec[81a], N. Lalloue[56], J.E. Lambert[124], S. Lammers[63], W. Lampl[6], C. Lampoudis[158], E. Lançon[27], U. Landgraf[50], M.P.J. Landon[90], V.S. Lang[50], J.C. Lange[51], R.J. Langenberg[100], A.J. Lankford[166], F. Lanni[27], K. Lantzsch[22], A. Lanza[68a], A. Lapertosa[53b,53a], J.F. Laporte[140], T. Lari[66a], F. Lasagni Manghi[21b], M. Lassnig[34], V. Latonova[136], T.S. Lau[60a], A. Laudrain[97], A. Laurier[32], M. Lavorgna[67a,67b], S.D. Lawlor[91], Z. Lawrence[98], M. Lazzaroni[66a,66b], B. Le[98], B. Leban[89], A. Lebedev[76], M. LeBlanc[34], T. LeCompte[5], F. Ledroit-Guillon[56], A.C.A. Lee[92], G.R. Lee[15], L. Lee[57], S.C. Lee[154], S. Lee[76], L.L. Leeuw[31c], B. Lefebvre[163a], H.P. Lefebvre[91], M. Lefebvre[171], C. Leggett[16], K. Lehmann[148], N. Lehmann[18], G. Lehmann Miotto[34], W.A. Leight[44], A. Leisos[158,w], M.A.L. Leite[78c], C.E. Leitgeb[44], R. Leitner[138], K.J.C. Leney[40], T. Lenz[22], S. Leone[69a], C. Leonidopoulos[48], A. Leopold[131], C. Leroy[107], R. Les[104], C.G. Lester[30], M. Levchenko[133], J. Levêque[4], D. Levin[103], L.J. Levinson[175], D.J. Lewis[19], B. Li[13b], B. Li[58b], C. Li[58a], C-Q. Li[58c,58d], H. Li[58a], H. Li[58b], H. Li[58b], J. Li[58c], K. Li[144], L. Li[58c], M. Li[13a,13d], Q.Y. Li[58a], S. Li[58d,58c,c], T. Li[58b], X. Li[44], Y. Li[44],

Z. Li[58b], Z. Li[130], Z. Li[101], Z. Li[88], Z. Liang[13a], M. Liberatore[44], B. Liberti[71a], K. Lie[60c], K. Lin[104], R.A. Linck[63], R.E. Lindley[6], J.H. Lindon[2], A. Linss[44], E. Lipeles[132], A. Lipniacka[15], T.M. Liss[168,ak], A. Lister[170], J.D. Little[7], B. Liu[13a], B.X. Liu[148], J.B. Liu[58a], J.K.K. Liu[35], K. Liu[58d,58c], M. Liu[58a], M.Y. Liu[58a], P. Liu[13a], X. Liu[58a], Y. Liu[44], Y. Liu[13c,13d], Y.L. Liu[103], Y.W. Liu[58a], M. Livan[68a,68b], A. Lleres[56], J. Llorente Merino[148], S.L. Lloyd[90], E.M. Lobodzinska[44], P. Loch[6], S. Loffredo[71a,71b], T. Lohse[17], K. Lohwasser[145], M. Lokajicek[136], J.D. Long[168], I. Longarini[70a,70b], L. Longo[34], R. Longo[168], I. Lopez Paz[12], A. Lopez Solis[44], J. Lorenz[111], N. Lorenzo Martinez[4], A.M. Lory[111], A. Lösle[50], X. Lou[43a,43b], X. Lou[13a], A. Lounis[62], J. Love[5], P.A. Love[87], J.J. Lozano Bahilo[169], G. Lu[13a,13d], M. Lu[58a], S. Lu[132], Y.J. Lu[61], H.J. Lubatti[144], C. Luci[70a,70b], F.L. Lucio Alves[13c], A. Lucotte[56], F. Luehring[63], I. Luise[151], L. Luminari[70a], O. Lundberg[150], B. Lund-Jensen[150], N.A. Luongo[127], M.S. Lutz[157], D. Lynn[27], H. Lyons[88], R. Lysak[136], E. Lytken[94], F. Lyu[13a], V. Lyubushkin[77], T. Lyubushkina[77], H. Ma[27], L.L. Ma[58b], Y. Ma[92], D.M. Mac Donell[171], G. Maccarrone[49], C.M. Macdonald[145], J.C. MacDonald[145], R. Madar[36], W.F. Mader[46], M. Madugoda Ralalage Don[125], N. Madysa[46], J. Maeda[80], T. Maeno[27], M. Maerker[46], V. Magerl[50], J. Magro[64a,64c], D.J. Mahon[37], C. Maidantchik[78b], A. Maio[135a,135b,135d], K. Maj[81a], O. Majersky[26a], S. Majewski[127], N. Makovec[62], B. Malaescu[131], Pa. Malecki[82], V.P. Maleev[133], F. Malek[56], D. Malito[39b,39a], U. Mallik[75], C. Malone[30], S. Maltezos[9], S. Malyukov[77], J. Mamuzic[169], G. Mancini[49], J.P. Mandalia[90], I. Mandić[89], L. Manhaes de Andrade Filho[78a], I.M. Maniatis[158], M. Manisha[140], J. Manjarres Ramos[46], K.H. Mankinen[94], A. Mann[111], A. Manousos[74], B. Mansoulie[140], I. Manthos[158], S. Manzoni[116], A. Marantis[158,w], G. Marchiori[131], M. Marcisovsky[136], L. Marcoccia[71a,71b], C. Marcon[94], M. Marjanovic[124], Z. Marshall[16], S. Marti-Garcia[169], T.A. Martin[173], V.J. Martin[48], B. Martin dit Latour[15], L. Martinelli[70a,70b], M. Martinez[12,x], P. Martinez Agullo[169], V.I. Martinez Outschoorn[100], S. Martin-Haugh[139], V.S. Martoiu[25b], A.C. Martyniuk[92], A. Marzin[34], S.R. Maschek[112], L. Masetti[97], T. Mashimo[159], J. Masik[98], A.L. Maslennikov[118b,118a], L. Massa[21b], P. Massarotti[67a,67b], P. Mastrandrea[69a,69b], A. Mastroberardino[39b,39a], T. Masubuchi[159], D. Matakias[27], T. Mathisen[167], A. Matic[111], N. Matsuzawa[159], J. Maurer[25b], B. Maček[89], D.A. Maximov[118b,118a], R. Mazini[154], I. Maznas[158], S.M. Mazza[141], C. Mc Ginn[27], J.P. Mc Gowan[101], S.P. Mc Kee[103], T.G. McCarthy[112], W.P. McCormack[16], E.F. McDonald[102], A.E. McDougall[116], J.A. Mcfayden[152], G. Mchedlidze[155b], M.A. McKay[40], K.D. McLean[171], S.J. McMahon[139], P.C. McNamara[102], R.A. McPherson[171,aa], J.E. Mdhluli[31f], Z.A. Meadows[100], S. Meehan[34], T. Megy[36], S. Mehlhase[111], A. Mehta[88], B. Meirose[41], D. Melini[156], B.R. Mellado Garcia[31f], A.H. Melo[51], F. Meloni[44], A. Melzer[22], E.D. Mendes Gouveia[135a], A.M. Mendes Jacques Da Costa[19], H.Y. Meng[162], L. Meng[34], S. Menke[112], M. Mentink[34], E. Meoni[39b,39a], C. Merlassino[130], P. Mermod[52,*], L. Merola[67a,67b], C. Meroni[66a], G. Merz[103], O. Meshkov[110,108], J.K.R. Meshreki[147], J. Metcalfe[5], A.S. Mete[5], C. Meyer[63], J-P. Meyer[140], M. Michetti[17], R.P. Middleton[139], L. Mijović[48], G. Mikenberg[175], M. Mikestikova[136], M. Mikuž[89], H. Mildner[145], A. Milic[162], C.D. Milke[40], D.W. Miller[35], L.S. Miller[32], A. Milov[175], D.A. Milstead[43a,43b], T. Min[13c], A.A. Minaenko[119], I.A. Minashvili[155b], L. Mince[55], A.I. Mincer[121], B. Mindur[81a], M. Mineev[77], Y. Minegishi[159], Y. Mino[83], L.M. Mir[12], M. Miralles Lopez[169], M. Mironova[130], T. Mitani[174], V.A. Mitsou[169], M. Mittal[58c], O. Miu[162], P.S. Miyagawa[90], Y. Miyazaki[85], A. Mizukami[79], J.U. Mjörnmark[94], T. Mkrtchyan[59a], M. Mlynarikova[117], T. Moa[43a,43b], S. Mobius[51], K. Mochizuki[107], P. Moder[44], P. Mogg[111], A.F. Mohammed[13a], S. Mohapatra[37], G. Mokgatitswane[31f], B. Mondal[147], S. Mondal[137], K. Mönig[44], E. Monnier[99], A. Montalbano[148], J. Montejo Berlingen[34], M. Montella[123], F. Monticelli[86], N. Morange[62], A.L. Moreira De Carvalho[135a], M. Moreno Llácer[169], C. Moreno Martinez[12], P. Morettini[53b], M. Morgenstern[156], S. Morgenstern[173], D. Mori[148], M. Morii[57], M. Morinaga[159], V. Morisbak[129], A.K. Morley[34], A.P. Morris[92], L. Morvaj[34], P. Moschovakos[34], B. Moser[116], M. Mosidze[155b], T. Moskalets[50], P. Moskvitina[115], J. Moss[29,o], E.J.W. Moyse[100], S. Muanza[99], J. Mueller[134], R. Mueller[18], D. Muenstermann[87], G.A. Mullier[94], J.J. Mullin[132], D.P. Mungo[66a,66b], J.L. Munoz Martinez[12], F.J. Munoz Sanchez[98], M. Murin[98], P. Murin[26b], W.J. Murray[173,139], A. Murrone[66a,66b], J.M. Muse[124], M. Muškinja[16], C. Mwewa[27], A.G. Myagkov[119,ag],

A.J. Myers[7], A.A. Myers[134], G. Myers[63], M. Myska[137], B.P. Nachman[16], O. Nackenhorst[45], A.Nag Nag[46], K. Nagai[130], K. Nagano[79], J.L. Nagle[27], E. Nagy[99], A.M. Nairz[34], Y. Nakahama[113], K. Nakamura[79], H. Nanjo[128], F. Napolitano[59a], R. Narayan[40], I. Naryshkin[133], M. Naseri[32], C. Nass[22], T. Naumann[44], G. Navarro[20a], J. Navarro-Gonzalez[169], R. Nayak[157], P.Y. Nechaeva[108], F. Nechansky[44], T.J. Neep[19], A. Negri[68a,68b], M. Negrini[21b], C. Nellist[115], C. Nelson[101], K. Nelson[103], S. Nemecek[136], M. Nessi[34,g], M.S. Neubauer[168], F. Neuhaus[97], J. Neundorf[44], R. Newhouse[170], P.R. Newman[19], C.W. Ng[134], Y.S. Ng[17], Y.W.Y. Ng[166], B. Ngair[33e], H.D.N. Nguyen[99], R.B. Nickerson[130], R. Nicolaidou[140], D.S. Nielsen[38], J. Nielsen[141], M. Niemeyer[51], N. Nikiforou[10], V. Nikolaenko[119,ag], I. Nikolic-Audit[131], K. Nikolopoulos[19], P. Nilsson[27], H.R. Nindhito[52], A. Nisati[70a], N. Nishu[2], R. Nisius[112], T. Nitta[174], T. Nobe[159], D.L. Noel[30], Y. Noguchi[83], I. Nomidis[131], M.A. Nomura[27], M.B. Norfolk[145], R.R.B. Norisam[92], J. Novak[89], T. Novak[44], O. Novgorodova[46], L. Novotny[137], R. Novotny[114], L. Nozka[126], K. Ntekas[166], E. Nurse[92], F.G. Oakham[32,al], J. Ocariz[131], A. Ochi[80], I. Ochoa[135a], J.P. Ochoa-Ricoux[142a], S. Oda[85], S. Odaka[79], S. Oerdek[167], A. Ogrodnik[81a], A. Oh[98], C.C. Ohm[150], H. Oide[160], R. Oishi[159], M.L. Ojeda[162], Y. Okazaki[83], M.W. O'Keefe[88], Y. Okumura[159], A. Olariu[25b], L.F. Oleiro Seabra[135a], S.A. Olivares Pino[142c], D. Oliveira Damazio[27], D. Oliveira Goncalves[78a], J.L. Oliver[166], M.J.R. Olsson[166], A. Olszewski[82], J. Olszowska[82], Ö.O. Öncel[22], D.C. O'Neil[148], A.P. O'neill[130], A. Onofre[135a,135e], P.U.E. Onyisi[10], R.G. Oreamuno Madriz[117], M.J. Oreglia[35], G.E. Orellana[86], D. Orestano[72a,72b], N. Orlando[12], R.S. Orr[162], V. O'Shea[55], R. Ospanov[58a], G. Otero y Garzon[28], H. Otono[85], P.S. Ott[59a], G.J. Ottino[16], M. Ouchrif[33d], J. Ouellette[27], F. Ould-Saada[129], A. Ouraou[140,*], Q. Ouyang[13a], M. Owen[55], R.E. Owen[139], K.Y. Oyulmaz[11c], V.E. Ozcan[11c], N. Ozturk[7], S. Ozturk[11c], J. Pacalt[126], H.A. Pacey[30], K. Pachal[47], A. Pacheco Pages[12], C. Padilla Aranda[12], S. Pagan Griso[16], G. Palacino[63], S. Palazzo[48], S. Palestini[34], M. Palka[81b], P. Palni[81a], D.K. Panchal[10], C.E. Pandini[52], J.G. Panduro Vazquez[91], P. Pani[44], G. Panizzo[64a,64c], L. Paolozzi[52], C. Papadatos[107], S. Parajuli[40], A. Paramonov[5], C. Paraskevopoulos[9], D. Paredes Hernandez[60b], S.R. Paredes Saenz[130], B. Parida[175], T.H. Park[162], A.J. Parker[29], M.A. Parker[30], F. Parodi[53b,53a], E.W. Parrish[117], J.A. Parsons[37], U. Parzefall[50], L. Pascual Dominguez[157], V.R. Pascuzzi[16], F. Pasquali[116], E. Pasqualucci[70a], S. Passaggio[53b], F. Pastore[91], P. Pasuwan[43a,43b], J.R. Pater[98], A. Pathak[176], J. Patton[88], T. Pauly[34], J. Pearkes[149], M. Pedersen[129], L. Pedraza Diaz[115], R. Pedro[135a], T. Peiffer[51], S.V. Peleganchuk[118b,118a], O. Penc[136], C. Peng[60b], H. Peng[58a], M. Penzin[161], B.S. Peralva[78a], M.M. Perego[62], A.P. Pereira Peixoto[135a], L. Pereira Sanchez[43a,43b], D.V. Perepelitsa[27], E. Perez Codina[163a], M. Perganti[9], L. Perini[66a,66b], H. Pernegger[34], S. Perrella[34], A. Perrevoort[116], K. Peters[44], R.F.Y. Peters[98], B.A. Petersen[34], T.C. Petersen[38], E. Petit[99], V. Petousis[137], C. Petridou[158], P. Petroff[62], F. Petrucci[72a,72b], M. Pettee[178], N.E. Pettersson[34], K. Petukhova[138], A. Peyaud[140], R. Pezoa[142d], L. Pezzotti[34], G. Pezzullo[178], T. Pham[102], P.W. Phillips[139], M.W. Phipps[168], G. Piacquadio[151], E. Pianori[16], F. Piazza[66a,66b], A. Picazio[100], R. Piegaia[28], D. Pietreanu[25b], J.E. Pilcher[35], A.D. Pilkington[98], M. Pinamonti[64a,64c], J.L. Pinfold[2], C. Pitman Donaldson[92], D.A. Pizzi[32], L. Pizzimento[71a,71b], A. Pizzini[116], M.-A. Pleier[27], V. Plesanovs[50], V. Pleskot[138], E. Plotnikova[77], P. Podberezko[118b,118a], R. Poettgen[94], R. Poggi[52], L. Poggioli[131], I. Pogrebnyak[104], D. Pohl[22], I. Pokharel[51], G. Polesello[68a], A. Poley[148,163a], A. Policicchio[70a,70b], R. Polifka[138], A. Polini[21b], C.S. Pollard[130], Z.B. Pollock[123], V. Polychronakos[27], D. Ponomarenko[109], L. Pontecorvo[34], S. Popa[25a], G.A. Popeneciu[25d], L. Portales[4], D.M. Portillo Quintero[163a], S. Pospisil[137], P. Postolache[25c], K. Potamianos[130], I.N. Potrap[77], C.J. Potter[30], H. Potti[1], T. Poulsen[44], J. Poveda[169], T.D. Powell[145], G. Pownall[44], M.E. Pozo Astigarraga[34], A. Prades Ibanez[169], P. Pralavorio[99], M.M. Prapa[42], S. Prell[76], D. Price[98], M. Primavera[65a], M.A. Principe Martin[96], M.L. Proffitt[144], N. Proklova[109], K. Prokofiev[60c], F. Prokoshin[77], S. Protopopescu[27], J. Proudfoot[5], M. Przybycien[81a], D. Pudzha[133], P. Puzo[62], D. Pyatiizbyantseva[109], J. Qian[103], Y. Qin[98], T. Qiu[90], A. Quadt[51], M. Queitsch-Maitland[34], G. Rabanal Bolanos[57], F. Ragusa[66a,66b], G. Rahal[95], J.A. Raine[52], S. Rajagopalan[27], K. Ran[13a,13d], D.F. Rassloff[59a], D.M. Rauch[44], S. Rave[97], B. Ravina[55], I. Ravinovich[175], M. Raymond[34], A.L. Read[129], N.P. Readioff[145],

D.M. Rebuzzi[68a,68b], G. Redlinger[27], K. Reeves[41], D. Reikher[157], A. Reiss[97], A. Rej[147], C. Rembser[34], A. Renardi[44], M. Renda[25b], M.B. Rendel[112], A.G. Rennie[55], S. Resconi[66a], E.D. Resseguie[16], S. Rettie[92], B. Reynolds[123], E. Reynolds[19], M. Rezaei Estabragh[177], O.L. Rezanova[118b,118a], P. Reznicek[138], E. Ricci[73a,73b], R. Richter[112], S. Richter[44], E. Richter-Was[81b], M. Ridel[131], P. Rieck[112], P. Riedler[34], O. Rifki[44], M. Rijssenbeek[151], A. Rimoldi[68a,68b], M. Rimoldi[44], L. Rinaldi[21b,21a], T.T. Rinn[168], M.P. Rinnagel[111], G. Ripellino[150], I. Riu[12], P. Rivadeneira[44], J.C. Rivera Vergara[171], F. Rizatdinova[125], E. Rizvi[90], C. Rizzi[52], B.A. Roberts[173], S.H. Robertson[101,aa], M. Robin[44], D. Robinson[30], C.M. Robles Gajardo[142d], M. Robles Manzano[97], A. Robson[55], A. Rocchi[71a,71b], C. Roda[69a,69b], S. Rodriguez Bosca[59a], A. Rodriguez Rodriguez[50], A.M. Rodríguez Vera[163b], S. Roe[34], A.R. Roepe[124], J. Roggel[177], O. Røhne[129], R.A. Rojas[142d], B. Roland[50], C.P.A. Roland[63], J. Roloff[27], A. Romaniouk[109], M. Romano[21b], A.C. Romero Hernandez[168], N. Rompotis[88], M. Ronzani[121], L. Roos[131], S. Rosati[70a], B.J. Rosser[132], E. Rossi[162], E. Rossi[4], E. Rossi[67a,67b], L.P. Rossi[53b], L. Rossini[44], R. Rosten[123], M. Rotaru[25b], B. Rottler[50], D. Rousseau[62], D. Rousso[30], G. Rovelli[68a,68b], A. Roy[10], A. Rozanov[99], Y. Rozen[156], X. Ruan[31f], A.J. Ruby[88], T.A. Ruggeri[1], F. Rühr[50], A. Ruiz-Martinez[169], A. Rummler[34], Z. Rurikova[50], N.A. Rusakovich[77], H.L. Russell[34], L. Rustige[36], J.P. Rutherfoord[6], E.M. Rüttinger[145], M. Rybar[138], E.B. Rye[129], A. Ryzhov[119], J.A. Sabater Iglesias[44], P. Sabatini[169], L. Sabetta[70a,70b], H.F-W. Sadrozinski[141], R. Sadykov[77], F. Safai Tehrani[70a], B. Safarzadeh Samani[152], M. Safdari[149], P. Saha[117], S. Saha[101], M. Sahinsoy[112], A. Sahu[177], M. Saimpert[140], M. Saito[159], T. Saito[159], D. Salamani[34], G. Salamanna[72a,72b], A. Salnikov[149], J. Salt[169], A. Salvador Salas[12], D. Salvatore[39b,39a], F. Salvatore[152], A. Salzburger[34], D. Sammel[50], D. Sampsonidis[158], D. Sampsonidou[58d,58c], J. Sánchez[169], A. Sanchez Pineda[4], V. Sanchez Sebastian[169], H. Sandaker[129], C.O. Sander[44], I.G. Sanderswood[87], J.A. Sandesara[100], M. Sandhoff[177], C. Sandoval[20b], D.P.C. Sankey[139], M. Sannino[53b,53a], Y. Sano[113], A. Sansoni[49], C. Santoni[36], H. Santos[135a,135b], S.N. Santpur[16], A. Santra[175], K.A. Saoucha[145], A. Sapronov[77], J.G. Saraiva[135a,135d], J. Sardain[99], O. Sasaki[79], K. Sato[164], C. Sauer[59b], F. Sauerburger[50], E. Sauvan[4], P. Savard[162,al], R. Sawada[159], C. Sawyer[139], L. Sawyer[93], I. Sayago Galvan[169], C. Sbarra[21b], A. Sbrizzi[64a,64c], T. Scanlon[92], J. Schaarschmidt[144], P. Schacht[112], D. Schaefer[35], U. Schäfer[97], A.C. Schaffer[62], D. Schaile[111], R.D. Schamberger[151], E. Schanet[111], C. Scharf[17], N. Scharmberg[98], V.A. Schegelsky[133], D. Scheirich[138], F. Schenck[17], M. Schernau[166], C. Schiavi[53b,53a], L.K. Schildgen[22], Z.M. Schillaci[24], E.J. Schioppa[65a,65b], M. Schioppa[39b,39a], B. Schlag[97], K.E. Schleicher[50], S. Schlenker[34], K. Schmieden[97], C. Schmitt[97], S. Schmitt[44], L. Schoeffel[140], A. Schoening[59b], P.G. Scholer[50], E. Schopf[130], M. Schott[97], J. Schovancova[34], S. Schramm[52], F. Schroeder[177], H-C. Schultz-Coulon[59a], M. Schumacher[50], B.A. Schumm[141], Ph. Schune[140], A. Schwartzman[149], T.A. Schwarz[103], Ph. Schwemling[140], R. Schwienhorst[104], A. Sciandra[141], G. Sciolla[24], F. Scuri[69a], F. Scutti[102], C.D. Sebastiani[88], K. Sedlaczek[45], P. Seema[17], S.C. Seidel[114], A. Seiden[141], B.D. Seidlitz[27], T. Seiss[35], C. Seitz[44], J.M. Seixas[78b], G. Sekhniaidze[67a], S.J. Sekula[40], L. Selem[4], N. Semprini-Cesari[21b,21a], S. Sen[47], C. Serfon[27], L. Serin[62], L. Serkin[64a,64b], M. Sessa[72a,72b], H. Severini[124], S. Sevova[149], F. Sforza[53b,53a], A. Sfyrla[52], E. Shabalina[51], R. Shaheen[150], J.D. Shahinian[132], N.W. Shaikh[43a,43b], D. Shaked Renous[175], L.Y. Shan[13a], M. Shapiro[16], A. Sharma[34], A.S. Sharma[1], S. Sharma[44], P.B. Shatalov[120], K. Shaw[152], S.M. Shaw[98], P. Sherwood[92], L. Shi[92], C.O. Shimmin[178], Y. Shimogama[174], J.D. Shinner[91], I.P.J. Shipsey[130], S. Shirabe[52], M. Shiyakova[77], J. Shlomi[175], M.J. Shochet[35], J. Shojaii[102], D.R. Shope[150], S. Shrestha[123], E.M. Shrif[31f], M.J. Shroff[171], E. Shulga[175], P. Sicho[136], A.M. Sickles[168], E. Sideras Haddad[31f], O. Sidiropoulou[34], A. Sidoti[21b], F. Siegert[46], Dj. Sijacki[14], J.M. Silva[19], M.V. Silva Oliveira[34], S.B. Silverstein[43a], S. Simion[62], R. Simoniello[34], S. Simsek[11b], P. Sinervo[162], V. Sinetckii[110], S. Singh[148], S. Singh[162], S. Sinha[44], S. Sinha[31f], M. Sioli[21b,21a], I. Siral[127], S.Yu. Sivoklokov[110], J. Sjölin[43a,43b], A. Skaf[51], E. Skorda[94], P. Skubic[124], M. Slawinska[82], K. Sliwa[165], V. Smakhtin[175], B.H. Smart[139], J. Smiesko[138], S.Yu. Smirnov[109], Y. Smirnov[109], L.N. Smirnova[110,s], O. Smirnova[94], E.A. Smith[35], H.A. Smith[130], M. Smizanska[87], K. Smolek[137], A. Smykiewicz[82],

A.A. Snesarev[108], H.L. Snoek[116], S. Snyder[27], R. Sobie[171,aa], A. Soffer[157], F. Sohns[51], C.A. Solans Sanchez[34], E.Yu. Soldatov[109], U. Soldevila[169], A.A. Solodkov[119], S. Solomon[50], A. Soloshenko[77], O.V. Solovyanov[119], V. Solovyev[133], P. Sommer[145], H. Son[165], A. Sonay[12], W.Y. Song[163b], A. Sopczak[137], A.L. Sopio[92], F. Sopkova[26b], S. Sottocornola[68a,68b], R. Soualah[64a,64c], A.M. Soukharev[118b,118a], Z. Soumaimi[33e], D. South[44], S. Spagnolo[65a,65b], M. Spalla[112], M. Spangenberg[173], F. Spanò[91], D. Sperlich[50], T.M. Spieker[59a], G. Spigo[34], M. Spina[152], D.P. Spiteri[55], M. Spousta[138], A. Stabile[66a,66b], R. Stamen[59a], M. Stamenkovic[116], A. Stampekis[19], M. Standke[22], E. Stanecka[82], B. Stanislaus[34], M.M. Stanitzki[44], M. Stankaityte[130], B. Stapf[44], E.A. Starchenko[119], G.H. Stark[141], J. Stark[99], D.M. Starko[163b], P. Staroba[136], P. Starovoitov[59a], S. Stärz[101], R. Staszewski[82], G. Stavropoulos[42], P. Steinberg[27], A.L. Steinhebel[127], B. Stelzer[148,163a], H.J. Stelzer[134], O. Stelzer-Chilton[163a], H. Stenzel[54], T.J. Stevenson[152], G.A. Stewart[34], M.C. Stockton[34], G. Stoicea[25b], M. Stolarski[135a], S. Stonjek[112], A. Straessner[46], J. Strandberg[150], S. Strandberg[43a,43b], M. Strauss[124], T. Strebler[99], P. Strizenec[26b], R. Ströhmer[172], D.M. Strom[127], L.R. Strom[44], R. Stroynowski[40], A. Strubig[43a,43b], S.A. Stucci[27], B. Stugu[15], J. Stupak[124], N.A. Styles[44], D. Su[149], S. Su[58a], W. Su[58d,144,58c], X. Su[58a], N.B. Suarez[134], K. Sugizaki[159], V.V. Sulin[108], M.J. Sullivan[88], D.M.S. Sultan[52], S. Sultansoy[3c], T. Sumida[83], S. Sun[103], S. Sun[176], X. Sun[98], O. Sunneborn Gudnadottir[167], C.J.E. Suster[153], M.R. Sutton[152], M. Svatos[136], M. Swiatlowski[163a], T. Swirski[172], I. Sykora[26a], M. Sykora[138], T. Sykora[138], D. Ta[97], K. Tackmann[44,y], A. Taffard[166], R. Tafirout[163a], E. Tagiev[119], R.H.M. Taibah[131], R. Takashima[84], K. Takeda[80], T. Takeshita[146], E.P. Takeva[48], Y. Takubo[79], M. Talby[99], A.A. Talyshev[118b,118a], K.C. Tam[60b], N.M. Tamir[157], A. Tanaka[159], J. Tanaka[159], R. Tanaka[62], Z. Tao[170], S. Tapia Araya[76], S. Tapprogge[97], A. Tarek Abouelfadl Mohamed[104], S. Tarem[156], K. Tariq[58b], G. Tarna[25b,f], G.F. Tartarelli[66a], P. Tas[138], M. Tasevsky[136], E. Tassi[39b,39a], G. Tateno[159], Y. Tayalati[33e], G.N. Taylor[102], W. Taylor[163b], H. Teagle[88], A.S. Tee[176], R. Teixeira De Lima[149], P. Teixeira-Dias[91], H. Ten Kate[34], J.J. Teoh[116], K. Terashi[159], J. Terron[96], S. Terzo[12], M. Testa[49], R.J. Teuscher[162,aa], N. Themistokleous[48], T. Theveneaux-Pelzer[17], O. Thielmann[177], D.W. Thomas[91], J.P. Thomas[19], E.A. Thompson[44], P.D. Thompson[19], E. Thomson[132], E.J. Thorpe[90], Y. Tian[51], V. Tikhomirov[108,ah], Yu.A. Tikhonov[118b,118a], S. Timoshenko[109], P. Tipton[178], S. Tisserant[99], S.H. Tlou[31f], A. Tnourji[36], K. Todome[21b,21a], S. Todorova-Nova[138], S. Todt[46], M. Togawa[79], J. Tojo[85], S. Tokár[26a], K. Tokushuku[79], E. Tolley[123], R. Tombs[30], M. Tomoto[79,113], L. Tompkins[149], P. Tornambe[100], E. Torrence[127], H. Torres[46], E. Torró Pastor[169], M. Toscani[28], C. Tosciri[35], J. Toth[99,z], D.R. Tovey[145], A. Traeet[15], C.J. Treado[121], T. Trefzger[172], A. Tricoli[27], I.M. Trigger[163a], S. Trincaz-Duvoid[131], D.A. Trischuk[170], W. Trischuk[162], B. Trocmé[56], A. Trofymov[62], C. Troncon[66a], F. Trovato[152], L. Truong[31c], M. Trzebinski[82], A. Trzupek[82], F. Tsai[151], A. Tsiamis[158], P.V. Tsiareshka[105,af], A. Tsirigotis[158,w], V. Tsiskaridze[151], E.G. Tskhadadze[155a], M. Tsopoulou[158], I.I. Tsukerman[120], V. Tsulaia[16], S. Tsuno[79], O. Tsur[156], D. Tsybychev[151], Y. Tu[60b], A. Tudorache[25b], V. Tudorache[25b], A.N. Tuna[34], S. Turchikhin[77], I. Turk Cakir[3b,u], R.J. Turner[19], R. Turra[66a], P.M. Tuts[37], S. Tzamarias[158], P. Tzanis[9], E. Tzovara[97], K. Uchida[159], F. Ukegawa[164], G. Unal[34], M. Unal[10], A. Undrus[27], G. Unel[166], F.C. Ungaro[102], K. Uno[159], J. Urban[26b], P. Urquijo[102], G. Usai[7], R. Ushioda[160], M. Usman[107], Z. Uysal[11d], V. Vacek[137], B. Vachon[101], K.O.H. Vadla[129], T. Vafeiadis[34], C. Valderanis[111], E. Valdes Santurio[43a,43b], M. Valente[163a], S. Valentinetti[21b,21a], A. Valero[169], L. Valéry[44], R.A. Vallance[19], A. Vallier[99], J.A. Valls Ferrer[169], T.R. Van Daalen[144], P. Van Gemmeren[5], S. Van Stroud[92], I. Van Vulpen[116], M. Vanadia[71a,71b], W. Vandelli[34], M. Vandenbroucke[140], E.R. Vandewall[125], D. Vannicola[157], L. Vannoli[53b,53a], R. Vari[70a], E.W. Varnes[6], C. Varni[16], T. Varol[154], D. Varouchas[62], K.E. Varvell[153], M.E. Vasile[25b], L. Vaslin[36], G.A. Vasquez[171], F. Vazeille[36], D. Vazquez Furelos[12], T. Vazquez Schroeder[34], J. Veatch[51], V. Vecchio[98], M.J. Veen[116], I. Veliscek[130], L.M. Veloce[162], F. Veloso[135a,135c], S. Veneziano[70a], A. Ventura[65a,65b], A. Verbytskyi[112], M. Verducci[69a,69b], C. Vergis[22], M. Verissimo De Araujo[78b], W. Verkerke[116], A.T. Vermeulen[116], J.C. Vermeulen[116], C. Vernieri[149], P.J. Verschuuren[91], M.L. Vesterbacka[121], M.C. Vetterli[148,al], A. Vgenopoulos[158], N. Viaux Maira[142d], T. Vickey[145],

O.E. Vickey Boeriu[145], G.H.A. Viehhauser[130], L. Vigani[59b], M. Villa[21b,21a], M. Villaplana Perez[169], E.M. Villhauer[48], E. Vilucchi[49], M.G. Vincter[32], G.S. Virdee[19], A. Vishwakarma[48], C. Vittori[21b,21a], I. Vivarelli[152], V. Vladimirov[173], E. Voevodina[112], M. Vogel[177], P. Vokac[137], J. Von Ahnen[44], S.E. von Buddenbrock[31f], E. Von Toerne[22], V. Vorobel[138], K. Vorobev[109], M. Vos[169], J.H. Vossebeld[88], M. Vozak[98], L. Vozdecky[90], N. Vranjes[14], M. Vranjes Milosavljevic[14], V. Vrba[137,*], M. Vreeswijk[116], N.K. Vu[99], R. Vuillermet[34], O.V. Vujinovic[97], I. Vukotic[35], S. Wada[164], C. Wagner[100], W. Wagner[177], S. Wahdan[177], H. Wahlberg[86], R. Wakasa[164], M. Wakida[113], V.M. Walbrecht[112], J. Walder[139], R. Walker[111], S.D. Walker[91], W. Walkowiak[147], A.M. Wang[57], A.Z. Wang[176], C. Wang[58a], C. Wang[58c], H. Wang[16], J. Wang[60a], P. Wang[40], R.-J. Wang[97], R. Wang[57], R. Wang[117], S.M. Wang[154], S. Wang[58b], T. Wang[58a], W.T. Wang[58a], W.X. Wang[58a], X. Wang[13c], X. Wang[168], Y. Wang[58a], Z. Wang[103], C. Wanotayaroj[34], A. Warburton[101], C.P. Ward[30], R.J. Ward[19], N. Warrack[55], A.T. Watson[19], M.F. Watson[19], G. Watts[144], B.M. Waugh[92], A.F. Webb[10], C. Weber[27], M.S. Weber[18], S.A. Weber[32], S.M. Weber[59a], C. Wei[58a], Y. Wei[130], A.R. Weidberg[130], J. Weingarten[45], M. Weirich[97], C. Weiser[50], T. Wenaus[27], B. Wendland[45], T. Wengler[34], S. Wenig[34], N. Wermes[22], M. Wessels[59a], K. Whalen[127], A.M. Wharton[87], A.S. White[57], A. White[7], M.J. White[1], D. Whiteson[166], L. Wickremasinghe[128], W. Wiedenmann[176], C. Wiel[46], M. Wielers[139], N. Wieseotte[97], C. Wiglesworth[38], L.A.M. Wiik-Fuchs[50], D.J. Wilbern[124], H.G. Wilkens[34], L.J. Wilkins[91], D.M. Williams[37], H.H. Williams[132], S. Williams[30], S. Willocq[100], P.J. Windischhofer[130], I. Wingerter-Seez[4], F. Winklmeier[127], B.T. Winter[50], M. Wittgen[149], M. Wobisch[93], A. Wolf[97], R. Wölker[130], J. Wollrath[166], M.W. Wolter[82], H. Wolters[135a,135c], V.W.S. Wong[170], A.F. Wongel[44], S.D. Worm[44], B.K. Wosiek[82], K.W. Woźniak[82], K. Wraight[55], J. Wu[13a,13d], S.L. Wu[176], X. Wu[52], Y. Wu[58a], Z. Wu[140,58a], J. Wuerzinger[130], T.R. Wyatt[98], B.M. Wynne[48], S. Xella[38], M. Xia[13b], J. Xiang[60c], X. Xiao[103], M. Xie[58a], X. Xie[58a], I. Xiotidis[152], D. Xu[13a], H. Xu[58a], H. Xu[58a], L. Xu[58a], R. Xu[132], T. Xu[58a], W. Xu[103], Y. Xu[13b], Z. Xu[58b], Z. Xu[149], B. Yabsley[153], S. Yacoob[31a], N. Yamaguchi[85], Y. Yamaguchi[160], M. Yamatani[159], H. Yamauchi[164], T. Yamazaki[16], Y. Yamazaki[80], J. Yan[58c], S. Yan[130], Z. Yan[23], H.J. Yang[58c,58d], H.T. Yang[16], S. Yang[58a], T. Yang[60c], X. Yang[58a], X. Yang[13a], Y. Yang[159], Z. Yang[103,58a], W-M. Yao[16], Y.C. Yap[44], H. Ye[13c], J. Ye[40], S. Ye[27], I. Yeletskikh[77], M.R. Yexley[87], P. Yin[37], K. Yorita[174], K. Yoshihara[76], C.J.S. Young[50], C. Young[149], R. Yuan[58b,j], X. Yue[59a], M. Zaazoua[33e], B. Zabinski[82], G. Zacharis[9], E. Zaid[48], A.M. Zaitsev[119,ag], T. Zakareishvili[155b], N. Zakharchuk[32], S. Zambito[34], D. Zanzi[50], S.V. Zeißner[45], C. Zeitnitz[177], J.C. Zeng[168], O. Zenin[119], T. Ženiš[26a], S. Zenz[90], S. Zerradi[33a], D. Zerwas[62], M. Zgubič[130], B. Zhang[13c], D.F. Zhang[13b], G. Zhang[13b], J. Zhang[5], K. Zhang[13a], L. Zhang[13c], M. Zhang[168], R. Zhang[176], S. Zhang[103], X. Zhang[58c], X. Zhang[58b], Z. Zhang[62], P. Zhao[47], Y. Zhao[141], Z. Zhao[58a], A. Zhemchugov[77], Z. Zheng[149], D. Zhong[168], B. Zhou[103], C. Zhou[176], H. Zhou[6], N. Zhou[58c], Y. Zhou[6], C.G. Zhu[58b], C. Zhu[13a,13d], H.L. Zhu[58a], H. Zhu[13a], J. Zhu[103], Y. Zhu[58a], X. Zhuang[13a], K. Zhukov[108], V. Zhulanov[118b,118a], D. Zieminska[63], N.I. Zimine[77], S. Zimmermann[50,*], J. Zinsser[59b], M. Ziolkowski[147], L. Živković[14], A. Zoccoli[21b,21a], K. Zoch[52], T.G. Zorbas[145], O. Zormpa[42], W. Zou[37], L. Zwalinski[34].

[1]Department of Physics, University of Adelaide, Adelaide; Australia.
[2]Department of Physics, University of Alberta, Edmonton AB; Canada.
[3(a)]Department of Physics, Ankara University, Ankara;[(b)]Istanbul Aydin University, Application and Research Center for Advanced Studies, Istanbul;[(c)]Division of Physics, TOBB University of Economics and Technology, Ankara; Turkey.
[4]LAPP, Univ. Savoie Mont Blanc, CNRS/IN2P3, Annecy ; France.
[5]High Energy Physics Division, Argonne National Laboratory, Argonne IL; United States of America.
[6]Department of Physics, University of Arizona, Tucson AZ; United States of America.
[7]Department of Physics, University of Texas at Arlington, Arlington TX; United States of America.
[8]Physics Department, National and Kapodistrian University of Athens, Athens; Greece.

[9]Physics Department, National Technical University of Athens, Zografou; Greece.
[10]Department of Physics, University of Texas at Austin, Austin TX; United States of America.
[11(a)]Bahcesehir University, Faculty of Engineering and Natural Sciences, Istanbul;[(b)]Istanbul Bilgi University, Faculty of Engineering and Natural Sciences, Istanbul;[(c)]Department of Physics, Bogazici University, Istanbul;[(d)]Department of Physics Engineering, Gaziantep University, Gaziantep; Turkey.
[12]Institut de Física d'Altes Energies (IFAE), Barcelona Institute of Science and Technology, Barcelona; Spain.
[13(a)]Institute of High Energy Physics, Chinese Academy of Sciences, Beijing;[(b)]Physics Department, Tsinghua University, Beijing;[(c)]Department of Physics, Nanjing University, Nanjing;[(d)]University of Chinese Academy of Science (UCAS), Beijing; China.
[14]Institute of Physics, University of Belgrade, Belgrade; Serbia.
[15]Department for Physics and Technology, University of Bergen, Bergen; Norway.
[16]Physics Division, Lawrence Berkeley National Laboratory and University of California, Berkeley CA; United States of America.
[17]Institut für Physik, Humboldt Universität zu Berlin, Berlin; Germany.
[18]Albert Einstein Center for Fundamental Physics and Laboratory for High Energy Physics, University of Bern, Bern; Switzerland.
[19]School of Physics and Astronomy, University of Birmingham, Birmingham; United Kingdom.
[20(a)]Facultad de Ciencias y Centro de Investigaciónes, Universidad Antonio Nariño, Bogotá;[(b)]Departamento de Física, Universidad Nacional de Colombia, Bogotá; Colombia.
[21(a)]Dipartimento di Fisica e Astronomia A. Righi, Università di Bologna, Bologna;[(b)]INFN Sezione di Bologna; Italy.
[22]Physikalisches Institut, Universität Bonn, Bonn; Germany.
[23]Department of Physics, Boston University, Boston MA; United States of America.
[24]Department of Physics, Brandeis University, Waltham MA; United States of America.
[25(a)]Transilvania University of Brasov, Brasov;[(b)]Horia Hulubei National Institute of Physics and Nuclear Engineering, Bucharest;[(c)]Department of Physics, Alexandru Ioan Cuza University of Iasi, Iasi;[(d)]National Institute for Research and Development of Isotopic and Molecular Technologies, Physics Department, Cluj-Napoca;[(e)]University Politehnica Bucharest, Bucharest;[(f)]West University in Timisoara, Timisoara; Romania.
[26(a)]Faculty of Mathematics, Physics and Informatics, Comenius University, Bratislava;[(b)]Department of Subnuclear Physics, Institute of Experimental Physics of the Slovak Academy of Sciences, Kosice; Slovak Republic.
[27]Physics Department, Brookhaven National Laboratory, Upton NY; United States of America.
[28]Universidad de Buenos Aires, Facultad de Ciencias Exactas y Naturales, Departamento de Física, y CONICET, Instituto de Física de Buenos Aires (IFIBA), Buenos Aires; Argentina.
[29]California State University, CA; United States of America.
[30]Cavendish Laboratory, University of Cambridge, Cambridge; United Kingdom.
[31(a)]Department of Physics, University of Cape Town, Cape Town;[(b)]iThemba Labs, Western Cape;[(c)]Department of Mechanical Engineering Science, University of Johannesburg, Johannesburg;[(d)]National Institute of Physics, University of the Philippines Diliman (Philippines);[(e)]University of South Africa, Department of Physics, Pretoria;[(f)]School of Physics, University of the Witwatersrand, Johannesburg; South Africa.
[32]Department of Physics, Carleton University, Ottawa ON; Canada.
[33(a)]Faculté des Sciences Ain Chock, Réseau Universitaire de Physique des Hautes Energies - Université Hassan II, Casablanca;[(b)]Faculté des Sciences, Université Ibn-Tofail, Kénitra;[(c)]Faculté des Sciences Semlalia, Université Cadi Ayyad, LPHEA-Marrakech;[(d)]LPMR, Faculté des Sciences, Université

Mohamed Premier, Oujda;[e] Faculté des sciences, Université Mohammed V, Rabat; Morocco.
[34] CERN, Geneva; Switzerland.
[35] Enrico Fermi Institute, University of Chicago, Chicago IL; United States of America.
[36] LPC, Université Clermont Auvergne, CNRS/IN2P3, Clermont-Ferrand; France.
[37] Nevis Laboratory, Columbia University, Irvington NY; United States of America.
[38] Niels Bohr Institute, University of Copenhagen, Copenhagen; Denmark.
[39(a)] Dipartimento di Fisica, Università della Calabria, Rende;[b] INFN Gruppo Collegato di Cosenza, Laboratori Nazionali di Frascati; Italy.
[40] Physics Department, Southern Methodist University, Dallas TX; United States of America.
[41] Physics Department, University of Texas at Dallas, Richardson TX; United States of America.
[42] National Centre for Scientific Research "Demokritos", Agia Paraskevi; Greece.
[43(a)] Department of Physics, Stockholm University;[b] Oskar Klein Centre, Stockholm; Sweden.
[44] Deutsches Elektronen-Synchrotron DESY, Hamburg and Zeuthen; Germany.
[45] Fakultät Physik , Technische Universität Dortmund, Dortmund; Germany.
[46] Institut für Kern- und Teilchenphysik, Technische Universität Dresden, Dresden; Germany.
[47] Department of Physics, Duke University, Durham NC; United States of America.
[48] SUPA - School of Physics and Astronomy, University of Edinburgh, Edinburgh; United Kingdom.
[49] INFN e Laboratori Nazionali di Frascati, Frascati; Italy.
[50] Physikalisches Institut, Albert-Ludwigs-Universität Freiburg, Freiburg; Germany.
[51] II. Physikalisches Institut, Georg-August-Universität Göttingen, Göttingen; Germany.
[52] Département de Physique Nucléaire et Corpusculaire, Université de Genève, Genève; Switzerland.
[53(a)] Dipartimento di Fisica, Università di Genova, Genova;[b] INFN Sezione di Genova; Italy.
[54] II. Physikalisches Institut, Justus-Liebig-Universität Giessen, Giessen; Germany.
[55] SUPA - School of Physics and Astronomy, University of Glasgow, Glasgow; United Kingdom.
[56] LPSC, Université Grenoble Alpes, CNRS/IN2P3, Grenoble INP, Grenoble; France.
[57] Laboratory for Particle Physics and Cosmology, Harvard University, Cambridge MA; United States of America.
[58(a)] Department of Modern Physics and State Key Laboratory of Particle Detection and Electronics, University of Science and Technology of China, Hefei;[b] Institute of Frontier and Interdisciplinary Science and Key Laboratory of Particle Physics and Particle Irradiation (MOE), Shandong University, Qingdao;[c] School of Physics and Astronomy, Shanghai Jiao Tong University, Key Laboratory for Particle Astrophysics and Cosmology (MOE), SKLPPC, Shanghai;[d] Tsung-Dao Lee Institute, Shanghai; China.
[59(a)] Kirchhoff-Institut für Physik, Ruprecht-Karls-Universität Heidelberg, Heidelberg;[b] Physikalisches Institut, Ruprecht-Karls-Universität Heidelberg, Heidelberg; Germany.
[60(a)] Department of Physics, Chinese University of Hong Kong, Shatin, N.T., Hong Kong;[b] Department of Physics, University of Hong Kong, Hong Kong;[c] Department of Physics and Institute for Advanced Study, Hong Kong University of Science and Technology, Clear Water Bay, Kowloon, Hong Kong; China.
[61] Department of Physics, National Tsing Hua University, Hsinchu; Taiwan.
[62] IJCLab, Université Paris-Saclay, CNRS/IN2P3, 91405, Orsay; France.
[63] Department of Physics, Indiana University, Bloomington IN; United States of America.
[64(a)] INFN Gruppo Collegato di Udine, Sezione di Trieste, Udine;[b] ICTP, Trieste;[c] Dipartimento Politecnico di Ingegneria e Architettura, Università di Udine, Udine; Italy.
[65(a)] INFN Sezione di Lecce;[b] Dipartimento di Matematica e Fisica, Università del Salento, Lecce; Italy.
[66(a)] INFN Sezione di Milano;[b] Dipartimento di Fisica, Università di Milano, Milano; Italy.
[67(a)] INFN Sezione di Napoli;[b] Dipartimento di Fisica, Università di Napoli, Napoli; Italy.
[68(a)] INFN Sezione di Pavia;[b] Dipartimento di Fisica, Università di Pavia, Pavia; Italy.
[69(a)] INFN Sezione di Pisa;[b] Dipartimento di Fisica E. Fermi, Università di Pisa, Pisa; Italy.

[70(a)]INFN Sezione di Roma;[(b)]Dipartimento di Fisica, Sapienza Università di Roma, Roma; Italy.
[71(a)]INFN Sezione di Roma Tor Vergata;[(b)]Dipartimento di Fisica, Università di Roma Tor Vergata, Roma; Italy.
[72(a)]INFN Sezione di Roma Tre;[(b)]Dipartimento di Matematica e Fisica, Università Roma Tre, Roma; Italy.
[73(a)]INFN-TIFPA;[(b)]Università degli Studi di Trento, Trento; Italy.
[74]Institut für Astro- und Teilchenphysik, Leopold-Franzens-Universität, Innsbruck; Austria.
[75]University of Iowa, Iowa City IA; United States of America.
[76]Department of Physics and Astronomy, Iowa State University, Ames IA; United States of America.
[77]Joint Institute for Nuclear Research, Dubna; Russia.
[78(a)]Departamento de Engenharia Elétrica, Universidade Federal de Juiz de Fora (UFJF), Juiz de Fora;[(b)]Universidade Federal do Rio De Janeiro COPPE/EE/IF, Rio de Janeiro;[(c)]Instituto de Física, Universidade de São Paulo, São Paulo; Brazil.
[79]KEK, High Energy Accelerator Research Organization, Tsukuba; Japan.
[80]Graduate School of Science, Kobe University, Kobe; Japan.
[81(a)]AGH University of Science and Technology, Faculty of Physics and Applied Computer Science, Krakow;[(b)]Marian Smoluchowski Institute of Physics, Jagiellonian University, Krakow; Poland.
[82]Institute of Nuclear Physics Polish Academy of Sciences, Krakow; Poland.
[83]Faculty of Science, Kyoto University, Kyoto; Japan.
[84]Kyoto University of Education, Kyoto; Japan.
[85]Research Center for Advanced Particle Physics and Department of Physics, Kyushu University, Fukuoka ; Japan.
[86]Instituto de Física La Plata, Universidad Nacional de La Plata and CONICET, La Plata; Argentina.
[87]Physics Department, Lancaster University, Lancaster; United Kingdom.
[88]Oliver Lodge Laboratory, University of Liverpool, Liverpool; United Kingdom.
[89]Department of Experimental Particle Physics, Jožef Stefan Institute and Department of Physics, University of Ljubljana, Ljubljana; Slovenia.
[90]School of Physics and Astronomy, Queen Mary University of London, London; United Kingdom.
[91]Department of Physics, Royal Holloway University of London, Egham; United Kingdom.
[92]Department of Physics and Astronomy, University College London, London; United Kingdom.
[93]Louisiana Tech University, Ruston LA; United States of America.
[94]Fysiska institutionen, Lunds universitet, Lund; Sweden.
[95]Centre de Calcul de l'Institut National de Physique Nucléaire et de Physique des Particules (IN2P3), Villeurbanne; France.
[96]Departamento de Física Teorica C-15 and CIAFF, Universidad Autónoma de Madrid, Madrid; Spain.
[97]Institut für Physik, Universität Mainz, Mainz; Germany.
[98]School of Physics and Astronomy, University of Manchester, Manchester; United Kingdom.
[99]CPPM, Aix-Marseille Université, CNRS/IN2P3, Marseille; France.
[100]Department of Physics, University of Massachusetts, Amherst MA; United States of America.
[101]Department of Physics, McGill University, Montreal QC; Canada.
[102]School of Physics, University of Melbourne, Victoria; Australia.
[103]Department of Physics, University of Michigan, Ann Arbor MI; United States of America.
[104]Department of Physics and Astronomy, Michigan State University, East Lansing MI; United States of America.
[105]B.I. Stepanov Institute of Physics, National Academy of Sciences of Belarus, Minsk; Belarus.
[106]Research Institute for Nuclear Problems of Byelorussian State University, Minsk; Belarus.
[107]Group of Particle Physics, University of Montreal, Montreal QC; Canada.

[108]P.N. Lebedev Physical Institute of the Russian Academy of Sciences, Moscow; Russia.
[109]National Research Nuclear University MEPhI, Moscow; Russia.
[110]D.V. Skobeltsyn Institute of Nuclear Physics, M.V. Lomonosov Moscow State University, Moscow; Russia.
[111]Fakultät für Physik, Ludwig-Maximilians-Universität München, München; Germany.
[112]Max-Planck-Institut für Physik (Werner-Heisenberg-Institut), München; Germany.
[113]Graduate School of Science and Kobayashi-Maskawa Institute, Nagoya University, Nagoya; Japan.
[114]Department of Physics and Astronomy, University of New Mexico, Albuquerque NM; United States of America.
[115]Institute for Mathematics, Astrophysics and Particle Physics, Radboud University/Nikhef, Nijmegen; Netherlands.
[116]Nikhef National Institute for Subatomic Physics and University of Amsterdam, Amsterdam; Netherlands.
[117]Department of Physics, Northern Illinois University, DeKalb IL; United States of America.
[118(a)]Budker Institute of Nuclear Physics and NSU, SB RAS, Novosibirsk;[(b)]Novosibirsk State University Novosibirsk; Russia.
[119]Institute for High Energy Physics of the National Research Centre Kurchatov Institute, Protvino; Russia.
[120]Institute for Theoretical and Experimental Physics named by A.I. Alikhanov of National Research Centre "Kurchatov Institute", Moscow; Russia.
[121]Department of Physics, New York University, New York NY; United States of America.
[122]Ochanomizu University, Otsuka, Bunkyo-ku, Tokyo; Japan.
[123]Ohio State University, Columbus OH; United States of America.
[124]Homer L. Dodge Department of Physics and Astronomy, University of Oklahoma, Norman OK; United States of America.
[125]Department of Physics, Oklahoma State University, Stillwater OK; United States of America.
[126]Palacký University, Joint Laboratory of Optics, Olomouc; Czech Republic.
[127]Institute for Fundamental Science, University of Oregon, Eugene, OR; United States of America.
[128]Graduate School of Science, Osaka University, Osaka; Japan.
[129]Department of Physics, University of Oslo, Oslo; Norway.
[130]Department of Physics, Oxford University, Oxford; United Kingdom.
[131]LPNHE, Sorbonne Université, Université Paris Cité, CNRS/IN2P3, Paris; France.
[132]Department of Physics, University of Pennsylvania, Philadelphia PA; United States of America.
[133]Konstantinov Nuclear Physics Institute of National Research Centre "Kurchatov Institute", PNPI, St. Petersburg; Russia.
[134]Department of Physics and Astronomy, University of Pittsburgh, Pittsburgh PA; United States of America.
[135(a)]Laboratório de Instrumentação e Física Experimental de Partículas - LIP, Lisboa;[(b)]Departamento de Física, Faculdade de Ciências, Universidade de Lisboa, Lisboa;[(c)]Departamento de Física, Universidade de Coimbra, Coimbra;[(d)]Centro de Física Nuclear da Universidade de Lisboa, Lisboa;[(e)]Departamento de Física, Universidade do Minho, Braga;[(f)]Departamento de Física Teórica y del Cosmos, Universidad de Granada, Granada (Spain);[(g)]Dep Física and CEFITEC of Faculdade de Ciências e Tecnologia, Universidade Nova de Lisboa, Caparica;[(h)]Instituto Superior Técnico, Universidade de Lisboa, Lisboa; Portugal.
[136]Institute of Physics of the Czech Academy of Sciences, Prague; Czech Republic.
[137]Czech Technical University in Prague, Prague; Czech Republic.
[138]Charles University, Faculty of Mathematics and Physics, Prague; Czech Republic.
[139]Particle Physics Department, Rutherford Appleton Laboratory, Didcot; United Kingdom.

[140]IRFU, CEA, Université Paris-Saclay, Gif-sur-Yvette; France.
[141]Santa Cruz Institute for Particle Physics, University of California Santa Cruz, Santa Cruz CA; United States of America.
[142(a)]Departamento de Física, Pontificia Universidad Católica de Chile, Santiago;[(b)]Universidad Andres Bello, Department of Physics, Santiago;[(c)]Instituto de Alta Investigación, Universidad de Tarapacá, Arica;[(d)]Departamento de Física, Universidad Técnica Federico Santa María, Valparaíso; Chile.
[143]Universidade Federal de São João del Rei (UFSJ), São João del Rei; Brazil.
[144]Department of Physics, University of Washington, Seattle WA; United States of America.
[145]Department of Physics and Astronomy, University of Sheffield, Sheffield; United Kingdom.
[146]Department of Physics, Shinshu University, Nagano; Japan.
[147]Department Physik, Universität Siegen, Siegen; Germany.
[148]Department of Physics, Simon Fraser University, Burnaby BC; Canada.
[149]SLAC National Accelerator Laboratory, Stanford CA; United States of America.
[150]Department of Physics, Royal Institute of Technology, Stockholm; Sweden.
[151]Departments of Physics and Astronomy, Stony Brook University, Stony Brook NY; United States of America.
[152]Department of Physics and Astronomy, University of Sussex, Brighton; United Kingdom.
[153]School of Physics, University of Sydney, Sydney; Australia.
[154]Institute of Physics, Academia Sinica, Taipei; Taiwan.
[155(a)]E. Andronikashvili Institute of Physics, Iv. Javakhishvili Tbilisi State University, Tbilisi;[(b)]High Energy Physics Institute, Tbilisi State University, Tbilisi; Georgia.
[156]Department of Physics, Technion, Israel Institute of Technology, Haifa; Israel.
[157]Raymond and Beverly Sackler School of Physics and Astronomy, Tel Aviv University, Tel Aviv; Israel.
[158]Department of Physics, Aristotle University of Thessaloniki, Thessaloniki; Greece.
[159]International Center for Elementary Particle Physics and Department of Physics, University of Tokyo, Tokyo; Japan.
[160]Department of Physics, Tokyo Institute of Technology, Tokyo; Japan.
[161]Tomsk State University, Tomsk; Russia.
[162]Department of Physics, University of Toronto, Toronto ON; Canada.
[163(a)]TRIUMF, Vancouver BC;[(b)]Department of Physics and Astronomy, York University, Toronto ON; Canada.
[164]Division of Physics and Tomonaga Center for the History of the Universe, Faculty of Pure and Applied Sciences, University of Tsukuba, Tsukuba; Japan.
[165]Department of Physics and Astronomy, Tufts University, Medford MA; United States of America.
[166]Department of Physics and Astronomy, University of California Irvine, Irvine CA; United States of America.
[167]Department of Physics and Astronomy, University of Uppsala, Uppsala; Sweden.
[168]Department of Physics, University of Illinois, Urbana IL; United States of America.
[169]Instituto de Física Corpuscular (IFIC), Centro Mixto Universidad de Valencia - CSIC, Valencia; Spain.
[170]Department of Physics, University of British Columbia, Vancouver BC; Canada.
[171]Department of Physics and Astronomy, University of Victoria, Victoria BC; Canada.
[172]Fakultät für Physik und Astronomie, Julius-Maximilians-Universität Würzburg, Würzburg; Germany.
[173]Department of Physics, University of Warwick, Coventry; United Kingdom.
[174]Waseda University, Tokyo; Japan.
[175]Department of Particle Physics and Astrophysics, Weizmann Institute of Science, Rehovot; Israel.
[176]Department of Physics, University of Wisconsin, Madison WI; United States of America.
[177]Fakultät für Mathematik und Naturwissenschaften, Fachgruppe Physik, Bergische Universität

Wuppertal, Wuppertal; Germany.
[178]Department of Physics, Yale University, New Haven CT; United States of America.
[a] Also at Borough of Manhattan Community College, City University of New York, New York NY; United States of America.
[b] Also at Bruno Kessler Foundation, Trento; Italy.
[c] Also at Center for High Energy Physics, Peking University; China.
[d] Also at Centro Studi e Ricerche Enrico Fermi; Italy.
[e] Also at CERN, Geneva; Switzerland.
[f] Also at CPPM, Aix-Marseille Université, CNRS/IN2P3, Marseille; France.
[g] Also at Département de Physique Nucléaire et Corpusculaire, Université de Genève, Genève; Switzerland.
[h] Also at Departament de Fisica de la Universitat Autonoma de Barcelona, Barcelona; Spain.
[i] Also at Department of Financial and Management Engineering, University of the Aegean, Chios; Greece.
[j] Also at Department of Physics and Astronomy, Michigan State University, East Lansing MI; United States of America.
[k] Also at Department of Physics and Astronomy, University of Louisville, Louisville, KY; United States of America.
[l] Also at Department of Physics, Ben Gurion University of the Negev, Beer Sheva; Israel.
[m] Also at Department of Physics, California State University, East Bay; United States of America.
[n] Also at Department of Physics, California State University, Fresno; United States of America.
[o] Also at Department of Physics, California State University, Sacramento; United States of America.
[p] Also at Department of Physics, King's College London, London; United Kingdom.
[q] Also at Department of Physics, St. Petersburg State Polytechnical University, St. Petersburg; Russia.
[r] Also at Department of Physics, University of Fribourg, Fribourg; Switzerland.
[s] Also at Faculty of Physics, M.V. Lomonosov Moscow State University, Moscow; Russia.
[t] Also at Faculty of Physics, Sofia University, 'St. Kliment Ohridski', Sofia; Bulgaria.
[u] Also at Giresun University, Faculty of Engineering, Giresun; Turkey.
[v] Also at Graduate School of Science, Osaka University, Osaka; Japan.
[w] Also at Hellenic Open University, Patras; Greece.
[x] Also at Institucio Catalana de Recerca i Estudis Avancats, ICREA, Barcelona; Spain.
[y] Also at Institut für Experimentalphysik, Universität Hamburg, Hamburg; Germany.
[z] Also at Institute for Particle and Nuclear Physics, Wigner Research Centre for Physics, Budapest; Hungary.
[aa] Also at Institute of Particle Physics (IPP); Canada.
[ab] Also at Institute of Physics, Azerbaijan Academy of Sciences, Baku; Azerbaijan.
[ac] Also at Institute of Theoretical Physics, Ilia State University, Tbilisi; Georgia.
[ad] Also at Instituto de Fisica Teorica, IFT-UAM/CSIC, Madrid; Spain.
[ae] Also at Istanbul University, Dept. of Physics, Istanbul; Turkey.
[af] Also at Joint Institute for Nuclear Research, Dubna; Russia.
[ag] Also at Moscow Institute of Physics and Technology State University, Dolgoprudny; Russia.
[ah] Also at National Research Nuclear University MEPhI, Moscow; Russia.
[ai] Also at Physics Department, An-Najah National University, Nablus; Palestine.
[aj] Also at Physikalisches Institut, Albert-Ludwigs-Universität Freiburg, Freiburg; Germany.
[ak] Also at The City College of New York, New York NY; United States of America.
[al] Also at TRIUMF, Vancouver BC; Canada.
[am] Also at Università di Napoli Parthenope, Napoli; Italy.
[an] Also at University of Chinese Academy of Sciences (UCAS), Beijing; China.

[ao] Also at Yeditepe University, Physics Department, Istanbul; Turkey.
[*] Deceased